

AD-R198 617

A STUDY OF DAMAGE TOLERANCE IN CURVED COMPOSITE PANELS

1/2

(U) AIR FORCE INST OF TECH WRIGHT-PATTERSON AFB OH

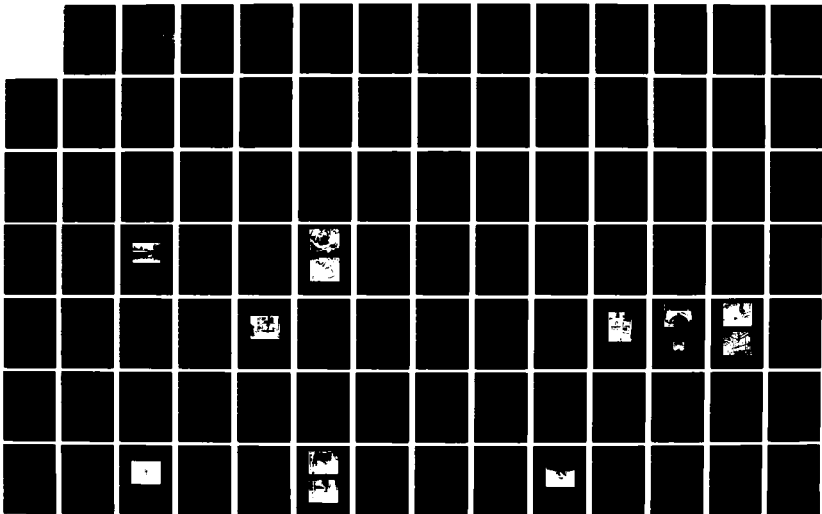
SCHOOL OF ENGINEERING B L WILDER MAR 88

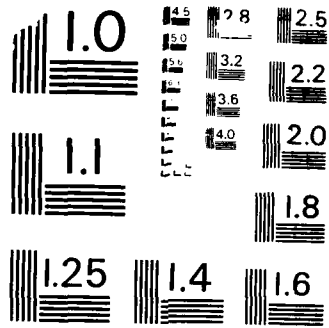
UNCLASSIFIED

AFIT/GA/AA/88M-3

F/G 11/4

NL





MICROCOPY RESOLUTION TEST CHART
NATIONAL BUREAU OF STANDARDS-1963-A

AD-A190 617

DTIC FILE COPY

1



DTIC
 ELECTRIC
 MAR 3 1 1988
 S & D

 A STUDY OF DAMAGE TOLERANCE
 IN CURVED COMPOSITE PANELS
 THESIS
 Brendan L. Wilder
 Captain, USAF

DISTRIBUTION STATEMENT A
 Approved for public release
 Distribution Unlimited

DEPARTMENT OF THE AIR FORCE
 AIR UNIVERSITY
AIR FORCE INSTITUTE OF TECHNOLOGY

Wright-Patterson Air Force Base, Ohio

88 3 30 054

1

AFIT/GA/AA/88M-3

A STUDY OF DAMAGE TOLERANCE
IN CURVED COMPOSITE PANELS

THESIS

Brendan L. Wilder
Captain, USAF

DTIC
ELECT
SEP 1 1988
Q

Approved for public release: distribution unlimited

**A STUDY OF DAMAGE TOLERANCE
IN CURVED COMPOSITE PANELS**

THESIS

Presented to the Faculty of the School of Engineering
of the Air Force Institute of Technology
Air University
In Partial Fulfillment of the
Requirements for the Degree of
Master of Science in Astronautical Engineering

Brendan L. Wilder
Captain, USAF

March 1988



Accession For	
NTIS GRA&I	<input checked="" type="checkbox"/>
DTIC TAB	<input type="checkbox"/>
Unannounced	<input type="checkbox"/>
Justification	
By	
Date	
Availability Codes	
Dist	Availability Codes
A-1	

ACKNOWLEDGMENTS

I would like to express my sincere gratitude to Doctor Anthony Palazotto, my thesis advisor, for his patience, his guidance, and his sense of humor throughout the course of this thesis work.

I would also like to thank the people of the AF Flight Dynamics lab who sponsored my work. Dr. R. S. Sandhu was kind enough to teach me to use his plane strain finite element code and gave me much assistance in modeling my problem. Patty Lache was invaluable in the experimental phase of my work as were Jack Smith, Don Cook, and Larry Bates. It was a true pleasure to work with professionals such as these.

Finally, I would like to thank my wife Denise for her love, her patience and her continuous support. This thesis is as much hers as it is mine.

"Rusty" Wilder

TABLE OF CONTENTS

Acknowledgment	ii
List of Symbols	v
List of Figures	vii
List of Tables	ix
Abstract	x
I. Introduction	1
Background	3
Purpose	10
Scope	11
II. Theory	13
Classical Laminate Theory	13
Bifurcation Buckling	19
STAGSC-1 Theory	23
III. Manufacturing and Experimental Procedure	28
Panel Manufacturing	32
Experimental Set-Up	48
Test Procedure	50
IV. Results and Discussion	57
Panel Identification	57
Panels with No Damage	58
Manufacturing Induced Defects.....	62
Surface Damage	66
Internal Delaminations	71
V. Analytical Technique	82
Introduction	82
Curved Panel - STAGSC-1 Model	89
Delamination - STAGSC-1 Model.....	92
Plane Strain Finite Element Model	101
Plane Strain Solution - No Delamination	105
Analytical Predictions	107

VI. Conclusion	112
Appendix A - Constitutive Matrices & Test Data.....	116
Appendix B - Sample STAGSC-1 Input Decks.....	123
Bibliography	134

LIST OF SYMBOLS

E_1	Longitudinal Modulus of Elasticity
E_2	Transverse Modulus of Elasticity
G_{12}	Shear Modulus
ν	Poisson's Ratio
$1, 2, 3$	Material Co-ordinate Directions
x, y, z	Global Co-ordinate Directions
X, Y, Z	Surface Co-ordinates of Shell
u, v, w	Displacements in the x, y, z Directions
a	Radius of Delamination
C	Panel Chord Length
D	$D = E \cdot h^3 / 12(1 - \nu^2)$
h	Thickness of Panel from Mid-Surface
k_x	Curvature with Respect to x
k_y	Curvature with Respect to y
L	Panel Height in x Direction
R	Radius of Curvature of Panel
t	Thickness of Panel
U	Internal Strain Energy
V	Potential Energy
W	Work
$w, _x$	Differential of w with respect to x
$w, _y$	Differential of w with respect to y
z	Distance from Panel Mid-Surface

A_{ij}	[A]	Extensional Stiffness Matrix
B_{ij}	[B]	Coupling Stiffness Matrix
D_{ij}	[D]	Bending Stiffness Matrix
Q_{ij}		Reduced Stiffness Matrix
\bar{Q}_{ij}		Transformed Reduced Stiffness
N_x N_y N_{xy}		Force Resultants
M_x M_y M_{xy}		Moment Resultants
σ		Normal Stress
τ		Shear Stress
ϵ		Strain
ϵ_{xy}		Sheer Strain
θ		Ply Orientation
ϕ		Rotation of a Tangent to the Panel's Mid-Surface

LIST OF FIGURES

Figure	Page
1.1 Panel Geometry	8
1.2 Panel Cross Section.....	9
2.1 Laminate Co-ordinate System.....	14
2.2 Geometry of N Layered Laminate.....	14
2.3 Equilibrium Path.....	20
2.4 Equilibrium Path for Cylindrical Shell.....	22
3.1 Blistering Due to Teflon Insert.....	30
3.2 Placing Bleeder in Steel Mold.....	33
3.3 Positioning Teflon Inserts in Panel.....	33
3.4 Prepreg Cutting Plan for 0° Plies.....	34
3.5 Prepreg Cutting Plan for 45° Plies.....	35
3.6 Prepreg Cutting Plan for 90° Plies.....	36
3.7 Bagging Sequence.....	38
3.8 Horban's [7] STAGSC-1 Results	42
3.9 Placement of Strain Guages on Panel.....	45
3.10 Compression Machine, Amps & Signal Conditioners....	46
3.11 Control Unit for Compression Machine.....	52
3.12 Top Support of Test Fixture.....	53
3.13 Vertical Support of Test Fixture.....	53
3.14 Panel Clamped in Bottom Fixture.....	54
3.15 Array of LVDT's.....	54
3.16 Load Displacement Curve for No Seating Load.....	55
3.17 Load Displacement Curve for 3000 lb Seating Load...	56
4.1 Load vs SG1 & SG2 - Q0-00-x Panel.....	60
4.2 Global Buckling for Q0-00-x Panel.....	61
4.3 Compressive Load vs Percent Voids.....	64
4.4 Percent Voids vs Panel Thickness.....	65
4.5 Load vs Laminate Thickness - Surface Damage.....	69
4.6 Load vs SG1 & SG2 for Surface Damage.....	70
4.7 Stereo X-ray of Delamination.....	72
4.8 Experimental vs STAGSC-1 Load for Delaminated Panels.....	74

4.9	Buckling of Sublamine in Q2-23 Panel.....	75
4.10	Buckling of Sublamine in Q4-23 Panel	75
4.11	Ideal Strain Reversal Curve.....	76
4.12	Plastic Deformation of Sublamine.....	79
4.13	Strain Reversal for Reloaded Panel.....	80
5.1	Plane Strain Assumption for Analytic Tech.....	84
5.2	QUAF 410 STAGSC-1 Element.....	91
5.3	Disc Convergence Meshes.....	94
5.4	Convergence Curve for Circular Disc.....	96
5.5	Divergence for Circular Disc - h=1.0000".....	96
5.6	9 x 33 Circular Mesh with 320 Element.....	98
5.7	TRINC 320 STAGSC-1 Element.....	99
5.7a	10 x33 Circular Mesh with 420 Element.....	100
5.8	Plane Strain Finite Element Model.....	102
5.9	Plane Strain Model at Crack Tip.....	102
5.10	Sublamine Snapping vs Analytic Predictions.....	110
A.1	Load vs Thickness for all Panels Tested.....	121
B.1	Typical STAGSC-1 Batch Job.....	124
B.2	STAGSC-1 Input Deck for 12" Panel.....	125
B.3	STAGSC-1 Input Deck for Circular Disc.....	127
B.4	STAGSC-1 Input Deck for 360° Disc Using the TRINC 320 Element.....	128
B.5	STAGSC-1 Model with Multiple Load Systems.....	129
B.6	Sample SQ5 Input Deck.....	131

LIST OF TABLES

Table	Page
3.1 Bagging Sequence.....	37
3.2 Autoclave Curing Cycle.....	39
3.3 Experimental Equipment List.....	47
4.1 Panel Identification.....	57
5.1 Overview of Analytic Technique.....	87
5.2 Convergence Study for STAGSC-1 Disc.....	97
5.2a Compilation of STAGSC-1 Results.....	97
5.3 Experimental Sublamine Snapping Loads.....	111
A.1 Experimental Test Results for Panels.....	120
A.2 Panel Lab Sheet - Voids, Density & Thickness...	122

ABSTRACT

As more and more composite materials are used in modern aircraft construction, the understanding of the damage tolerance of this relatively stiff, brittle, anisotropic material becomes important to designers. These composites may suffer surface damage due to abrasions and burns, material damages such as excess voids due to careless manufacturing techniques, or unseen damage in the forms of delaminations due to a low speed impact. These damages all cause eccentricities which result in lower panel buckling values when the panel is compressively loaded.

This thesis investigated the behavior of a cylindrical composite panel made of AS4/3501-6 graphite/epoxy with ply orientations $[0/-45/45/90]_S$. Abrasion and burn surface damage was physically modeled in the panels by removing a portion of the exterior plies. The panels were then tested by compressively loading them and a comparison was made to buckling predictions obtained using a STAGSC-1 shell program. These tests indicated that panels which have suffered minor surface damage do not deviate significantly from buckling predictions obtained using a STAGSC-1 linear bifurcation model.

Panels were also tested which had varying thicknesses and variations in void content due to faulty manufacturing techniques. These panels were also compressively loaded, and it was found that high void content increased panel thickness, which resulted in higher compressive strengths.

Composite laminates subjected to a low speed impact, such as a dropped tool or a manufacturing load, often develop an internal delamination. This delamination may result in the reduction of the panel's strength when subjected to compressive load.

Since curved panels are 3-dimensional, and buckling is a non-linear phenomenon, the compressive load which will cause curved panels to become unstable is extremely hard to predict analytically. This thesis presents a technique whereby the local buckling loads at the delamination may be predicted using a 2-dimensional model with a plane strain correction. This model yielded predictions of local instability within 30 percent of experimental values.

A STUDY OF DAMAGE TOLERANCE IN CURVED COMPOSITE PANELS

I. Introduction

Composite materials are being used more and more frequently in the design and construction of modern aircraft. Composites are used for aircraft skins, for major structural components and for small component parts.

Composites have many advantages over the more homogeneous, isotropic metals such as aluminum and titanium that have been used in classical aircraft construction. Modern designers can choose from a wide variety of composite fibers and matrix resins to tailor their strength and stiffness to a given application. Composites can be chosen which have higher strength at high temperatures than metals, or which are more dimensionally stable over a wider temperature range than metals. Composites have a much higher specific stiffness and specific strength than metals, with stiffness ranging from 2×10^6 psi to 18×10^6 psi and strengths ranging from 10 ksi to over 200 ksi. Fatigue limits are far in excess of those in aluminum, with a much greater vibrational damping.

The ability to achieve great strength at reduced weight has had a significant impact on spacecraft and aircraft design. Composites are currently being used in aircraft such as the Grumman X-29 Advanced Technology

Fighter, the General Dynamics F-16 Falcon and the McDonnell Douglas F-15 Eagle. They are also being used in the Space program where weight savings and dimensional stability over a wide temperature range are critical. Currently, the world's largest composite structures are the carbon-fiber reinforced motor casings for the space shuttle's solid fuel rockets. Composites are also used in space frames such as the shuttle's retractable boom, and in the trusses used to stabilize the spot beam reflectors for the Intelesat V communications satellite. [5]

Graphite epoxy laminates are perhaps the most versatile and prevalent of composite materials. They have been in wide use for a number of years and are readily available. In the early 1970's, the increased use of graphite epoxy in commercial products such as fishing rods, skis, and tennis racquet has resulted in a continuing drop in the cost of graphite/epoxy. Not only are they becoming less expensive, but they can give strength comparable to aluminum at weight savings of 15 to 30 percent. With the use of computer controlled and advanced robotics, automated filament windings are possible. As a result, parts can be consolidated, and the post fabrication machining often used for metal parts can be reduced. Up to 50% reductions in fabrication costs are the end result.

However, there are also potential disadvantages to the use of composites. The design of composite structures is

much more complicated, and less intuitive than design with isotropic materials. Careful consideration must be given to the rotational effects caused by variations in temperature and ply lay-up in a composite. A composite panel can peel due to air friction in a high performance aircraft, and damage to composite structures is frequently more complicated and time consuming to repair than damage to metal structures. Damage to a composite caused by a low velocity impact such as a dropped tool, manufacturing loads or strikes from runway debris is not easily detected and can cause serious reductions in the strength of the structure resulting in the collapse of the structure at loads which are much smaller than the design load.

BACKGROUND

The problem of shell collapse has been discussed in the literature for many years, and analytic techniques have been developed to predict the buckling load for simple isotropic materials with simple geometries. Stability equations for cylindrical shells were first developed in the late 1800's. In 1911, a closed form solution for the collapse of a cylindrical shell was presented by Lorenz. In 1932, Flugge presented a comprehensive treatment of cylindrical shell stability for shells subjected to compression and bending loads [2]. Flugge tested a series

of shells and found that his experimental values were approximately 50 percent of his closed form predictions. In 1933, Donnell presented a study which treated the class of shells known as quasi-shallow shells. These shells were relatively flat as are most structural shells, and because of the simplicity of his solution, Donnell's equations became widely used. Donnell's experimental values for thin cylindrical aluminum shells, however, were even farther from his predictions than Flugge's had been [2]. Finally, von Karman and Tsien performed an analysis in 1941 on the post buckling paths of compressed cylindrical shells. Their work showed that the secondary path dropped sharply downward from the bifurcation point. As a result, slight imperfections in a shell induced rotational effects which caused the actual equilibrium path to fall at a lower load level than the theoretical linear path. Hence, for shells with a slight imperfection, the actual collapse values could be quite small compared to predictions.

As composite panels came on the scene, the problem of shell instability was compounded. A composite panel which contained a delamination often had a thin section of delaminated plies attached to a thicker base laminate. As a result, the delaminated plies were more flexible than the base laminate, and were often the first portion of the laminate to experience instability.

Early work with delaminations in composite materials was done by attaching a thin composite layer to a thick isotropic base material such as aluminum. This technique allowed the introduction of pure compression loads without having to worry about rotational effects in the base material. In 1981, Whitcomb [17] used this technique to study a rectangular delamination in a graphite/epoxy panel. He used a thin teflon film to prevent bonding of the delaminated region to the base material. Using this technique, he was able to study Mode I and Mode II strain energy release rates and their effects on interlaminar stresses at the delamination crack tip.

In 1984, Whitcomb [18] substituted the aluminum base material for a thick quasi-isotropic graphite/epoxy base laminate. Still, using a piece of teflon to form rectangular strip delaminations in a flat plate, Whitcomb found that buckling can cause high interlaminar stresses at the delamination crack tip and that buckling strain is an important phenomenon in assessing potential for strength loss due to a delamination. In this study, Whitcomb [18] analyzed the complicated non-linear buckling phenomenon using the superposition of several minor linear problems.

Actual delaminations caused by an impact were found to be elliptical in shape, however. These elliptical delaminations in flat plates were studied by Shivakumar and Whitcomb in 1984 [13]. This study also used flat quasi-isotropic plates, and developed a simple Rayleigh Ritz

solution based on the Trefftz criterion to predict local buckling of delaminated plies (referred to as the sublaminates) from a quasi-isotropic base laminate. They found that there were no interlaminar stresses in the region of the delamination until the onset of buckling and that the size of the delamination was an important parameter in the stress intensity at the delamination. However, this technique gave inaccurate results for highly anisotropic sublaminates, and the technique wasn't extended to curved shells. This study attempts to address the problem of the buckling of an anisotropic (0/-45) sublaminate in a curved composite shell.

All of the studies involving composite materials that were mentioned above had involved a flat plate geometry. Since most real structural shells are not flat, generalizations made from these studies sometimes couldn't be applied to a curved surface. In the early 1970's, a researcher at General Dynamics named Wilkens began using a fixture to test curved laminate panels [20]. About this time, Dr. Anthony Palazotto initiated research at AFIT into the behavior of curved laminate panels. In 1977, Nelson studied the buckling behavior of curved, stiffened panels with cutouts. In 1979, Becker compared experimental buckling loads in composite panels to analytic predictions. Later, Bauld investigated the effects of the aspect ratio of the panels on buckling loads. In 1984,

another AFIT student, Siefert investigated the effects of centrally located delaminations on composite panel strength [12]. Horban [7] continued this research in 1985 by using a non-linear STAGS finite element code to study multiple delaminations in curved panels.

Composite panels present other unique problems to the designer. Laminates tend to develop large interlaminar stresses which depend to a large extent on the orientations of the laminate's fibers and the locations of singularities such as holes or boundaries. Due to the expense and complexity of computer models required to model a delamination in a composite panel, most of the work involving discontinuities in a composite panel have been done analytically. However, analytic results have only been developed for a narrow range of geometries which neglect any defects in the material such as surface imperfections or internal delaminations. This study attempts to address this problem by developing a technique whereby the effects of a delamination in a curved composite panel can be modeled using relatively inexpensive linear shell models with a plane strain correction.

PURPOSE

The purpose of this thesis was to experimentally study the tolerance of a curved composite panel to damage. Damages investigated included surface damage due to abrasion or burning, higher than normal void contents due to faulty manufacturing, and delamination damage due to low speed impact. This study also attempted to develop an inexpensive two dimensional model using the superposition of linear buckling finite element codes to predict the non-linear three dimensional phenomenon of sublaminar buckling in a thin curved panel. This investigation involved both analytical work and experimental work to verify the predicted local buckling values.

Internal delaminations in a composite panel can develop as a result of a low velocity impact caused by a dropped tool, a projectile, or as a result of manufacturing loads. These delaminations weaken the panel and reduce the load at which panel "global" buckling will occur. Another phenomenon that has been noted [7] is the snapping effect of the delaminated plies as they reach their local buckling load. This snap out may occur at a load which is much less than the global buckling load of the panel. Since curved composite panels are 3-dimensional and buckling is a non-linear problem, the compressive load which will cause the panel to become unstable is extremely hard to predict

analytically. Another purpose of this study is to develop a method which will use a 2-dimensional linear finite element model and a plane strain correction to accurately predict this initial instability.

SCOPE

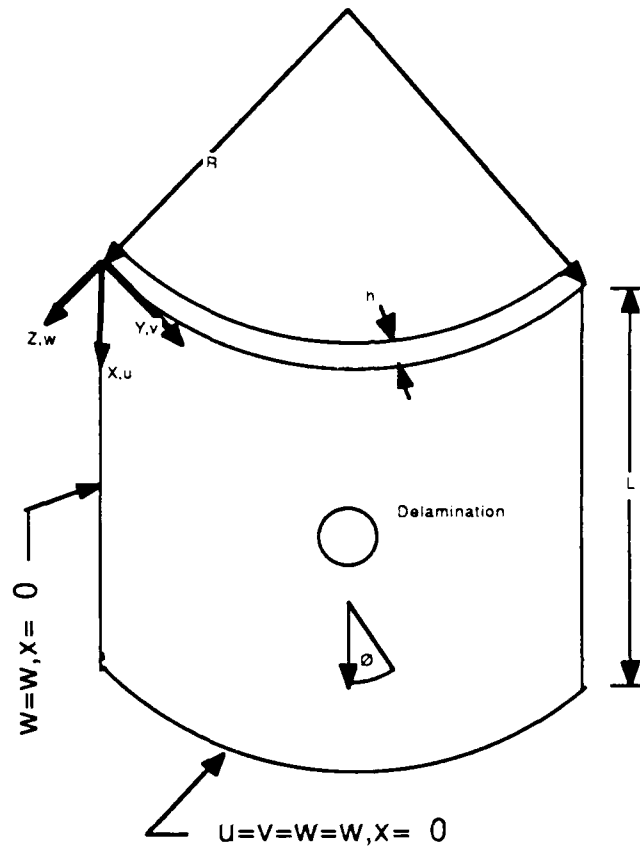
The panels used in this study were quasi-isotropic cylindrical composite panels made of AS4/3501-6 graphite/epoxy with ply orientations of $(0/-45/+45/90)_s$. Their height was 12 inches and they had a radius of curvature of 12 inches. (fig 1.1) The actual experimental panels, however, were trimmed slightly oversize to allow for mounting in a test fixture.

Previous work done by Horban and Palazotto [7] has shown that a teflon film placed between plies during panel layup will cause a total internal delamination in the panel. Therefore, 0.5 mil teflon discs were placed at the geometric centers of the panels between plies 2-3 on the panels' concave side, and between plies 6-7 on the convex side (fig 1.2). Panels were manufactured with a four inch and two inch diameter delamination and with no delaminations.

Panels were also manufactured with a teflon disc placed between plies 1-2 and between plies 7-8. The delaminations caused by placing inserts adjacent to the

exterior ply resulted in delaminations that were externally visible. The delamination appeared to be a circular blister approximately the size of the insert, with fractures in the matrix running parallel to the fiber orientation of the blistered ply. Since the blistered portion of the external ply could take no compressive load, it was removed and the panel was used to model a panel which has suffered external damage resulting from abrasion, chafing, or burning. These panels were then experimentally tested to determine the effect of this damage on panel strength.

The boundary conditions (see fig 1.1) used in the experimental fixture were: simply supported sides ($u=v=w_y=\text{free}$ $w=w_x=0$), a clamped bottom edge ($u=v=w=w_x=0$), and a clamped top edge ($u=\text{free}$ $v=w=w_x=0$). A constant displacement load was introduced at the top edge of the panel.



- X, Y, Z Surface Coordinates
- u, v, w Displacements
- h Panel Thickness
- R Panel Radius
- L Panel Height
- ϕ Ply Orientation

Figure 1.1 - Panel Geometry

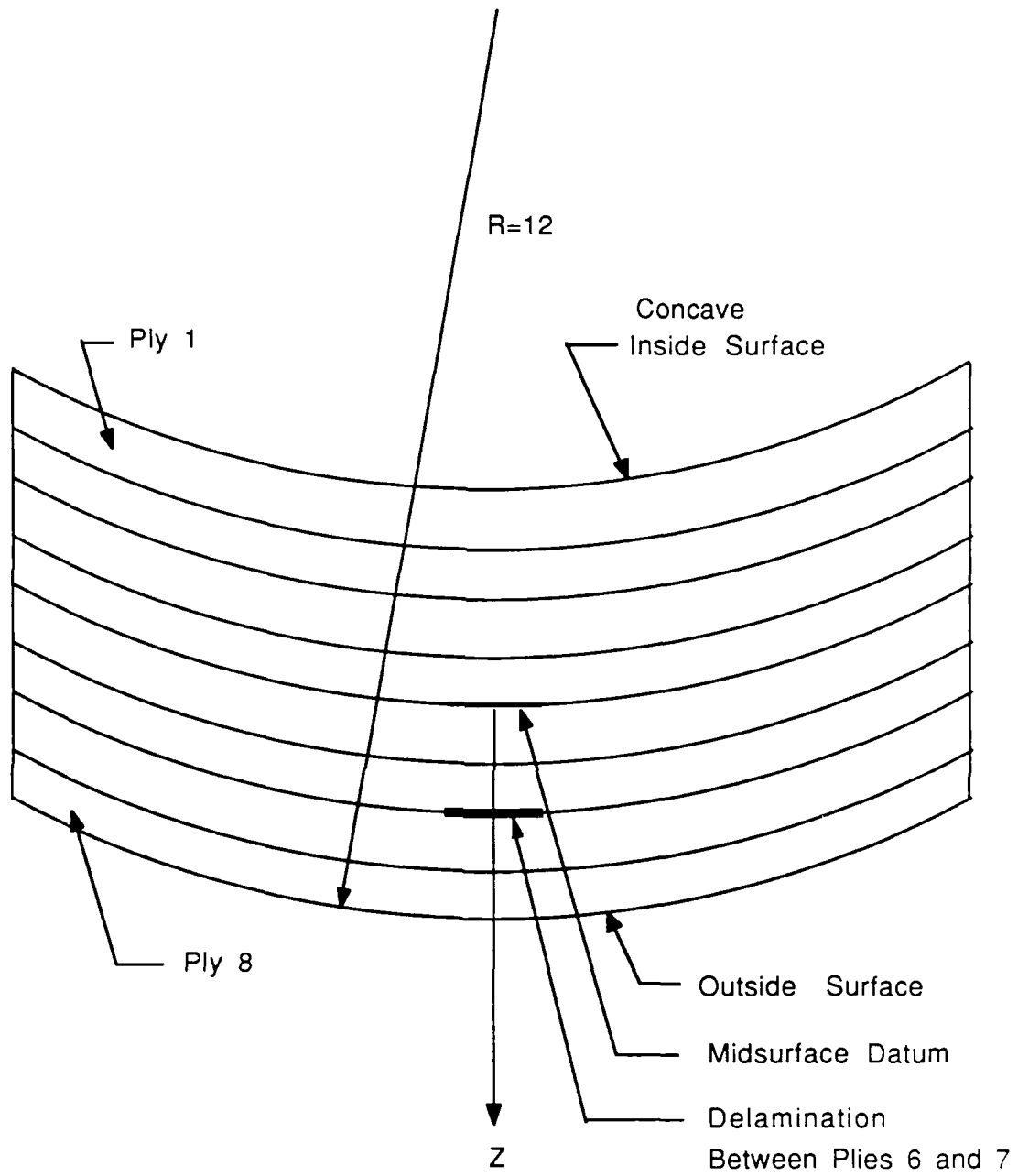


Figure 1.2 - Cross Section of Panel

II. THEORY

Classical Laminated Plate Theory

An overview of classical laminate plate theory is presented here for readers not familiar with the behavior of composite materials and the associated notation. Interested readers may read Jone's text [8] for a more in-depth treatment of this material. This section is a condensation of Jone's text, Section II of the SQ5 user manual [11] and some work presented in previous theses [6,7,12].

Co-ordinates in an orthotropic layer of a laminate are defined with respect to the material's fiber orientation. The 1-direction is defined as the direction parallel to the fiber, and the 2-direction is the direction normal to the fibers in the plane of the laminate layer (see fig 2.1).

To form the constitutive relations in terms of the 1-2 directions, the four independent material properties ($E_1, E_2, G_{12}, \nu_{12}$) are used:

$$\begin{bmatrix} \sigma_1 \\ \sigma_2 \\ \tau_{12} \end{bmatrix} = \begin{bmatrix} Q_{11} & Q_{12} & 0 \\ Q_{12} & Q_{22} & 0 \\ 0 & 0 & Q_{66} \end{bmatrix} \begin{bmatrix} \epsilon_1 \\ \epsilon_2 \\ \gamma_{12} \end{bmatrix} \quad (2.1)$$

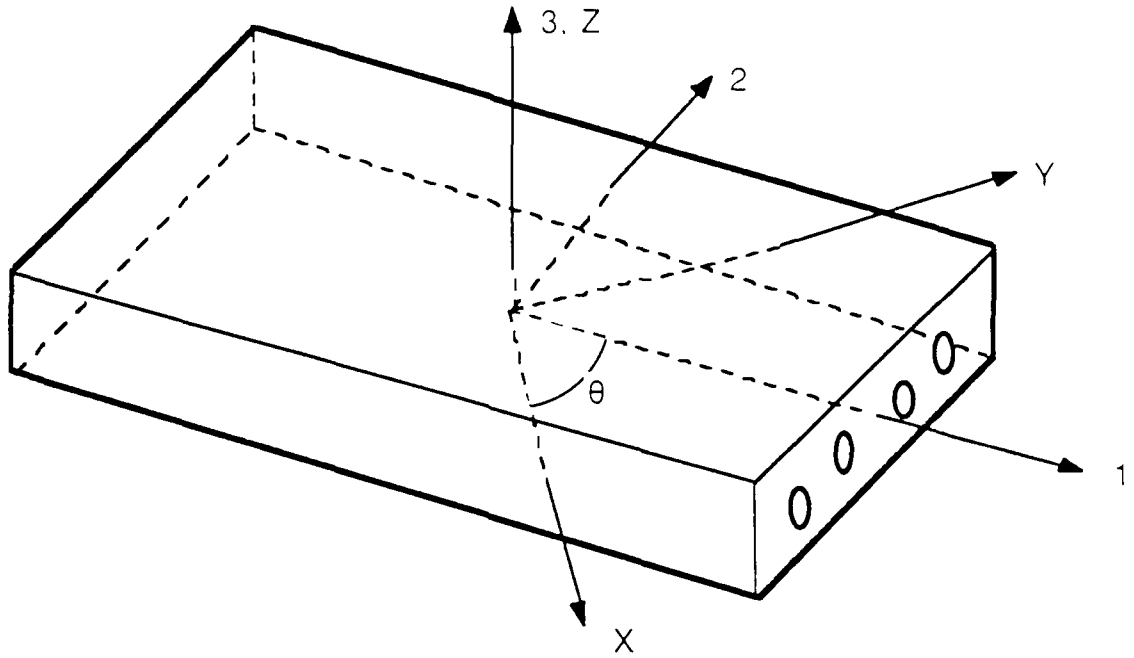


Figure 2.1 - Laminate C0-Ordinate Axes

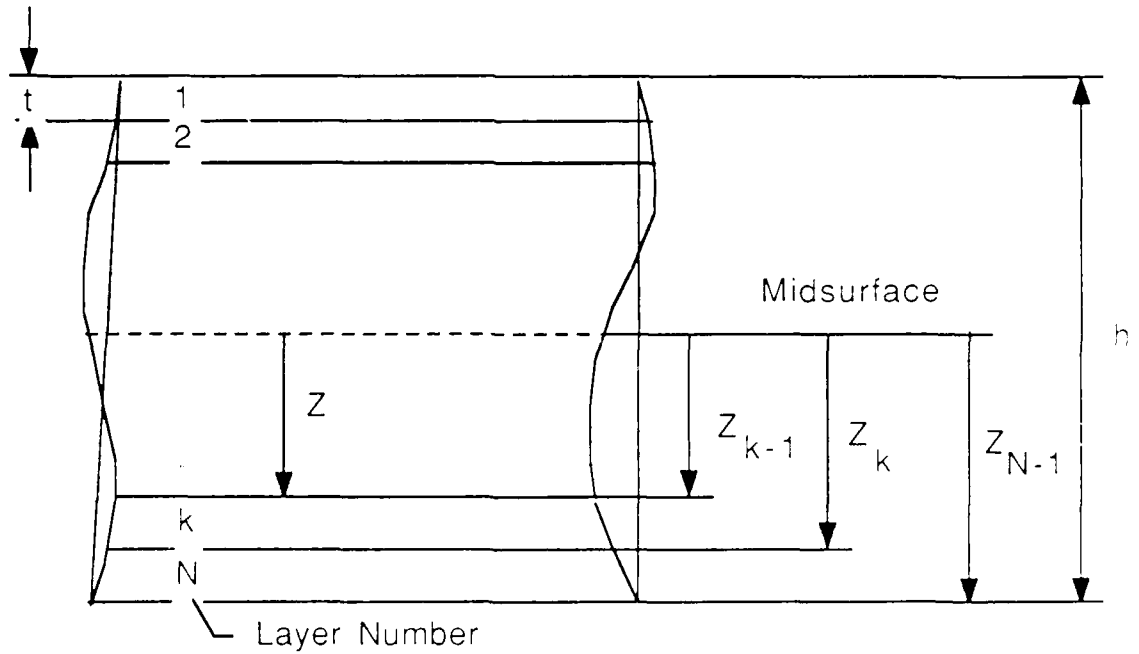


Figure 2.2 - Geometry of N Layered Laminate

The Q_{ij} reduced stiffness terms are given by:

$$\begin{aligned}
 Q_{11} &= E_{11} / (1 - \nu_{12}\nu_{21}) \\
 Q_{22} &= E_{22} / (1 - \nu_{12}\nu_{21}) \\
 Q_{12} &= \nu_{21}E_{11} / (1 - \nu_{12}\nu_{21}) = \nu_{12}E_{22} / (1 - \nu_{12}\nu_{21}) \\
 Q_{66} &= G_{12}
 \end{aligned}
 \tag{2.2}$$

When the designer is interested in stresses in directions other than the 1-2 directions, then the Q_{ij} matrix is transformed by the angle θ between the 1 axis and the new x axis of interest (see fig 2.1). When this transformation is performed for each Q_{ij} term, the following relation results:

$$\begin{bmatrix} \sigma_x \\ \sigma_y \\ \tau_{xy} \end{bmatrix} = \begin{bmatrix} \bar{Q}_{11} & \bar{Q}_{12} & \bar{Q}_{16} \\ \bar{Q}_{12} & \bar{Q}_{22} & \bar{Q}_{26} \\ \bar{Q}_{16} & \bar{Q}_{26} & \bar{Q}_{66} \end{bmatrix} \begin{bmatrix} \epsilon_x \\ \epsilon_y \\ \gamma_{xy} \end{bmatrix}
 \tag{2.3}$$

Where the \bar{Q} are the stiffness terms transformed by the rotation θ of the 1-2 axes into the x-y axes.

The displacements at any point in the laminate cross section are defined in terms of the strains at the midsurface of the laminate ($\epsilon_x^0, \epsilon_y^0, \gamma_{xy}^0$) and the plate curvatures (k_x, k_y, k_{xy}):

$$\begin{bmatrix} \epsilon_x \\ \epsilon_y \\ \epsilon_{xy} \end{bmatrix} = \begin{bmatrix} \epsilon_x^0 \\ \epsilon_y^0 \\ \epsilon_{xy}^0 \end{bmatrix} + z \begin{bmatrix} k_x \\ k_y \\ k_{xy} \end{bmatrix}
 \tag{2.4}$$

For the relation given in (2.4), a couple of assumptions must be made. First, the laminae are assumed to be very thin with displacements continuous across the laminae thickness. Second, the Kirchhoff-Love assumption applies. This assumption says that normals to the mid-surface remain plane and normal to the mid-surface after bending. For relatively thin laminates with small rotations relative to the neutral axis, this is not a bad assumption. For a cylindrical shell, the strains and curvatures expressed in equation (2.4) above are defined as follows, with strains at the midsurface given by:

$$\begin{aligned}
 \epsilon_x^{\circ} &= u_{,x} + \frac{1}{2} \left[\theta_x^2 + \theta^2 \right] \\
 \epsilon_y^{\circ} &= v_{,x} + \frac{1}{2} \left[\theta_y^2 + \theta^2 \right] + \frac{w}{R} \\
 \gamma_{xy}^{\circ} &= v_{,x} + u_{,y} + \theta_x \theta_y
 \end{aligned}
 \tag{2.5}$$

and curvatures given by:

$$\begin{aligned}
 k_x &= \theta_{x,x} \\
 k_y &= \theta_{y,y} \\
 k_{xy} &= \frac{1}{2} \left[\theta_{y,x} + \theta_{x,y} + \frac{\theta}{R} \right]
 \end{aligned}
 \tag{2.6}$$

In equations (2.5) and (2.6) above, R is the panel's radius of curvature; u,v,w are the axial, circumferential, and radial displacements of the shells mid-surface; and the

θ 's are rotational components which are expressed in terms of displacement as follows:

$$\begin{aligned}\theta_x &= -w_{,x} \\ \theta_y &= -w_{,y} + \frac{v}{R} \\ \theta &= \frac{1}{2} [v_{,x} - u_{,y}]\end{aligned}\quad (2.7)$$

Now that the stresses have been computed for each individual ply using equation (2.3), the force resultants (N_x, N_y, N_{xy}), and the moment resultants (M_x, M_y, M_{xy}) can be computed by integrating the laminae stresses over the laminate thickness in the z direction.

$$\begin{Bmatrix} N_x \\ N_y \\ N_{xy} \end{Bmatrix} = \int_{-t/2}^{t/2} \begin{Bmatrix} \sigma_x \\ \sigma_y \\ \tau_{xy} \end{Bmatrix} dz \quad (2.8)$$

$$\begin{Bmatrix} M_x \\ M_y \\ M_{xy} \end{Bmatrix} = \int_{-t/2}^{t/2} \begin{Bmatrix} \sigma_x \\ \sigma_y \\ \tau_{xy} \end{Bmatrix} z dz \quad (2.9)$$

Now we substitute equation (2.3) into (2.8) and (2.9).

In matrix notation, we get the following equations:

$$[N] = \sum_{k=1}^n \left\{ \int_{h_{k-1}}^{h_k} [\bar{Q}]_k \{\epsilon^0\} dz + \int_{h_{k-1}}^{h_k} [\bar{Q}]_k \{k\} z dz \right\} \quad (2.10)$$

$$[M] = \sum_{k=1}^n \left\{ \int_{h_{k-1}}^{h_k} [\bar{Q}]_k \{\epsilon^0\} z dz + \int_{h_{k-1}}^{h_k} [\bar{Q}]_k \{k\} z^2 dz \right\} \quad (2.11)$$

Defining the quantities:

$$A_{ij} = \sum (\bar{Q}_{ij})_k (h_k - h_{k-1}) \quad (2.12)$$

$$B_{ij} = \sum (\bar{Q}_{ij})_k (h_k^2 - h_{k-1}^2) \quad (2.13)$$

$$D_{ij} = \sum (\bar{Q}_{ij})_k (h_k^3 - h_{k-1}^3) \quad (2.14)$$

We can now write equations (2.10) and (2.11) in terms of the extensional stiffness matrix [A], the coupling stiffness matrix [B], and the bending stiffness matrix [D], where [A], [B] and [D] are each a 3x3 matrix whose values are given in appendix A. Now we can write an expression for N and M in matrix notation:

$$\begin{bmatrix} N_x \\ N_y \\ N_{xy} \\ M_x \\ M_y \\ M_{xy} \end{bmatrix} = \begin{bmatrix} [A] & [B] \\ [B] & [D] \end{bmatrix} \begin{bmatrix} \epsilon_x^0 \\ \epsilon_y^0 \\ \gamma_{xy} \\ k_x \\ k_y \\ k_{xy} \end{bmatrix} \quad (2.15)$$

Equation (2.15) is the total constitutive relation for a laminated plate. The coupling of inplane extension and bending is seen to be a result of the [B] matrix. For a laminate that is symmetric about the midplane, the $[B_{ij}]$ terms are zero, and there is no coupling of extension with bending.

Bifurcation

In linear mechanics, displacements are assumed to be proportional to loads. This approximation is often made for the initial portion of the stress strain curve that is nearly linear. As a compressive load is increased in a structure, deflections from the center line increase, local slopes increase, and rotations increase. As a result of these rotations, the load deflection curve responds in a non-linear manner. However, for the initial portion of the load vs deflection curve, these rotations are assumed to be so small that non-linear interactions between rotations and loads may be neglected.

The resulting load versus deflection curve is known as the equilibrium path since the structure is in static equilibrium for a given deflection and load along the curve. As the load increases even further, an instability point on the equilibrium path will eventually be reached. At this point, there is more than one equilibrium path that the structure may follow (fig 2.3). The continuation of the straight line portion of the curve is the unstable path. The secondary path at lower values of load is the stable path and is the asymptote which the actual curve will approach. The intersection of the equilibrium paths is known as the bifurcation point, and the load associated with this point is called the critical load. The bifurcation point is the theoretical value that the load on

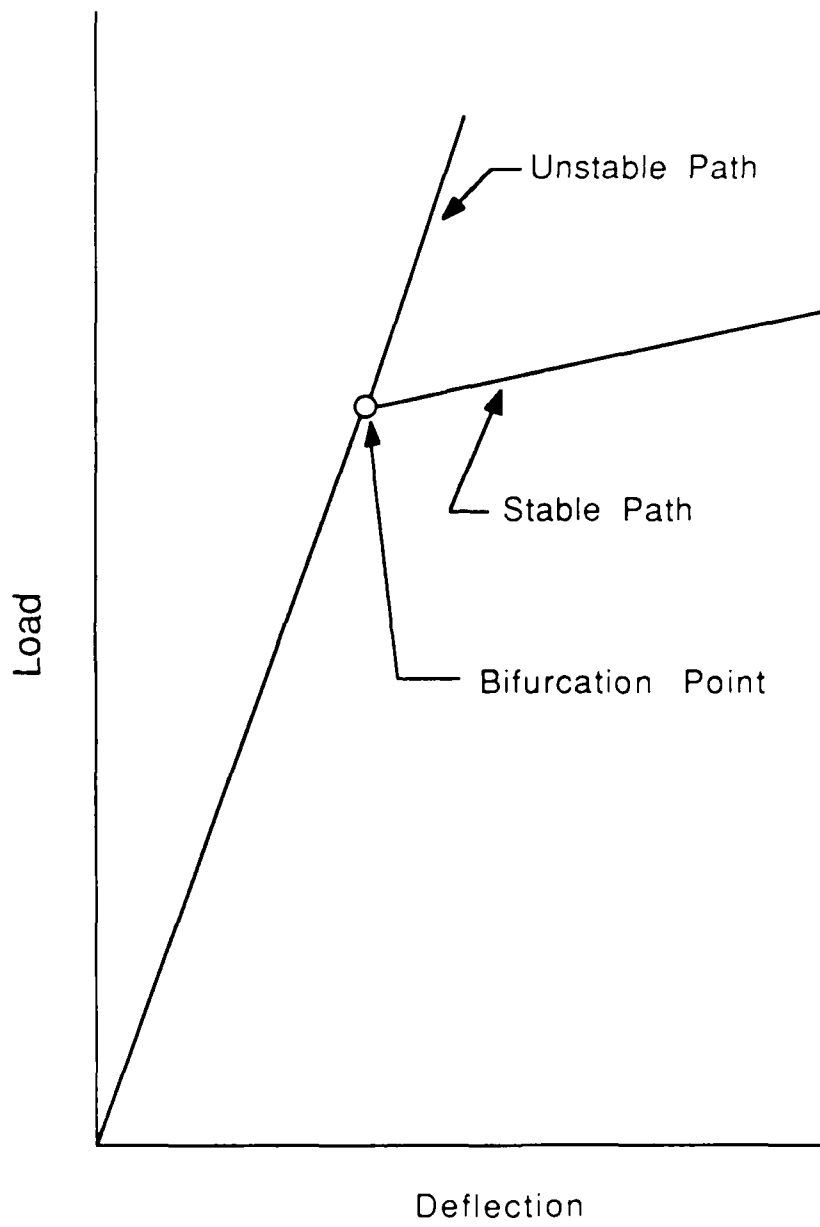


Figure 2.3 - Equilibrium Path

a structure will reach when second order rotational effects are neglected and is the point at which the structure will become unstable and buckle.

Figure 2.4 represents the equilibrium path for a perfect circular cylindrical shell. No structure is perfect, however, and for the case of cylindrical shells, very slight shell imperfections result in large reductions of the buckling load. Experimental collapse loads for axially compressed cylindrical shells may even be as low as 20% of the theoretical values [1].

The reason for this large difference in theoretical vs actual load can be seen by observing figure 2.4. For circular cylindrical shells, the secondary equilibrium path drops sharply downward from the bifurcation point. Since the equilibrium path is the path for a perfect structure, a slight imperfection in the shell will induce eccentricities which increase the second order rotational effects and result in the actual curve falling somewhat below the ideal curve. Therefore, the critical load will occur at a smaller value, and no post buckling increase in load can result. The reduction in the actual strength of a shell from the critical load at bifurcation is known as knockdown and is essentially the percent difference between predicted values and experimental values. Horban [7] and Siefert [12] used this knockdown factor in their work with cylindrical composite panels to compare experimental results with the higher STAGSC-1 bifurcation predictions.

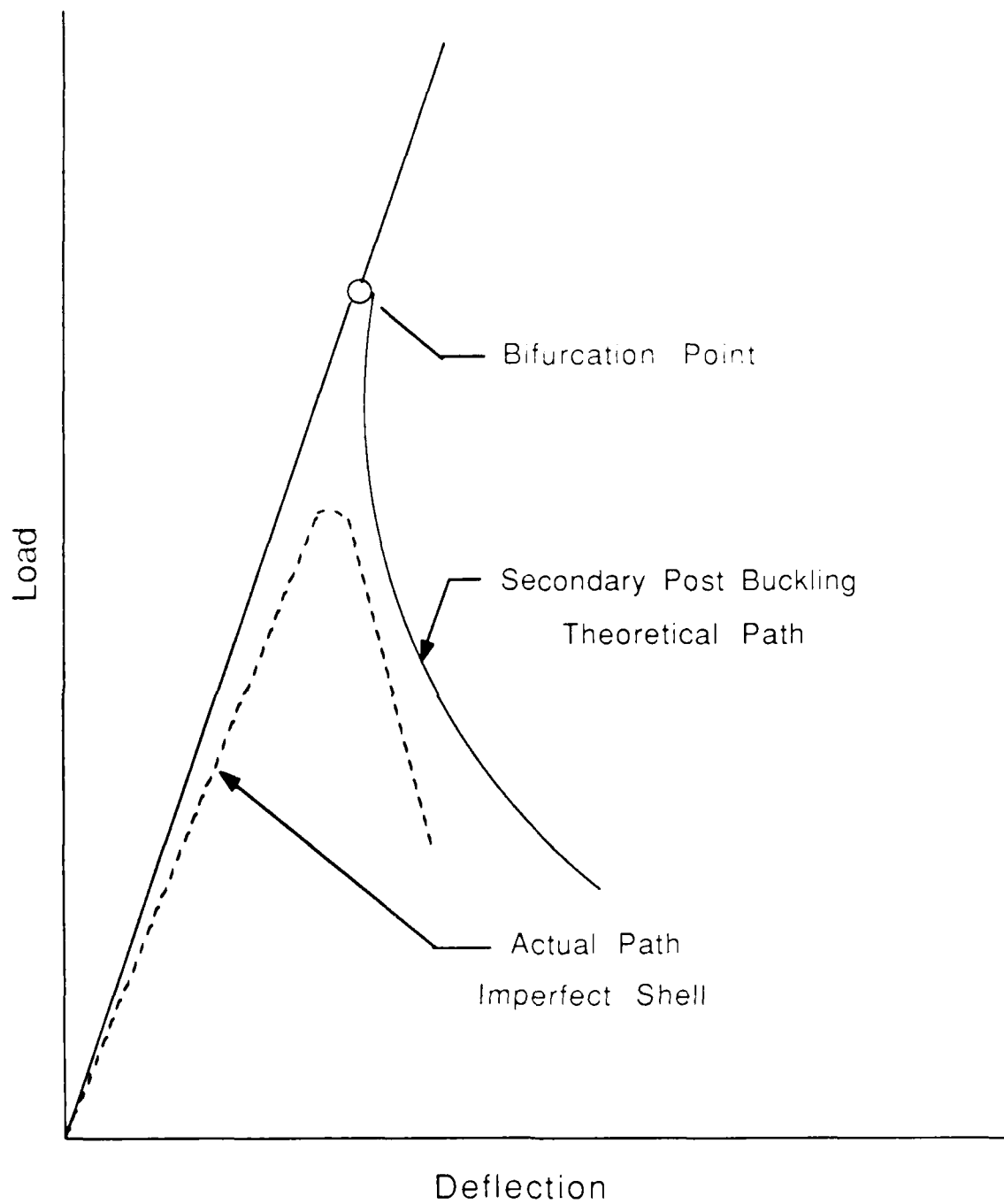


Figure 2.4 - Equilibrium Path for Cylindrical Shell

STAGSC-1 Theory

STAGSC-1 (Structural Analysis of General Shells) is an energy based finite element program for thin shells. STAGSC-1 began its development in 1967 under government contract to Lockheed Palo Alto Research Laboratory, and its development has continued for the past twenty years under various contracts through NASA Langley Research Center. The first version, known as STAGS, was a finite difference program for the non-linear analysis of thin shells with outputs. A linear version for shells of revolution was developed in 1968, and buckling and thermal capabilities were added in 1970. The code evolved further in 1970 with the addition of more elements to its library and an inelastic capability. In 1973, a version called STAGSA had evolved which included transient response, dynamic eigenvalue analysis, and dynamic buckling response routines. STAGSC-1 was released in 1979. The new code was entirely transformed to a finite element based program, and was particularly useful for bifurcation analysis and dynamic analysis of thin shells [14].

The latest version of STAGSC-1 was released in 1986 and addresses the full collapse of a structure. Also, previous versions of STAGS were limited to problems in the small rotation class (less than 10 degrees). The present version addresses this problem using an element-independent

co-rotational formulation for all static non-linear collapse problems, and it can now be used for structures with large rotations (greater than 10 degrees) at small strains. The 1986 version also uses the Riks algorithm for non-linear collapse evaluation typical of optimized shells made of the new lightweight materials [10]. The new Riks method is an efficient nonlinear solver which can extend STAGS solutions into the post buckled portion of the load versus deflection curve. The 1986 program is the version that is used for this research.

The STAGSC-1 computer program is made up of four main parts: STAGS1, STAGS2, POSTP, and STAPL. The STAGS1 portion is the part of the program which compiles the input deck, performs model generation, and begins performing preliminary calculations. The STAGS2 module does the bulk of the numerical calculations performed in a finite element analysis. STAGS2 performs such tasks as matrix decomposition, linear and non-linear stress analysis, eigenvalue analysis, thermal gradient determination, and the calculation of stress resultants, moments and deflections. POSTP is a post-processor for determining secondary solutions from previously calculated displacements which have been saved to TAPE22. The STAPL module is a plotting routine which can be used to plot the undeformed finite element mesh, the deformed mesh, and contour plots of the structure's deflections [19]. Readers

interested in running the STAPL module should refer to the STAGSC-1 user manual [1] and to Tisler [15], appendix B for sample input decks for restart and STAPL runs.

The 1986 version of STAGSC-1 that was used for this research has two routines which are both called STAGS2. Either routine can be loaded in the computer under the name STAGS2. The first routine performs a linear bifurcation analysis state, while the second performs its computations using a non-linear buckling routine. "It is suggested that users of STAGSC-1 utilize the non-linear module, as it will give more accurate results at approximately the same cost in computer time. True linear problems will converge very quickly using the non-linear version, so there is usually no real advantage in running a linear model." [10] If a user should encounter problems with a model that does not run, he should check the B1 card in the input deck to ensure that the analysis being performed is compatible with the STAGS2 module called on the system [19].

Another unique aspect of STAGSC-1 is its use of surface co-ordinates on the shell surface. This allows any point on the mesh to be defined in terms of two independent surface co-ordinates; or conversely, a user can use the system's global frame to define the grid points. Also, shell units consisting of various elements and material properties may be formed. These shell units can then be interconnected using the STAGS G1 card to form a continuous

compatible shell. This feature is useful when modeling stiffeners, beams, or shells whose geometries change along the surface.

The STAGSC-1 program calculates the bifurcation point using variational potential energy techniques. The static equilibrium path is calculated using minimum potential energy such that static equilibrium is achieved for a given input load or deflection (summation of external forces equal zero at equilibrium). Potential energy, V , is the internal strain energy, U , minus the work done by external forces, W ; where work is the product of external forces and their associated deformations.

$$V = U - W \quad (2.16)$$

$$U = 1/2 \int \{\epsilon\}^T [N] \{\epsilon\} dA \quad (2.17)$$

$$W = \sum \{x\}^T \{F\} \quad (2.18)$$

where: $\{\epsilon\}$ \equiv vector of strains and curvatures
 $[N]$ \equiv matrix of A_{ij} , B_{ij} , and D_{ij} terms
 $\{x\}$ \equiv vector of displacements
 $\{F\}$ \equiv vector of applied external forces

For static equilibrium, the potential energy, V , must be a minimum; therefore, the first variation of potential

energy, δV , must equal zero. At the bifurcation points for a conservative mechanical system, the second variation of potential energy, $\delta^2 V$ must be equal to zero. The $\delta^2 V$ terms represent the second order potential energy terms which result from a small virtual displacement to the structure. The critical load for a structure occurs when the structure first loses its stability. For stability in a structure, the second variation must be positive definite.

STAGSC-1 performs an eigenvalue solution to find the bifurcation point. Readers are referred to Brush and Almroth [2] for an in-depth development of potential energy formulations and bifurcation analysis, and to Rankin [10] for the 1986 updates to the STAGSC-1 computer code.

III. MANUFACTURING & EXPERIMENTAL TECHNIQUES

Introduction

Forty curved panels were fabricated and tested for this research. The panels were constructed of Hercules AS4/3501-6 Graphite/Epoxy 12 inch prepreg tape. All panels were laid up with a (0/-45/45/90)_s quasi-isotropic geometry. The panels were cylindrical shells having a radius of curvature of 12 inches measured to the outside convex surface of the panel. They had a trimmed height of 13 inches, and an arc length of 12.5 inches (fig 1.1). The material properties were assumed to be:

$$E_1 = 18.844 \times 10^6 \text{ psi}$$

$$E_2 = 1.468 \times 10^6 \text{ psi}$$

$$G_{12} = 0.91 \times 10^6 \text{ psi}$$

$$\nu_{12} = 0.28$$

$$\nu_{21} = 0.022$$

Four of the panels were built with no internal delaminations. These panels were to serve as control panels to check the accuracy of computer models, and to compare with previous work done by Horban [7] and Siefert [12]. Internal delaminations caused by low speed impacts were modeled by incorporating 0.5 mil teflon discs between plies

during lay up. Two inch diameter and four inch diameter delaminations were used.

Previous work [7,12] had shown that a complete delamination will occur in a panel if a teflon insert is placed in the panel during lay up. This work indicated that it was desirable to use a thin layer of material (0.5 mil mylar) to avoid matrix fracture when the delaminations are placed within one ply of the outer surface of the panel. Horban also found that mylar inserts only resulted in a partial delamination, while teflon discs resulted in a total delamination in the panel. Therefore, 0.5 mil teflon was chosen as the delamination causing insert for this research.

Initially, delaminations were caused by placing two discs of DuPont 300 A, 0.5 mil FEP teflon film back to back between plies during lay up. The discs were coated with RAM 225 release agent prior to being placed in the panel to ensure 100% debonding . Originally, delaminations were to be placed between plies 1-2, 2-3, 6-7 and 7-8 (fig 1.2). The inserts placed between plies 2-3, and 6-7 formed the desired delamination. However, problems were encountered when the teflon discs were placed only one ply in from the exterior surface (between plies 1-2 and 7-8). After the panels were removed from the autoclave, the delaminations were externally visible (fig 3.1). They appeared to be a low, circular blister approximately the size of the teflon

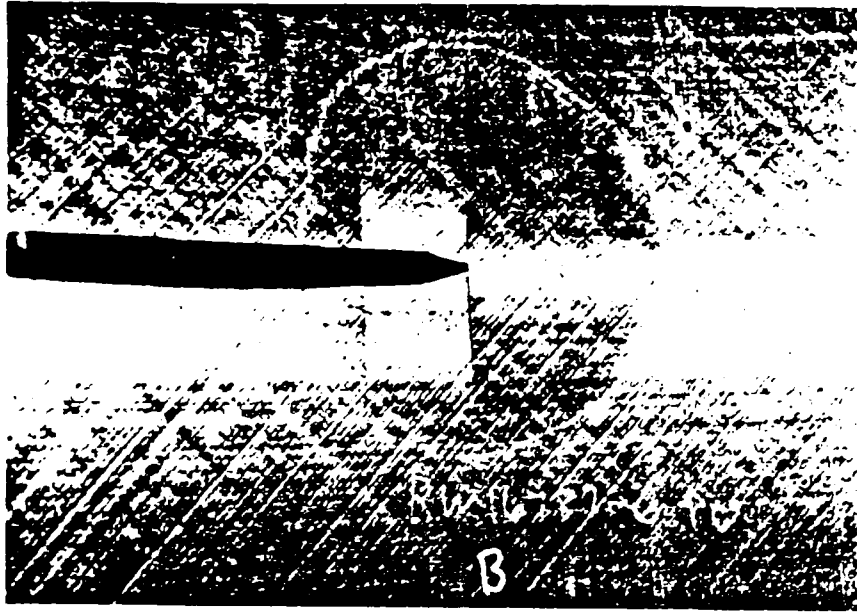


Figure 3.1 - Blistered Sublaminare due to Teflon Insert

insert, with fractures in the matrix running parallel to the 0° fiber orientation of the exterior blistered ply.

Horban [7] had previously noted this problem when he used one mil mylar inserts. He had then tried using 0.5 mil mylar inserts, and found that he observed no matrix cracking and no blistering effect. As a result of Horban's experience, it was thought that using one 0.5 mil teflon insert with RAM 225 release agent as opposed to the two inserts placed back to back would give acceptable results.

Four panels were manufactured in this manner. Two of the panels had two inch diameter inserts while the other two had four inch diameter inserts. All four panels exhibited the matrix cracking and blistering seen previously. At this point it was not known what was causing the blisters to form. Panels were constructed using one 0.5 mil teflon disc with no RAM 225 release agent applied. Blisters still occurred. It was then thought that perhaps volatiles in a gaseous state were being trapped beneath the teflon disc resulting in a vapor pressure as the panels were heated in the autoclave. Panels were then constructed using one 0.5 mil teflon disc that had been perforated with 20 small holes. Blisters still occurred. A finite element model was run to determine if residual curing stresses might be causing this blistering. No residual stresses were found in the model. Due to time constraints, and the number of panels allowed for this research, no further experimental investigation was attempted. However, it was decided to use

the panels with the blistered delamination to carry out further experimental work. Since the blistered portion of the external ply could take no load, the blistered portion was removed using a razor knife, and the panel was used to model a panel which has suffered external damage as a result of abrasion, chafing or burning. These panels were then experimentally tested to determine the effect of this damage on the panel's buckling strength.

Another type of damage studied in this thesis is panel damage due to manufacturing variabilities. Panels were tested that had laminate thicknesses ranging from 39.3 to 42.6, and which had void contents ranging from 0.10 percent to 4.4 percent. These variations could result from faulty manufacturing procedures or from mechanical difficulties such as a faulty vacuum during curing in the autoclave.

Panel Lay Up and Curing

The panels were laid up in curved steel molds with a 12 inch radius of curvature (fig 3.2) . The 12 inch prepreg was cut and placed as shown in the fabrication plan (figs 3.5-3.7). Panels that were to receive teflon inserts were carefully measured to the center of the intended delamination using a steel scale, and the teflon was placed using a RAM 225 release agent to ensure total delamination.



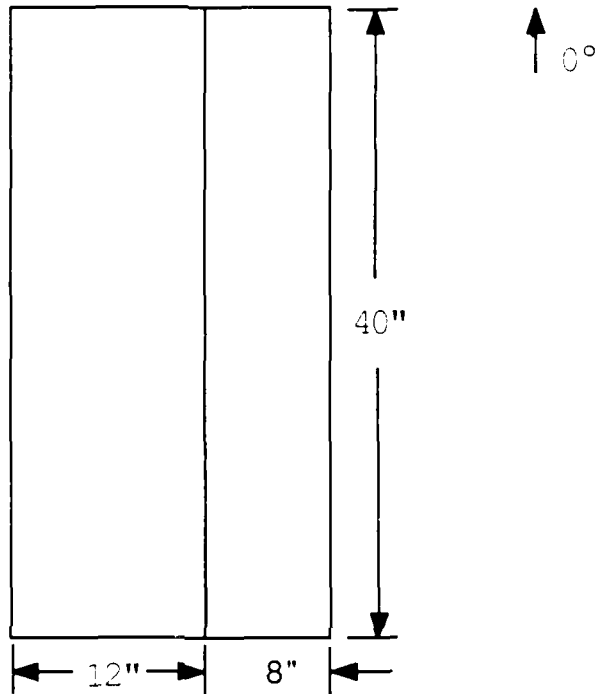
Figure 3.2 - Placing Bleeder in Steel Mold



Figure 3.3 - Positioning Teflon Inserts During Lay-up

AFIT Curved Panels
15.5" X 32" Panel - 12" wide mat'l

0° Plies:



For One Panel:

Cut 2 - 40" long X 12" wide pieces

Cut 2 - 40" long X 8" wide pieces

(Save the extra 4" wide X 40" long piece for the 90° plies)

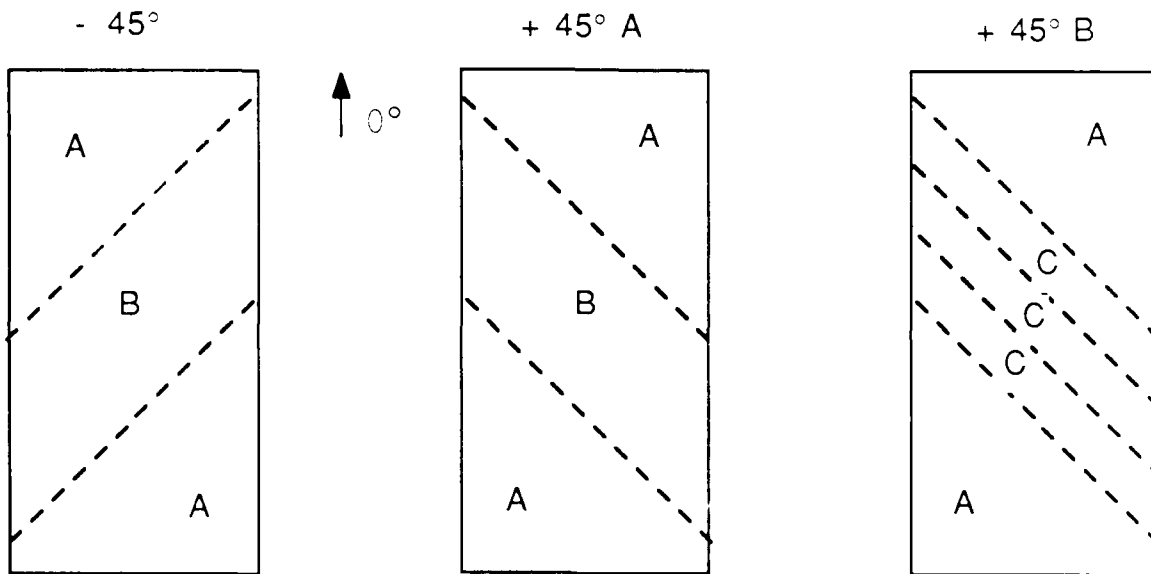
For All 17 Panels:

Cut 34 - 40" long X 12" wide pieces

Cut 34 - 40" long X 8" wide pieces (Save the 4" wide X 40" long pieces for the 90° plies)

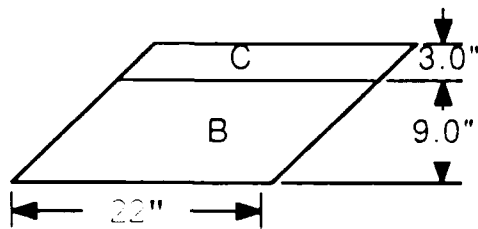
Figure 3.4 - Prepreg Cutting Plan for 0 Plies

AFIT Curved Panels
 15.5" X 32" Panel - 12" wide mat'l
 ±45° Plies:

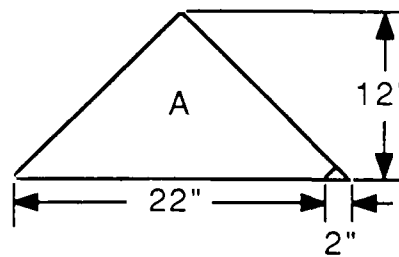


Cut Prepreg as Indicated Below

For One Panel:
 Cut and Trim 3 pieces:



Cut and Trim 8 pieces:



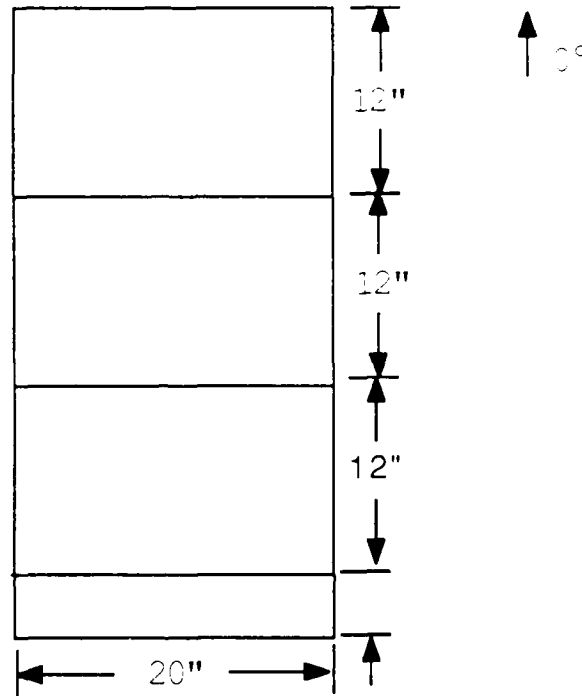
For All 17 Panels:

Cut and trim 51 pieces of B and C
 Cut and trim 136 pieces of A

Figure 3.5 - Preprep Cutting Plan for 45 Plies

AFIT Curved Panels
15.5" X 32" Panel - 12" wide mat'l

90° Plies:



For One Panel:

Cut 6 - 20" long X 12" wide pieces

Trim the 4" wide X 40" long piece into 2 - 4" wide X 20" long pieces

For All 17 Panels:

Cut 102 - 20" long X 12" wide pieces

Trim the 4" wide X 40" long pieces into 34 - 20" long X 4" wide pieces

Figure 3.6 - Prepreg Cutting Plan for 90 Plies

The bagging sequence listed in table 3.1 below and illustrated in figure 3.7 was identical for all of the laminates manufactured:

1. Vacuum bag
2. Vent blanket breather (Air Weave SS-FR)
3. Perforated mylar (seal to coroprene edge)
4. Mochburg bleeder
5. Perforated mylar (seal to coroprene dam)
6. TX 1040 porous teflon coated glass cloth
7. Eight ply laminate
8. TX 1040
9. Mylar
10. 12 inch radius of curvature steel mold

Table 3.1 - Bagging Sequence [3]

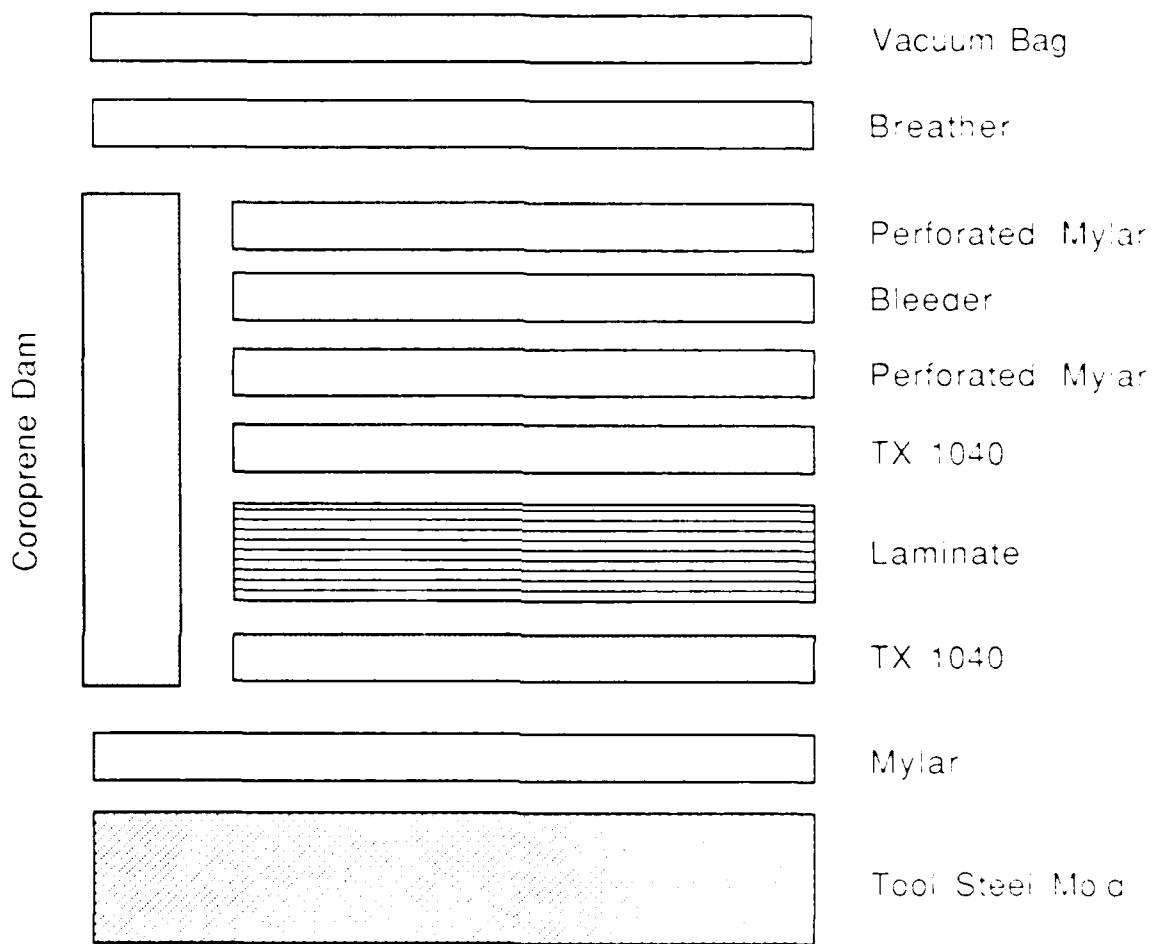


Figure 3.7 - Bagging Sequence [3]

The laminates were then cured in an autoclave according to cycle B-240-T, Rev A as shown in table 3.2 below:

1. Apply Vacuum, 25 in Hg and 85 psi minimum
2. Heat air to 240 F in 30 : 5 min
3. Hold part at 240 : 5 F for 60 min under 85 psi and full vacuum
4. Increase pressure to 100 psi and vent vacuum
5. Heat air to 350 F in 30 : 5
6. Hold part at 350 : 5 F and 100 psi for 120 minutes
7. Cool part below 150 F in no less than 120 min
8. When part is below 150 F, vent pressure

Table 3.2 - Autoclave curing cycle used [3]

After curing, the panels were removed from the bagging and visually inspected. At this time, it was noted that one mold produced a panel which had a glossier sheen than the other panels. A resin analysis showed that these panels had a higher than normal void content, with a range of 2.0 to 4.5 percent voids. Normally these panels would have been discarded, but it was decided to test them to determine the effects of this manufacturing defect on panel strength.

After subsequent autoclave runs, it was discovered that one of the autoclave's vacuum lines was partially blocked and was not producing a sufficient vacuum, thus resulting in the higher void contents in the affected panels.

After removal from the molds, the panels were C-scanned using a hand scanner to insure that no large voids or delaminations were present. During the C-scanning process, the inserted delaminations were marked so that the panels could be accurately trimmed. The panels were then checked at 13 locations to determine the average panel thickness and the average ply thickness. Thickness variation within individual panels was small (on the order of 0.2%); however, the average panel thickness variations from panel to panel amongst the group of panels tested was 6.8%.

For a given panel size and a material with constant properties, the only variability that will affect the critical buckling load is the panel thickness, h . Therefore, for panels with an aspect ratio of one, panel buckling strength should vary by the ratio [4]:

$$P_2 = P_1 (h_2/h_1)^n \quad (3.1)$$

For flat plates, n is equal to three; but for the curved panels used in this study, a value of $n=3$ gave collapse loads that diverged from STAGSC-1 predictions.

However, from equation (3.1), the buckling load for panels is seen to be sensitive to the thickness of the panel. This variation can cause scattering of the test data and experimental strengths that are other than the predicted values. Equation (3.1) was applied to Horban's STAGSC-1 buckling loads for curved panels, and an empirical regression relation was derived for panels with a 12 inch radius of curvature (see fig 3.8):

$$P_2 = P_1 (h_2/h_1)^{2.06} \quad (3.2)$$

This relation proved very useful in this thesis since a typical STAGSC-1 linear bifurcation analysis used from 120 to 150 cp seconds of computer time. Using equation (3.2), the largest calculated error was 0.86 percent. Therefore, a STAGSC-1 run was not necessary for every panel thickness in the test group, and the number of STAGS computer runs was substantially reduced.

Next, two test panels were cut from each mold panel using a curved steel fixture to hold the panel and a radial arm saw with a water lubricated, seven inch, diamond tipped blade. The panels were trimmed to a 13 inch height by a 12.5 inch arc length to allow for mounting in the test fixture. The unsupported dimension of the panel when in the fixture was 12 inches by 12 inches.

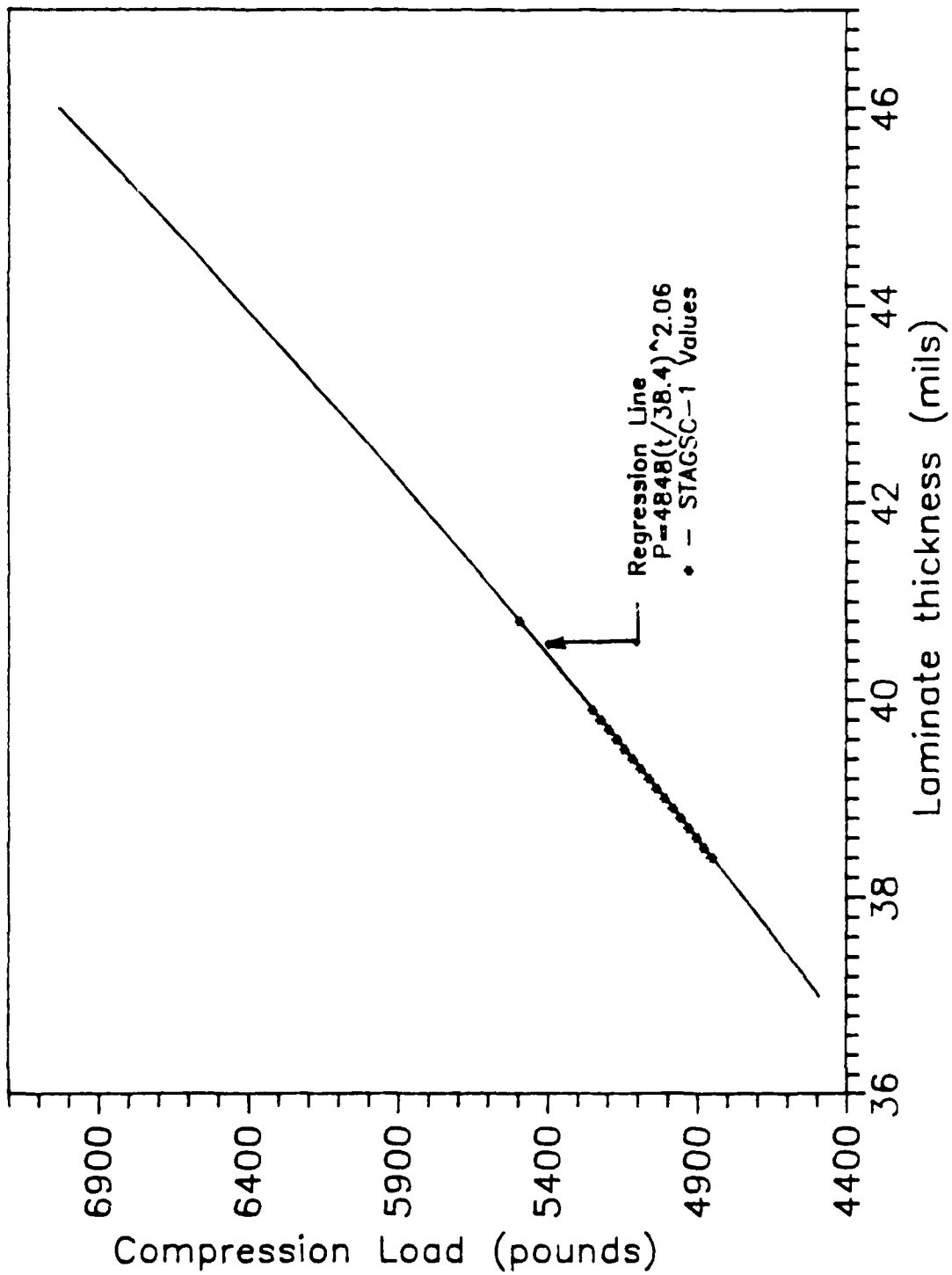


Figure 3.8 - STAGSC-1 Regression Curve for 12" Curved Panels

Strain gauges (M&M CEA-250-350UW-350) were placed on each panel to determine the uniformity of load introduction to the panel and to determine the load at which strain reversal occurred at the delamination (fig 3.9). Strain gauges 1 and 2 (SG1 and SG2) were placed on the concave and convex sides of the panel respectively. These gauges were at the center of the panels' damaged area so that moments, eccentricities and strain differentials due to panel damage could be determined. This panel damage is seen as a strain reversal between SG1 and SG2 as moments due to panel damage cause bending in the damaged region of the panel. Gauges SG3 and SG4 were placed at the top edge of the panel to track the uniformity at which the top edge displaced during the loading process.

From previous work [6,7,12], it was determined that the maximum tolerance in panel height should be held to 0.01 inches to ensure an even load distribution within the panel. When this tolerance is exceeded, non-symmetric buckling may result. Horban found that the machine shop that cut his panels was able to trim his panels to within 3 mils of the prescribed length. Variations of the arc length dimension weren't as critical since a simple knife edge, vertical support was used, and since no transverse load was applied.

Scrap pieces left over after trimming were tested for void content, resin content, volatile content, and density.

Void content is an excellent indicator of panel uniformity (see table A.1). Therefore, panels were tested which had high void contents to determine the effects of this defect on panel strength. Croop [3] wrote a report detailing these deviations in panels that Horban [7] and Siefert [12] had used for their research. Based on the data collected by Croop, it was assumed that panels with void contents much above 0.8% had suffered degradation during panel manufacture, and their material properties were suspect.

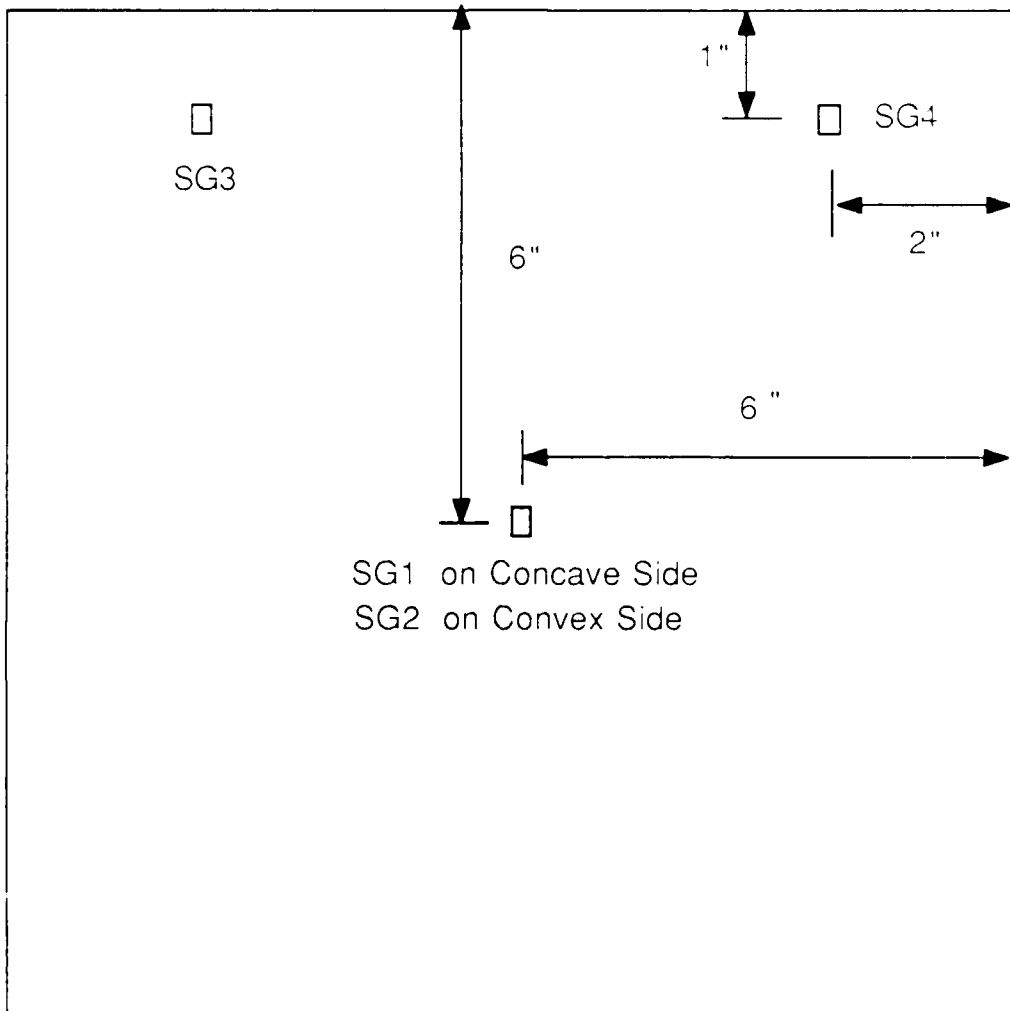


Figure 3.9 - Placement of Strain Guages on Panels

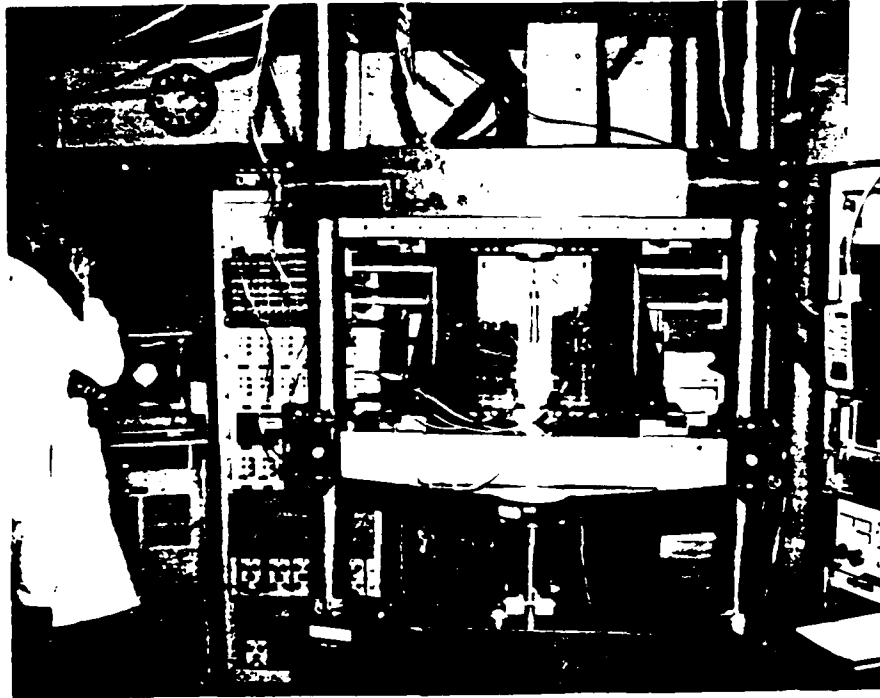


Figure 3.10 - Compression Machine Used for Experimentation

Prepreg - Hercules 12 inch tape, AS4/3501-6

Release Agent - RAM mold release 225, a tooling release
manufactured by RAM chemicals

Teflon Inserts - DuPont Teflon FEP flourocarbon film,
0.5 mil 300A film

Strain Guages - Micro Measurements CEA-250UW-350
uniaxial strain guages

Load Cell - Intarface model 1220-BF, 25k pound

Control Panel - MTS model 413.05
MTS 406 controller
MTS 436 control unit
Hewlett Packard 3450A

Amplifiers - NEF 126

Signal Conditioners - PPM model SG-15-2

Table 3.3 - Experimental Equipment List

Experimental Setup

The test fixture used in this thesis is a modification of the original General Dynamics 1974 design that was used by Wilkens [20] in his early work with curved composite panels. Since curved fixtures of this type are rare, experimental results should be particularly valuable to designers working with curved panel geometries.

The panel test device consists of a 25,000 pound capacity MTS compression machine with an Intarface model 1220-BF load cell (see material list - table 3.3). The panel is mounted in a fixture (fig 3.11) which clamps the top and bottom edges of the panel, and applies a knife edge support with negligible restraining moments to the side supports. These boundary conditions can be thought of as representative of the edge restraints caused by a continuous panel restrained against rotation at one end by a major structural support while being restrained by panel stiffeners in the transverse direction.

The clamped conditions on the top and bottom edges are achieved by using the machined steel plates shown in figure 3.12. and a series of six steel chucks which are machined so that they have a 12 inch radius of curvature at their interface with the curved panel. The chucks are 1/2 inch high and are held firmly against the panel using two set screws per chuck.

The vertical supports (fig 3.13) are designed to apply a knife edge support which will allow displacement in the x and y directions and rotations in the x, y direction while restraining displacements in the z direction. The rubber "o" rings cause the knife edge supports to place a constant normal force on each panel. A piece of teflon tape was attached to both sides of each panel tested to further aid in the panel's freedom to move in the x and y directions.

The fixture gives the following edge supports:

Top edge: $v=w=w_x=0$ $u=\text{free}$

Bottom edge: $u=v=w=w_x=0$

Vertical edges: $w=w_x=0$ $u=v=w_y=\text{free}$

The fixture's vertical supports allow 1/4 inch of the panel to protrude above the top of the supports, to allow for loading head displacement. An aluminum flange located at the center of the base plate provides a mount for an LVDT (Linear Variable Differential Transducer) which measures the vertical displacement. And, since the bottom test fixture is not permanently attached to the compression machine, this flange also provides a mount to secure the bottom test head in a uniform position for each test (fig 3.14). An array of 15 LVDT's was used to measure relative movement of the panel in the z direction during panel buckling (fig 3.15).

Test Procedure

After the panel was placed in the test fixture, a 300 pound seating load was applied and all of the supports were tightened. The purpose of this seating load was to insure that the panel's top and bottom edges are clamped parallel to the heads and to reduce the chance of introducing a moment load at the supports. Tests with previous panels with no seating load indicated a large displacement was induced before the panel began taking load (fig 3.16). The displacement was actually the seating of the panel in the clamped supports. The seating load was then removed, and all of the channels were set to zero.

The panels were then compressively loaded with a constant 0.05 inch per minute displacement with a load cell measuring the applied load. The displacement was introduced at the top edge of the panel and is measured using a LVDT which measures the relative movement of the top head with respect to the bottom head of the compression machine. A matrix of 15 LVDT's was positioned normal to the convex side of the panel to measure deflections in the z direction during panel loading. These LVDT's were positioned at $x=3$, 6, and 9 inches with the LVDT's equally spaced along the rows.

Data was recorded three times per second for the 16 LVDT's, the load cell, and the four strain gauges with each

instrument assigned to its own channel. The data was saved on a VAX 11/780 computer and later to magnetic tape backup so that experimental graphs could be plotted. In addition, a CRT was used which allowed the channels to be monitored during loading so that the progression of panel loading could be tracked during the test.

When global buckling of the panel occurred, the load was put on hold and the buckled regions were outlined with a silver pencil and photographed. The load was then removed by releasing the hydraulic pressure.

Ten of the panels tested had a 3000 pound seating load applied prior to testing. This large seating load was used to determine if there was a difference in the strain reversal at the delamination as a result of ply separation brought about by the high initial load. This seating load had the effect of smoothing the introduction of the test load since there was very little initial displacement of the panel in the supports at initial test loads (fig 3.17). However, this seating load had no apparent effect on the load at which snapping occurred and didn't seem to effect the shape of the strain separation curve. By observing this curve, it can also be seen that the assumption of linear material properties and linear bifurcation is an accurate approximation.



Figure 3.11 - Compression Machine and Control Unit

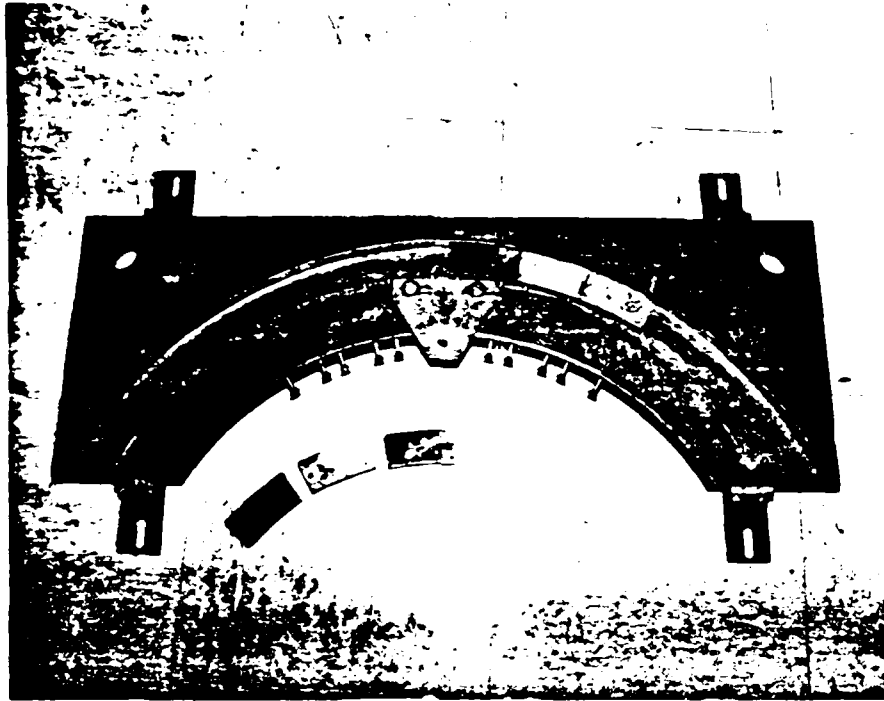


Figure 3.12 - Top Test Fixture with Steel Chucks

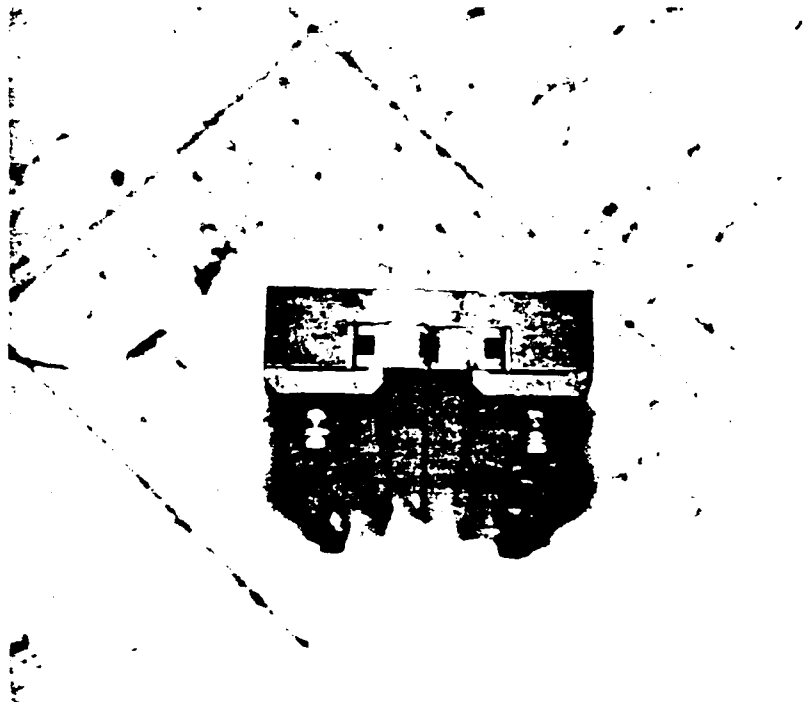


Figure 3.13 - Top View of Vertical Test Fixture

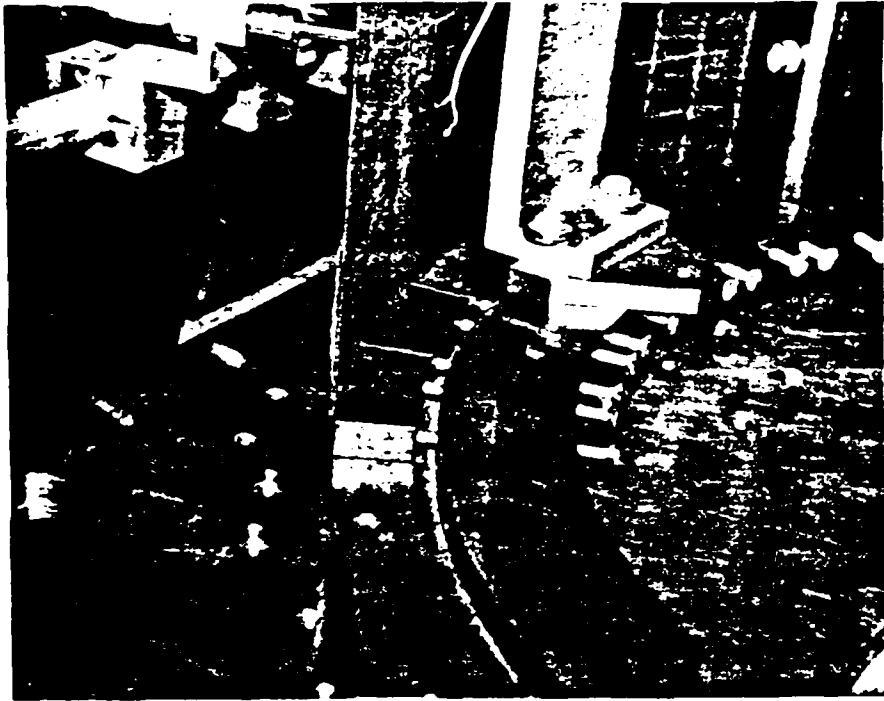


Figure 3.14 - Panel Clamped in Bottom Fixture

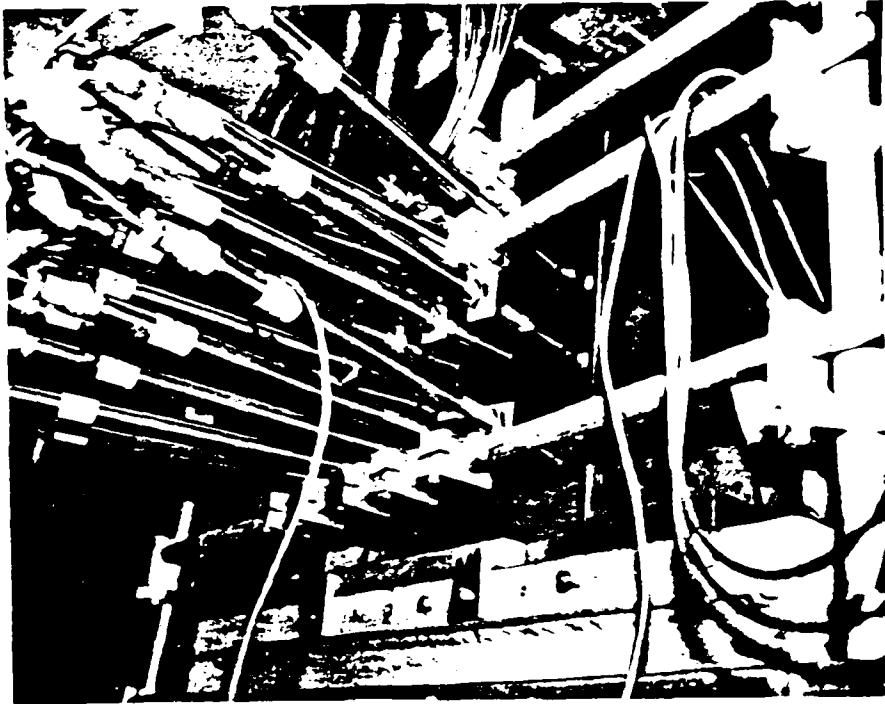


Figure 3.15 - Array of 15 LVDT's

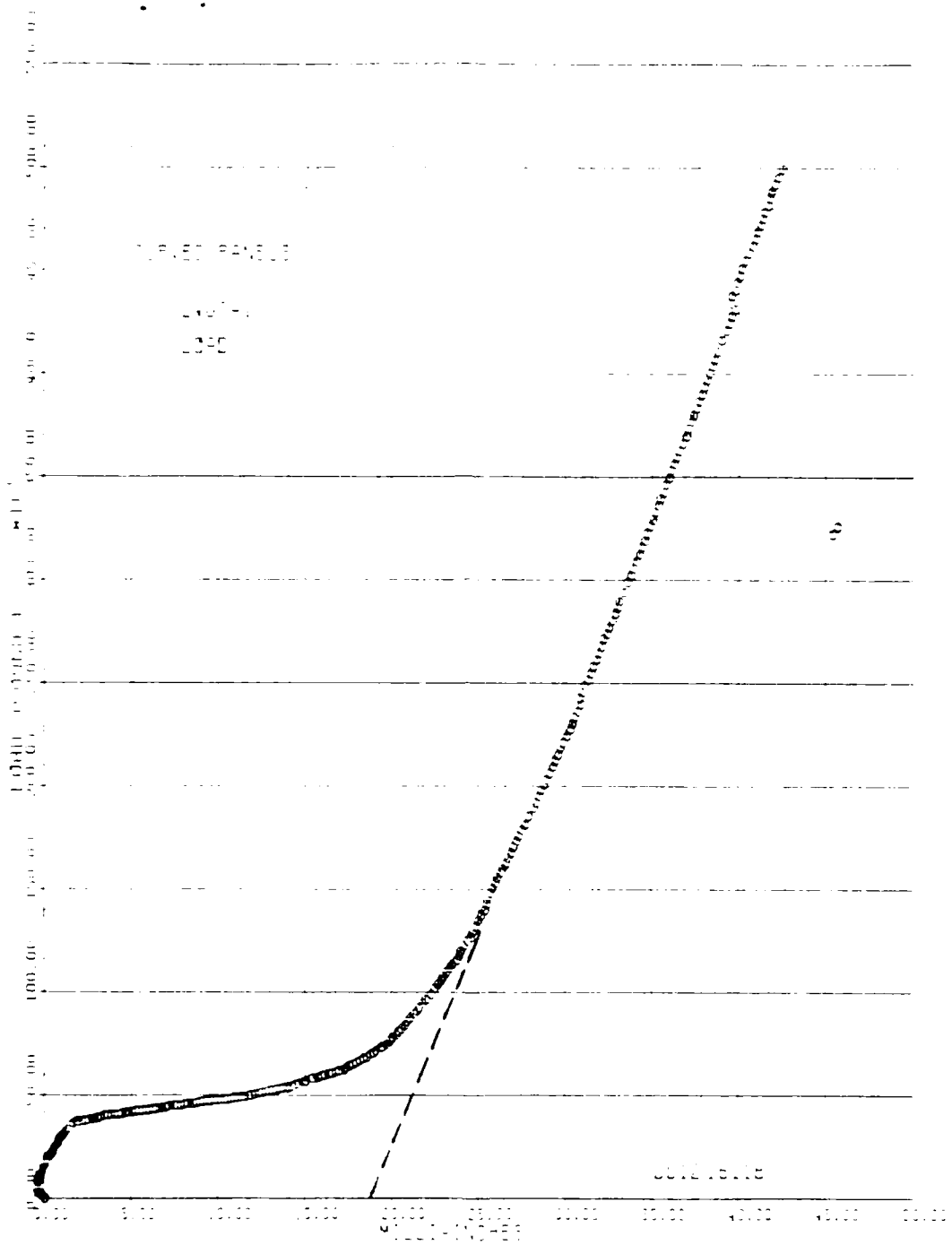


Figure 3.16 - Load vs Displacement - No Seating Load

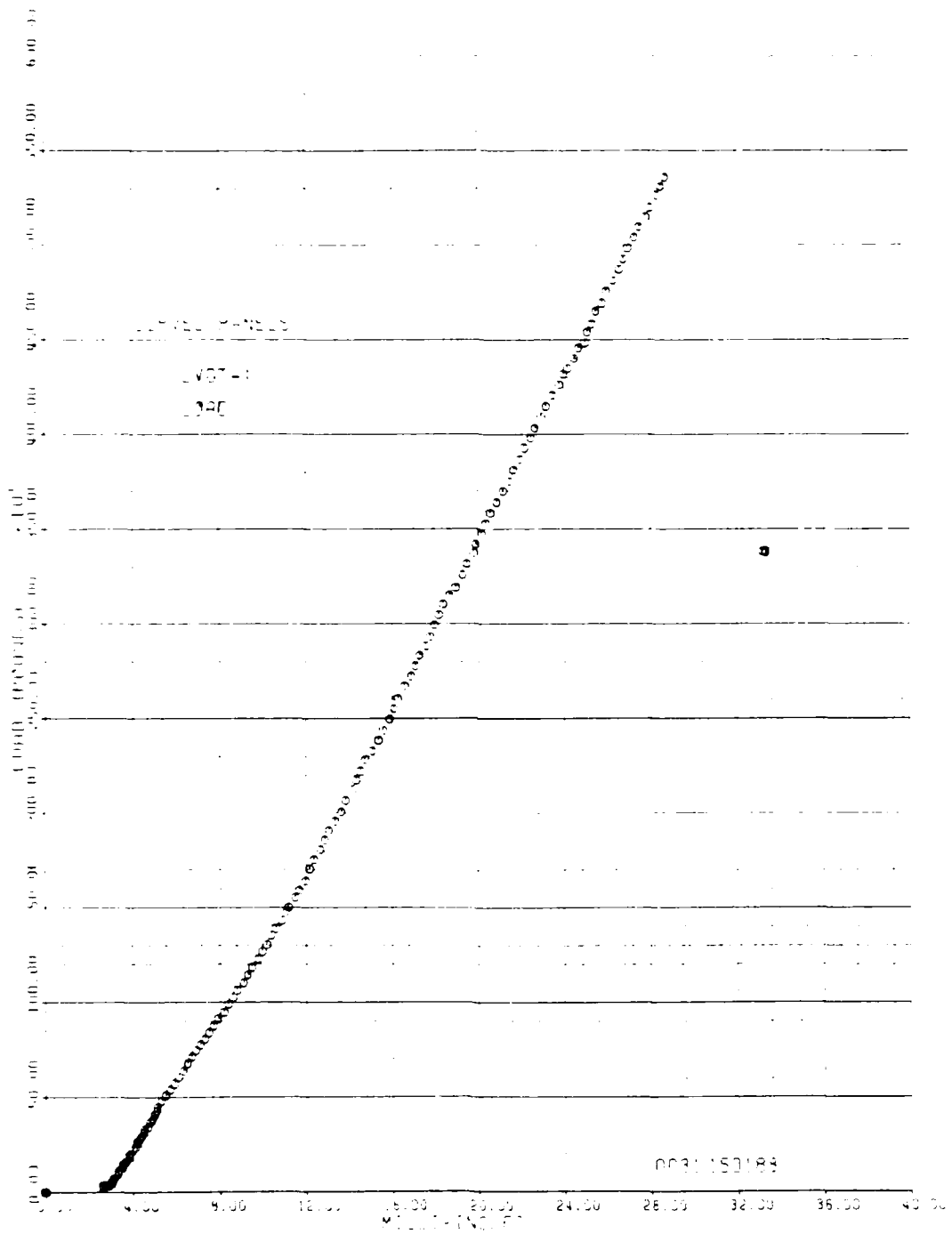


Figure 3.17- Load vs Displacement - 3000 lb Seating Load

IV. EXPERIMENTAL RESULTS AND DISCUSSION

Panel Identification

A panel identification nomenclature similar to Horban's [7] was adopted for this thesis and is shown in table 4.1 below. Tabulations of experimental results can be seen in tables 5.3 and A.1.

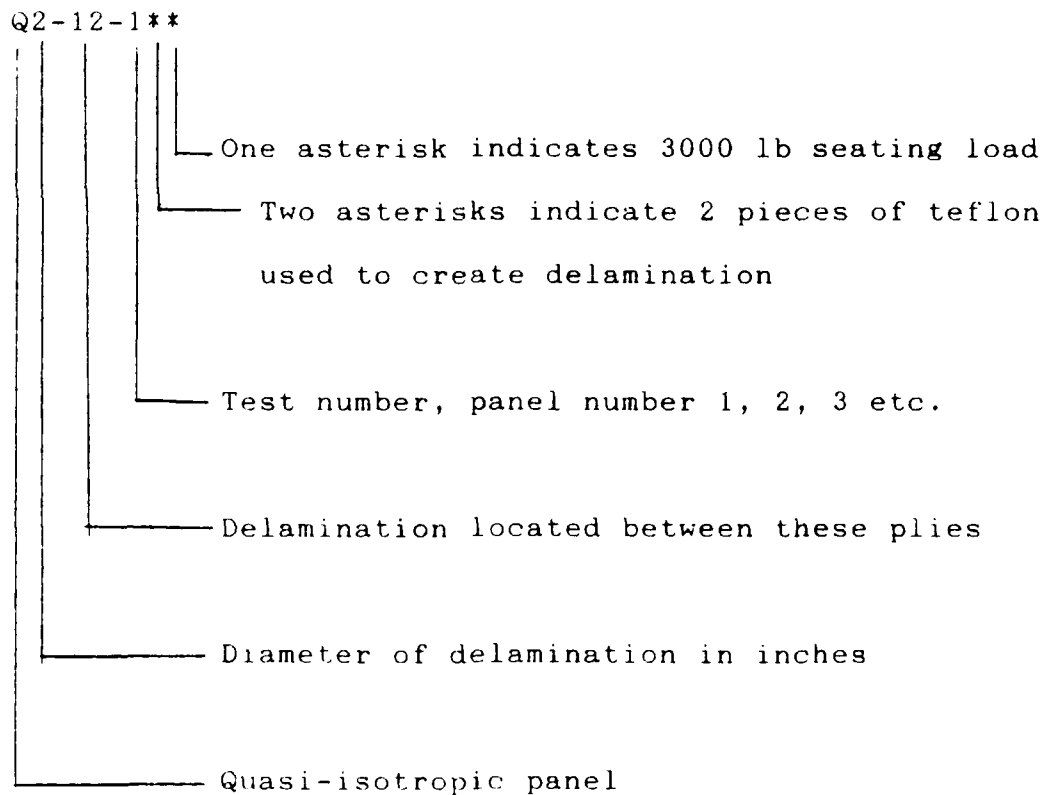


Table 4.1 - Panel Identification

Panels with varying levels of damage were experimentally tested by applying a uniform rate of end displacement. The panels tested for this thesis had damage due to faulty manufacturing of the panels, surface damage similar to that caused by burning or chafing, or an internal delamination of the type that might occur as a result of a low velocity impact. Other panels with no damage were tested as a control group. The panels were loaded until global panel buckling occurred, and the buckling load, buckling strain and the buckled shape of the panels were noted. The responses of the panels in their damaged regions were recorded both visually and through the use of strain gauges centered on either side of the damaged region.

Panels with No Damage - Q0-00-x

Panels which had no surface damage and no internal delaminations were experimentally tested. These panels all had void contents within an acceptable limit of one percent and exhibited no discontinuities when C-scanned. Therefore, it was assumed that no manufacturing induced defects were present. This group of control panels had strain gauges SG1 and SG2 positioned at the center of the panel in the same manner as for the damaged panels. These strain gauges indicated a uniform rate of strain at the center of the

panel with no difference in strain between SG1 on the first ply and SG2 on the eighth ply (fig 4.1). This uniform state of strain was interpreted as a state of axial strain without bending in a vertical strip of the panel through the panels center. This approximation is valid since the strip is flat in the longitudinal direction and has a relatively flat radius of curvature and is not restrained in the transverse direction. If moments or eccentric loading had been present, their effects would have shown up as a differential state of strain between SG1 and SG2. This uniform strain was observed for each of the Q0-00-x panels tested.

The panels' global buckling values were recorded and compared to a STAGSC-1 finite element model prediction. The experimental values were lower than STAGSC-1 predictions by a mean of 12.9 percent with a standard deviation of 2.8 (fig 4.2). The fact that predicted buckling loads were somewhat higher than experimental loads was expected, since for cylindrical shells, a very slight surface imperfection can result in a large decrease in buckling loads. Also, the STAGSC-1 model was a linear bifurcation model which was expected to yield higher buckling values than the experimental tests.

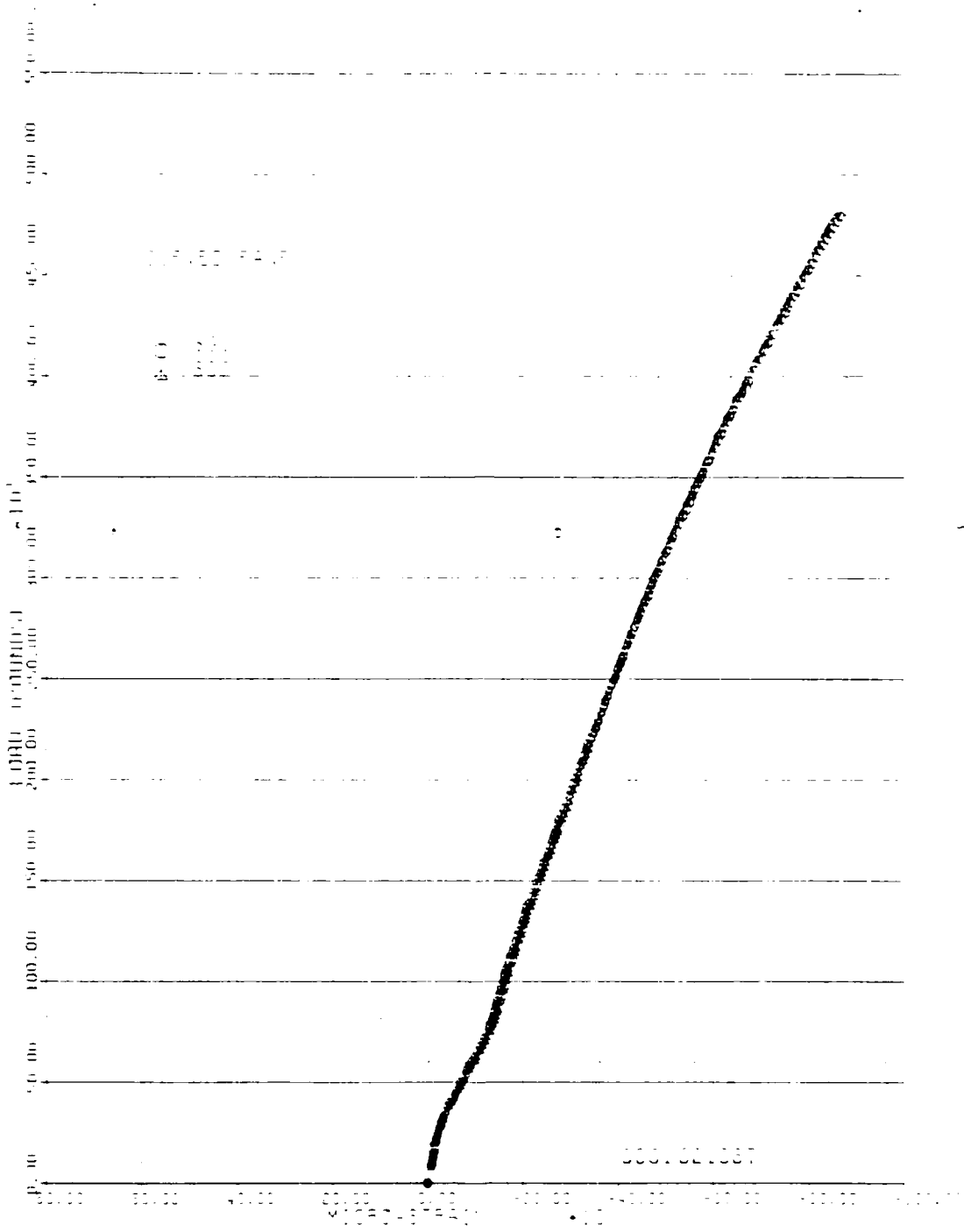


Figure 4.1 - Load vs SG1 & SG2 - Q0-00-x Panels

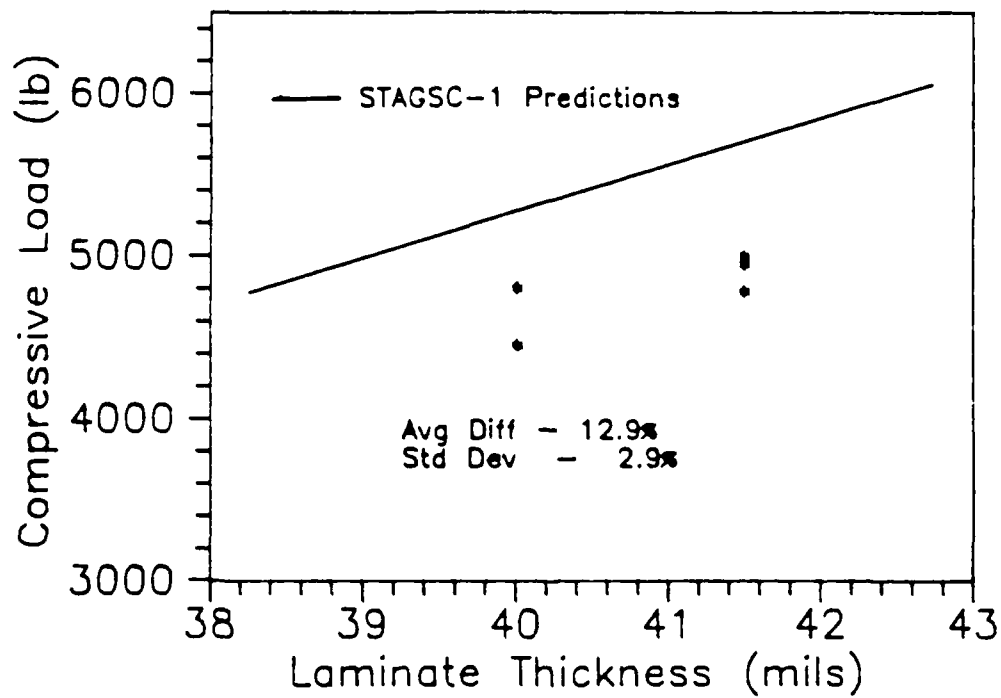


Figure 4.2 - Global Buckling for Q0-00-x Panel

Manufacturing Induced Defects

When the first sets of panels manufactured for this thesis were removed from the autoclave, it was noted that one of the four molds produced a panel which had a glossy sheen as stated previously. The panel appeared normal in every other respect and there were no other visible signs of defects. This panel was C-scanned along with the rest of its group, and when no voids or cracks were detected, it was trimmed to its test dimensions. The pieces trimmed from the panels were analyzed for density, fiber content, resin content and void content (see ref. 3). It was found that the panel with the sheen, had a much higher than normal void content (on the order of 2 to 4 percent as opposed to the less than 1 percent void content for a "normal" panel).

In the mean time, other autoclave runs had produced panels with the same glossy appearance, all from the same mold. When a lab analysis of these panels was carried out, it was found that they also had a higher than normal void content. At this time the autoclave was investigated, and it was found that one of the sets of vacuum lines was partially blocked with resin, and wasn't pulling sufficient vacuum on the bagged samples. Apparently, this resulted in the incomplete removal of volatiles during panel curing causing inadequate consolidation of the panels and higher void contents. After the autoclave was repaired, all panels had a void content below one percent.

Since the number of panels allowed for this research was limited, it was decided to test the panels with high void contents and observe their buckling characteristics. These panels were assumed to have the same material properties as low void panels. They were compressively loaded, and it was found that they had buckling loads which were within a mean of 9.6 percent of their STAGSC-1 values.

This result was unexpected. It was thought that a high void content was an indicator of a faulty specimen and that these panels would have greater flexibility due to the voids which would result in reduced buckling loads. When percent voids was plotted against compressive load at failure and the best fit line was plotted (fig 4.3), it was found that strength was increasing as void content increased. This phenomenon was explained by checking the average thickness of the panels. Voidy panels were thicker than "normal" panels (fig 4.4), and the increase in thickness was stiffening the panels and thus compensating for the higher void contents. As a result, the panels with a higher percentage of voids had a higher average buckling strength than the panels with a normal void content. However, in general, high void contents should be avoided in a composite panel. As the void content increases, the amount of matrix bonded to each fiber decreases which results in a reduction of load transfer through shear stress. Moisture absorption and subsequent material degradation could also be expected to increase.

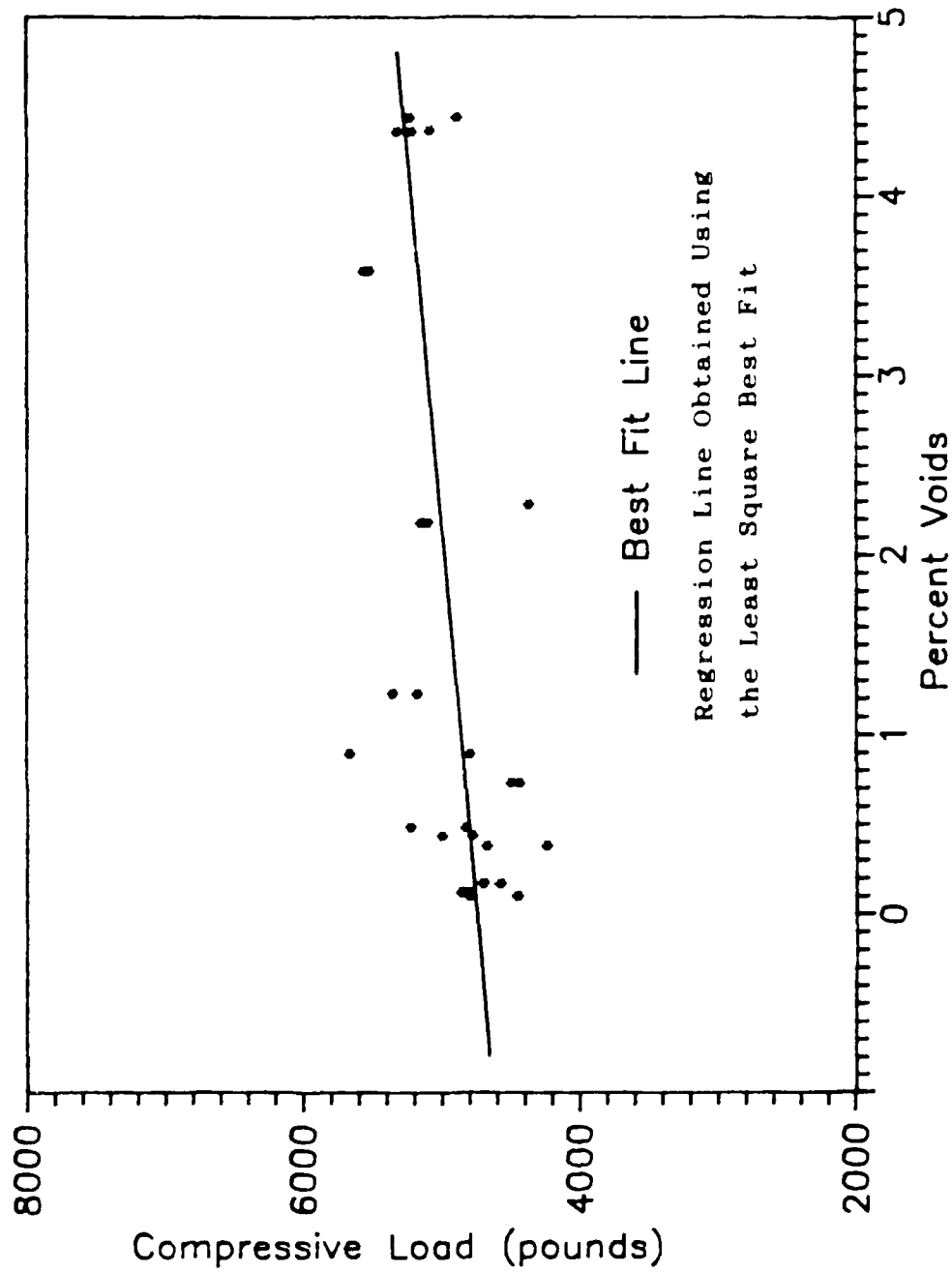


Figure 4.3 - Compressive Load vs Percent Voids

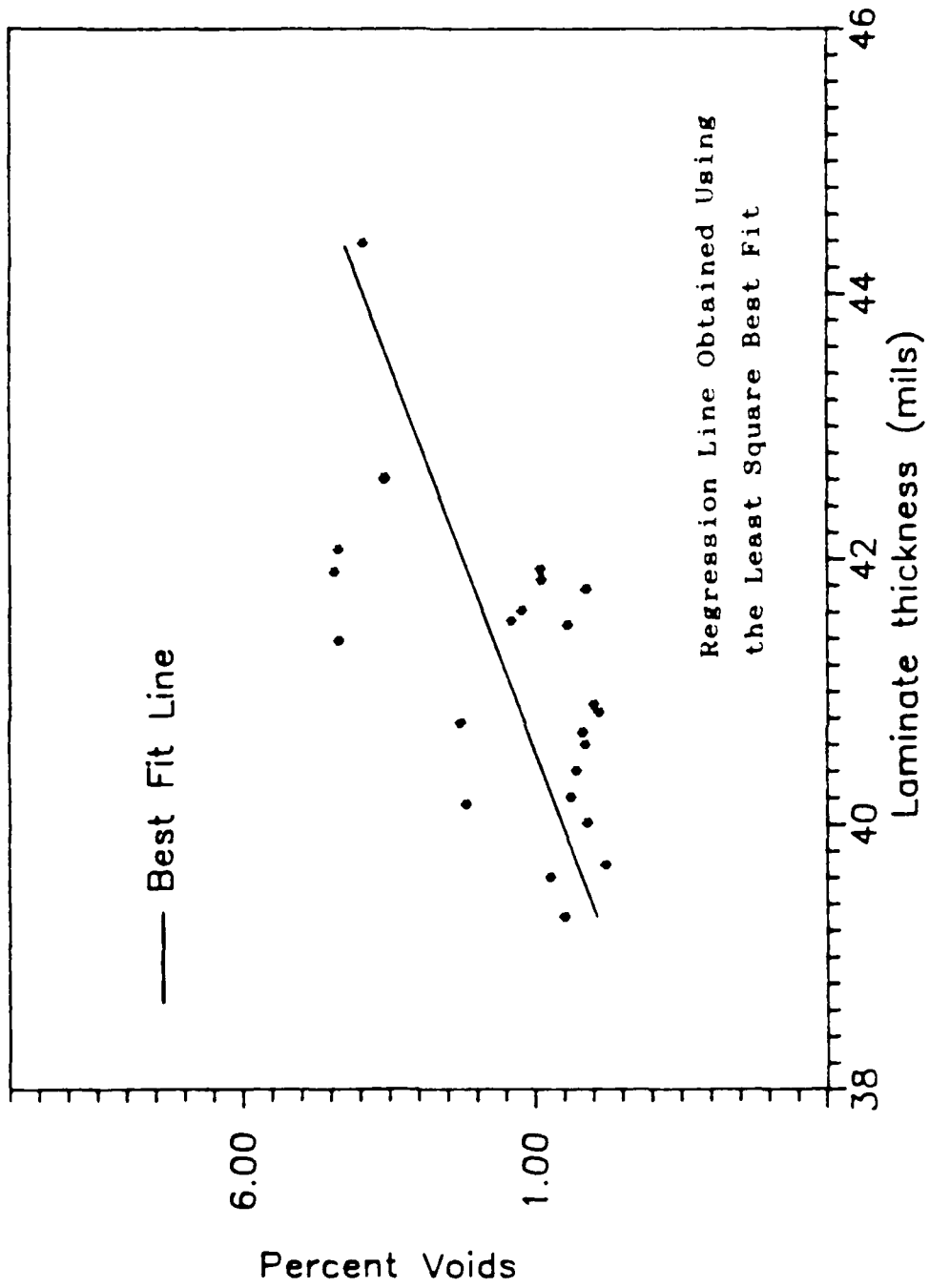


Figure 4.4 - Percent Voids vs Panel Thickness

Surface Damage

Surface damage in a composite panel may occur to the exterior surface or to the interior surface of the panel as the result of burning, chafing or abrasion. These types of surface damages were modeled in this thesis by the removal of a circular portion of an exterior 0 ply. The panels were then tested experimentally to determine the effects of this damage on the panels' buckling strength.

These Q2-12, Q2-78, Q4-12 and Q4-78 panels were manufactured with a teflon disc placed between plies 1-2 and between plies 7-8. The delaminations caused by placing inserts adjacent to the exterior ply resulted in the delaminations that were clearly failed (fig 3.1). Since the blistered portion of the external ply was failed during the manufacturing process, it was removed and SG1 and SG2 were placed at the center of the damaged region on the exterior of the 90 and the 45 plies. These strain gauges were used to detect differential strain in the damaged region which would indicate the presence of eccentric loading and moments due to the damage. It was thought that the additional moments caused by this eccentricity would trigger buckling at lower values than those observed for non-delaminated panels. But, the experimental buckling loads differed from the STAGSC-1 predictions by a mean of only 9.8 percent with a standard deviation of 5.6 percent (fig 4.5). There was no

observable difference between panels with surface damage on the convex side as opposed to panels with damage to the concave surface. The buckling values for these panels were actually higher buckling loads than were recorded for the non-delaminated panels and are very close to the values recorded for panels with high void content. This fact may be explained by noting that very thin eight ply panels were used for this thesis. All surfaces are very close to the neutral axis; and therefore, bending moments, which change by the distance from the neutral axis cubed, are small. As a result, eccentricities caused by this surface damage are minuscule; however, for thicker panels with deeper surface damage, these moments could increase and could cause reduced panel buckling loads. The total volume of panel that is removed as a result of this surface damage is also a very small percent of the total panel volume. For a four inch diameter surface damage in the outer ply of the panel, only 1.1 percent of the panel's volume is removed. As a result, the panels are seen to respond locally to surface damage, while little effect is seen on global panel buckling.

The local effects of this damage can be seen by observing figure 4.6. A large strain differential in the region of the damage is seen to occur at about 4000 pounds. It is thought that this represents local instability of the damaged region. At about 4600 pounds, the panel begins to deform just prior to global buckling. When the panels which contained two inch diameter abrasions were tested, it was

noted that the strain gauge located on the damaged surface was placed in compression. This was true both for the Q2-12 and Q2-78 panels, and was as expected. Moments caused by an eccentricity of this type would tend to put the plies on the damaged surface in compression relative to the plies on the opposite surface.

However, when the Q4-12 and Q4-78 panels were tested, an opposite state of relative strain existed. For these panels, the strain gauge on the damaged surface was placed in tension relative to the gauge on the undamaged surface. Also noted was a dramatic increase in the relative strain differential at the center of the damaged region at global panel buckling (fig 4.6).

This strain reversal could be explained if the damaged region were to be thought of as a plate. As compressive load is applied, a load is reached which triggers instability of the damaged region. The damaged region is restrained from buckling by the surrounding panel which acts as a clamped support, but it eventually reaches a load at which local buckling occurs. For larger damaged regions, such as the four inch diameter abrasion, a second mode buckling may occur causing a reversal of relative strain on a line drawn thru the damaged region and thus tension at the center of the damaged area. More experimental or finite element work would have to be done to determine the strain states in the damaged region and to check the validity of this hypothesis.

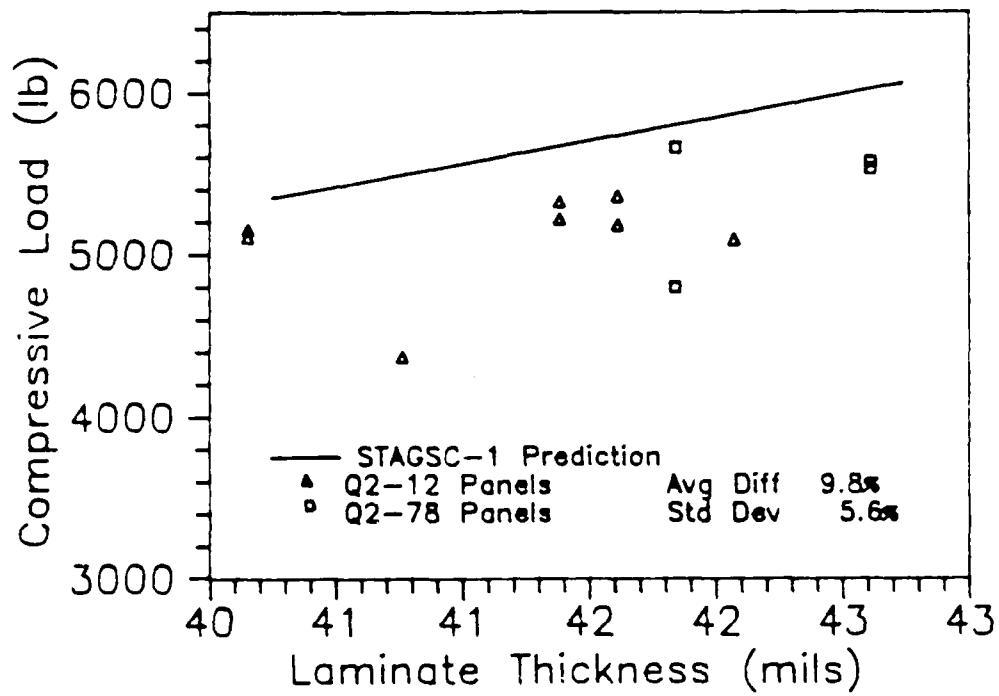


Figure 4.5 - Load vs Laminate Thickness - Surface Damage

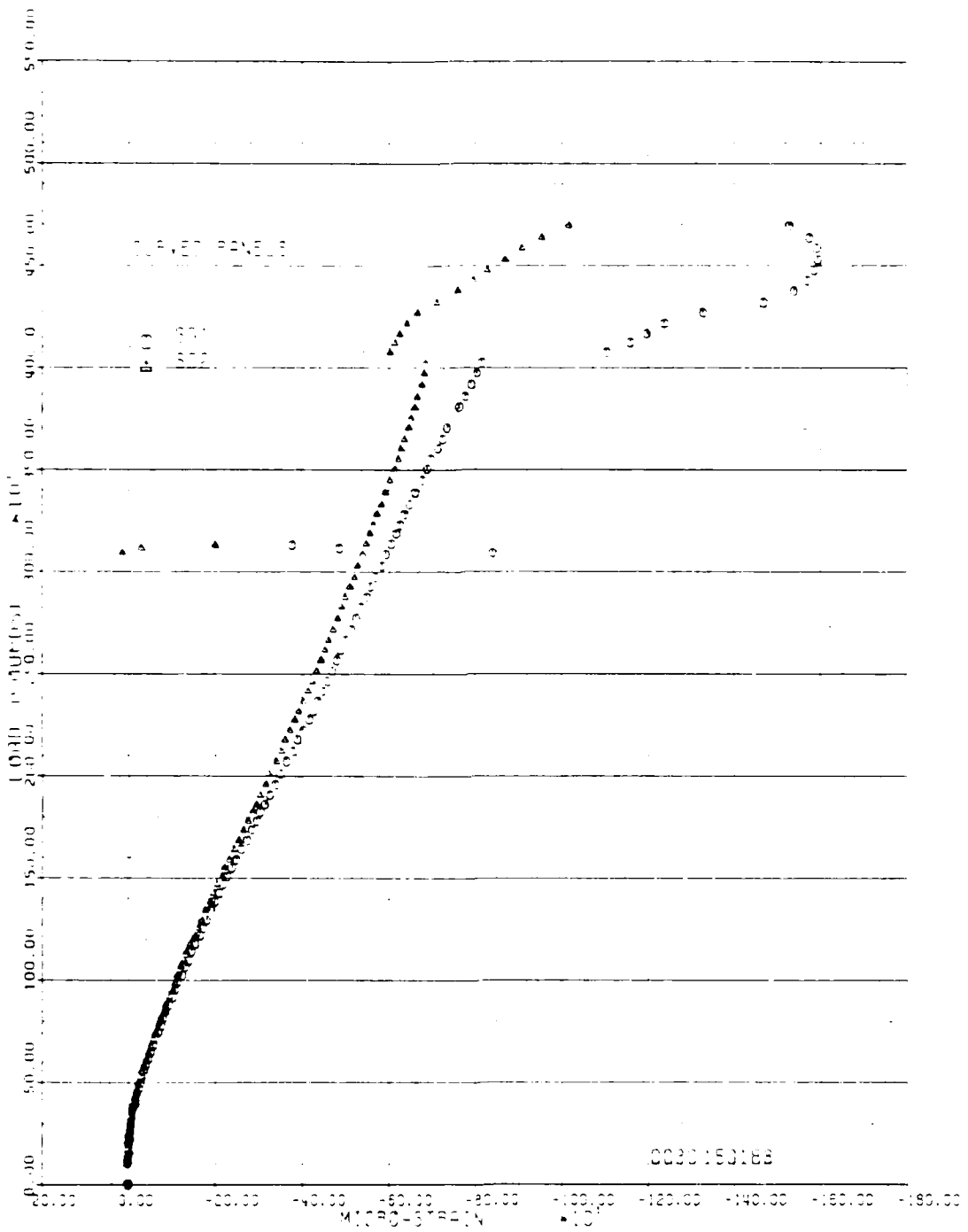


Figure 4.6 - Load vs SG1 & SG2 - Surface Damage

Internal Delamination

Impact damage to a composite shell is usually in the form of an internal delamination. This type of damage was modeled using teflon disc inserts to prevent bonding between adjacent plies. In previous work [7], it had been found that some insert materials didn't create total debonding. Therefore, to determine if 100 percent delamination at the inserts was occurring, a panel was tested by C-scanning and by using stereo x-ray. The C-scan indicated that a discontinuity existed at the approximate boundaries of the delamination. The stereoscopic x-ray confirmed that 100 percent delamination was being achieved.

The delaminated area of one of the panels is shown in figure 4.7. This stereo-scopic x-ray was produced by introducing a radioactive isotope penetrant, tetrabromomethane, into the panel through a 3/8 inch hole. After approximately half an hour, the penetrant had worked its way via capillary action into all accessible cavities. These areas show up as light areas on the photograph. By looking closely, an observer can easily see the outline of the circular delamination, and can determine that complete delamination has occurred. This test was only done on one panel since extensive work had been done previously by Horban [7] to determine the extent of delaminations in composite panels.

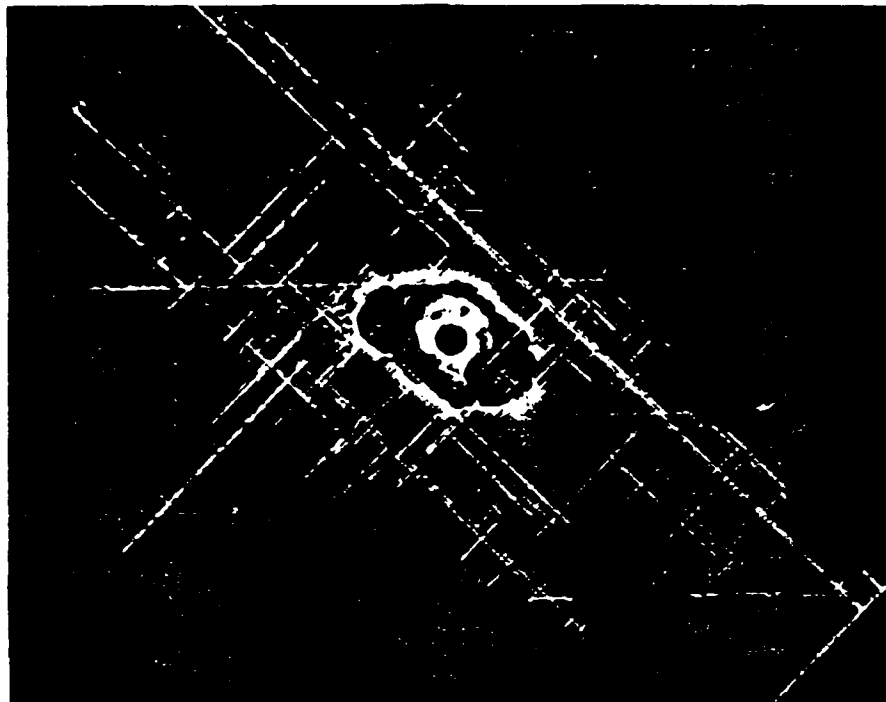


Figure 4.7 - Stereo X-ray of Delamination

Panels with two inch delaminations were then tested experimentally. These Q2-23 and Q2-67 panels experienced global panel buckling at a load which was a mean of 13.2 percent lower than STAGSC-1 predictions with a standard deviation of 5.5 percent (fig 4.8). Similar panels tested by Horban had average buckling loads that were 19.6 percent lower than the predicted loads. These experimental buckling loads for delaminated panels were only slightly lower than the experimental buckling loads for undamaged panels. However, initial sublaminare instability was detected at a much lower load. When these panels were compressively loaded, the delaminated region (the sublaminare) would reach its local critical load and buckle or "snap". This snapping effect can be detected visually as a blistered region at the delamination (fig 4.9 and 4.10) or it can be detected experimentally through the use of SG1 and SG2 centered over the delamination.

This local sublaminare snapping causes a release of strain energy and a lessening of the compression on the strain gauge attached to the sublaminare. A strain reversal effect results, an ideal depiction of which can be seen in figure 4.11. In this figure, the strain reversal is seen to occur at approximately 1900 pounds. At local sublaminare buckling, SG1 on the base laminate is in compression, while SG2 on the sublaminare is seen to have its compressive strain relieved. SG2 goes into tension as the delaminated

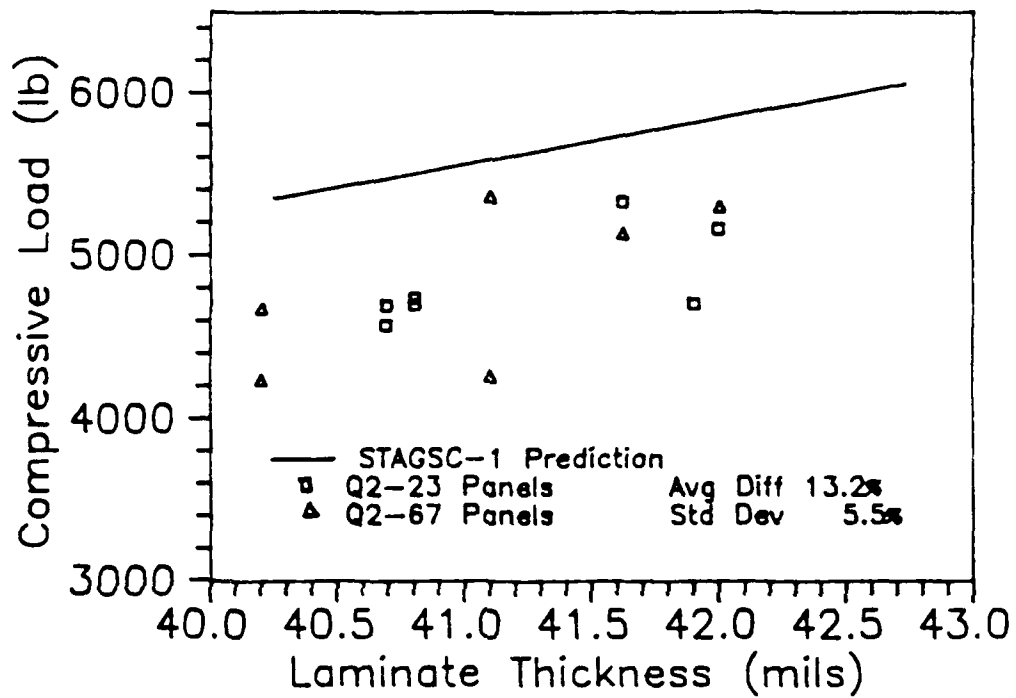


Figure 4.8 - Experimental Load vs STAGSC-1 Load
for Delaminated Panels

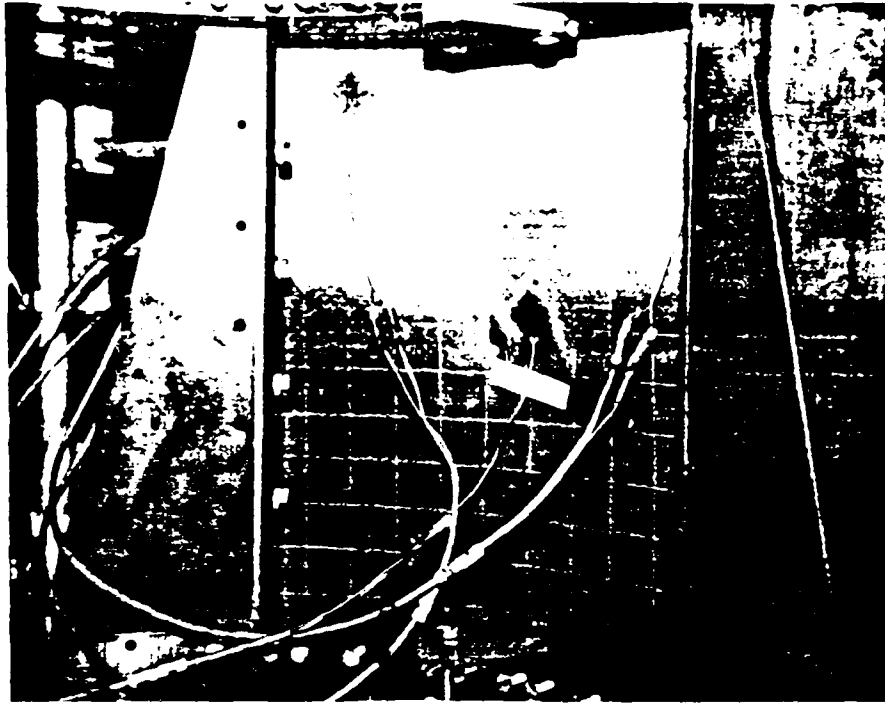


Figure 4.9 - Buckling Pattern of 2" Sublaminates

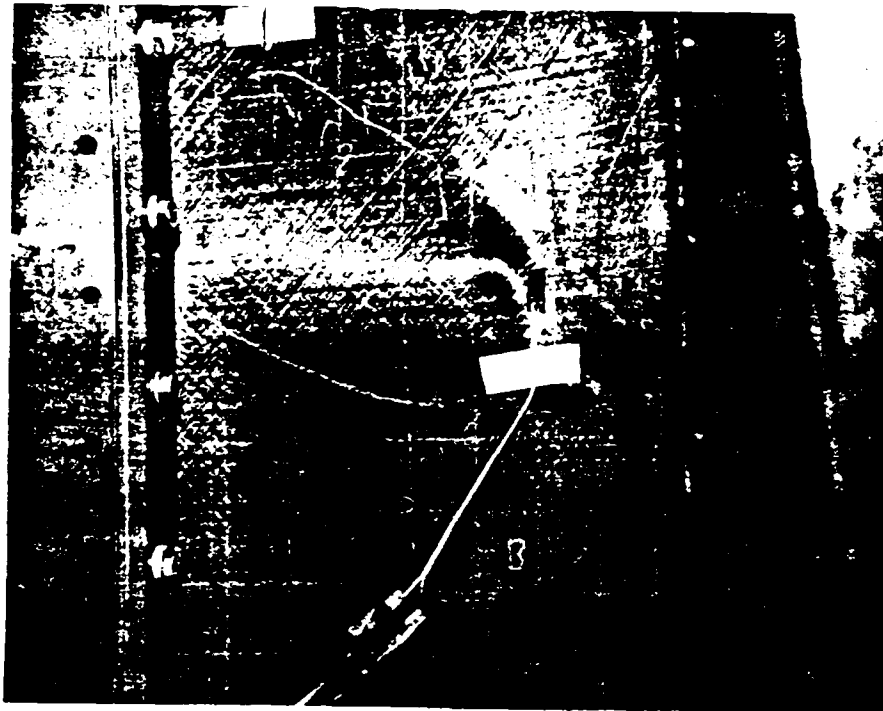


Figure 4.10 - Buckling Pattern of 4" Sublaminates

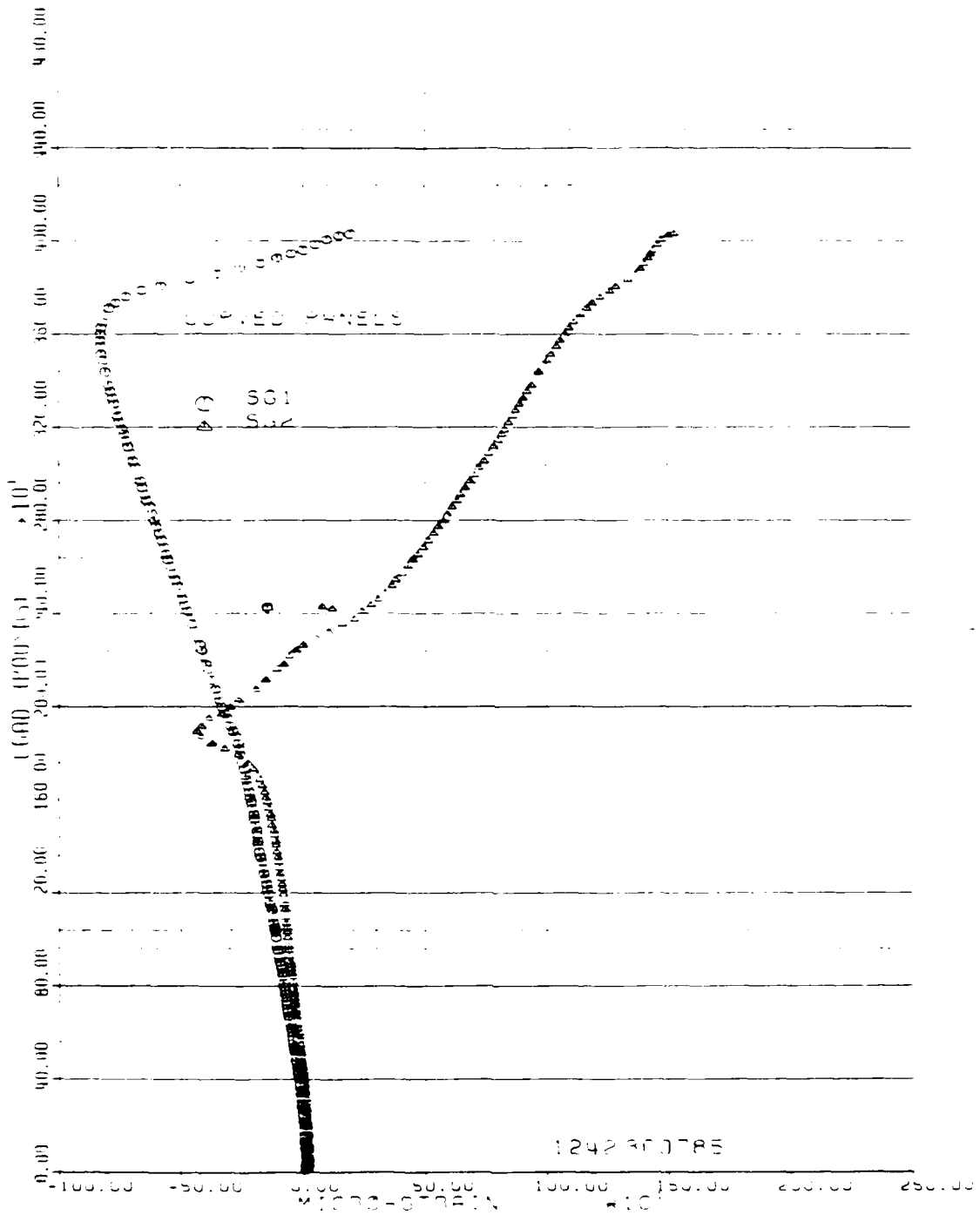


Figure 4.11 - Ideal Strain Reversal Curve

plies snap out. Another effect that can be seen by observing figure 4.11 is the lessening of compression on the base laminate at approximately 3700 pounds. It is thought that this corresponds to an initial panel deformation just prior to global panel buckling. An attempt was made in this thesis to predict this sublaminata instability through the use of the linear superposition of simple finite element models and a plane strain adjustment. This method will be presented in chapter five.

During the experimental testing of the panels, strain was only observed in the axial direction. Also, an axial load was applied to the panel in the plane of the panel. This led to the observation that a state of plane strain could be approximated for the panel in a strip in the region of the delamination.

The delaminated region of the panel was closely observed after experimental testing. This region was observed to have undergone a plastic deformation as a result of panel buckling. When the panel was unloaded and removed from the test fixture, the delaminated area was clearly visible, and retained the same general deformed shape it had attained under buckling load (fig 4.12). This indicated that this region had undergone plastic deformation and indicated a possibility of delamination growth.

At this point, a number of panels were placed back into the test fixture and compressively loaded for a second

time. The expected strain reversal of SG1 vs SG2 did not occur, but at a much lower value of load than for the initial test. Figure 4.13 shows that local sublaminate buckling is occurring at a load of approximately 400 pounds as opposed to the 1900 pound load seen for the initial test of the panel (fig 4.11). This lowering of the buckling load for the delaminated plies was expected, since a plastic deformation of the sublaminates would reduce its stiffness, would substantially increase the load eccentricity due to out of plane deformations, and would cause the second order rotational terms to become more dominant to local buckling. As a result, the critical load for local buckling would be decreased for subsequent panel loadings.

When panels were reloaded after their initial buckling failure, a small decrease in global panel buckling load was also noted. It can be seen that the panel in figure 4.13, which has undergone plastic deformation, buckles at 3300 pounds, as opposed to the 4100 pound load required to buckle the undamaged panel shown in figure 4.11. This decrease in global panel strength would occur as a result of the increased instability of the delaminated region which has suffered permanent deformation. It is postulated that subsequent cyclic panel loadings would cause delamination growth at the delamination crack tip and would cause a gradual deterioration of the panel's ability to carry load. This was beyond the scope of this thesis, but is an

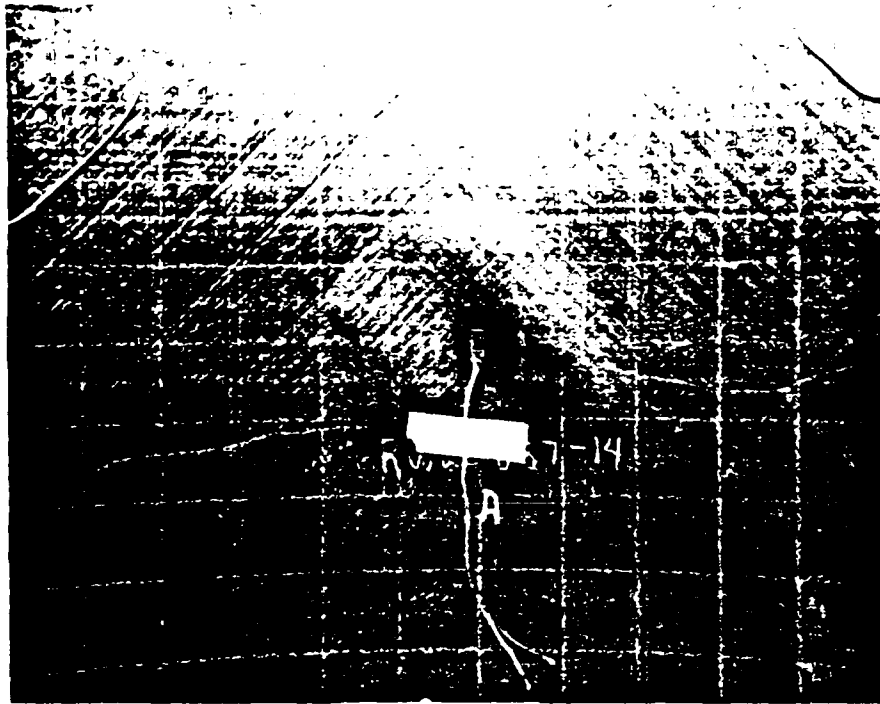


Figure 4.12 - Plastic Deformation of Sublamine

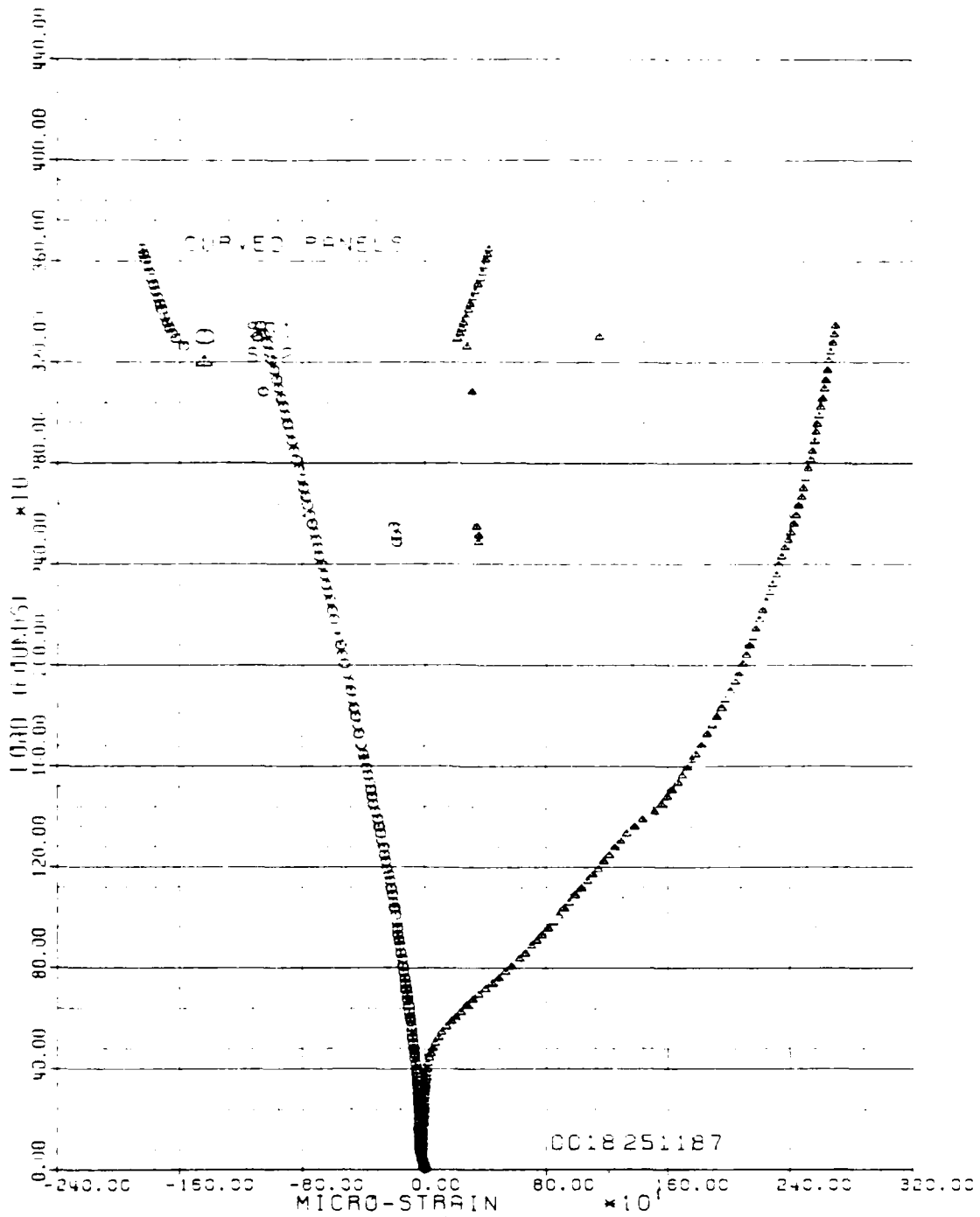


Figure 4.13 - Strain Reversal for Reloaded Panel

important problem since a panel in an aircraft could be expected to undergo cyclic loadings prior to detection of delamination damage.

Another phenomenon that was noted was the shape of the buckled sublaminates. Most of the two inch delaminations would snap out into a single blistered region that appeared to be a low bubble on the surface of the panel. The four inch sublaminates, on the other hand, would snap into a pattern of "ridges and valleys" that were oriented at approximately a 45° angle to the 1-direction (fig 4.10). This would indicate that shear stresses were developing at the sublaminates boundary, and that shear, or a combination of shear and compression was causing buckling for the larger diameter sublaminates.

It is also thought that the base laminate, which was in contact with the sublaminates, was laterally bracing the delaminated plies and causing them to buckle at higher modes. This phenomenon would tend to increase the critical load at which larger sublaminates initially become unstable relative to an unrestrained sublaminates.

V. ANALYTIC TECHNIQUE

Introduction

Composite laminates subjected to a low speed impact, such as a dropped tool or a manufacturing load, often develop an internal delamination. Delaminations in composite panels cause a reduction of local stiffness of the panel plies in the region of the delamination. As a result, when the panel is subjected to loading, this area is the first portion of the panel to become unstable and buckle. This local buckling of the delaminated plies precedes the global buckling of the panel and occurs at a much smaller load.

The effects of this local buckling will become more important to engineers and designers as composites are used more often in modern high-speed aircraft. Local surface defects can cause drastic disturbances in air flow, and a weakened area of a panel may experience peeling and dramatic delamination growth as the surface is exposed to increased aerodynamic loading.

Since curved panels are 3-dimensional, and buckling is a nonlinear phenomenon due to the large rotations and moments, the compressive load which will cause curved panels to become unstable is extremely hard to predict analytically. This thesis presents a technique whereby the local buckling loads

at the delamination may be predicted within approximately 30% of experimental values by using a 2-dimensional model with a plane strain correction. This approach to predicting local sublaminar instability is based upon the principle of linear superposition. During the experimental phase of this research, certain physical responses of the panels led to certain simplifying assumptions. It was observed that the local instability and snapping of the delaminated plies occurred at a much lower value of load than the global panel buckling for the 12 inch curved panels. It was thought that there existed a value of strain which when applied to the circular delamination would cause the sublaminar to buckle. This value of strain in the two ply sublaminar should be related to a value of strain in the eight ply curved panel. Some method of relating these two values of strain was required.

Therefore, a strip of the panel in the vicinity of the delaminations was considered. This strip, shown by the dashed lines in figure 5.1, would be flat in the longitudinal direction (which is the direction of loading), and slightly curved in the transverse direction. In the transverse y-direction, the strip is restrained against deformation by the eight ply thickness of panel between the strip and the fixture's vertical support, while in the x-direction the strip is unrestrained against deformation. A load displacement is applied in the x-direction.

AD-A198 617

A STUDY OF DAMAGE TOLERANCE IN CURVED COMPOSITE PANELS

2/2

(U) AIR FORCE INST OF TECH WRIGHT-PATTERSON AFB OH

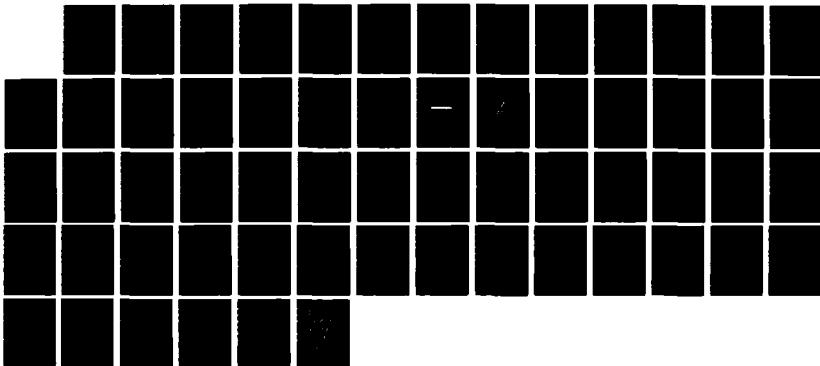
SCHOOL OF ENGINEERING B L WILDER MAR 88

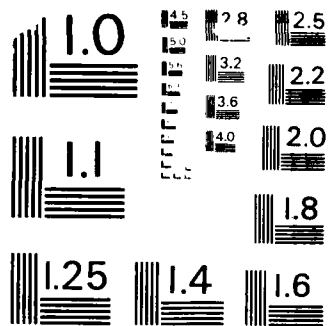
UNCLASSIFIED

AFIT/GA/RA/88M-3

F/G 11/4

ML





MICROCOPY RESOLUTION TEST CHART
NATIONAL BUREAU OF STANDARDS-1963-A

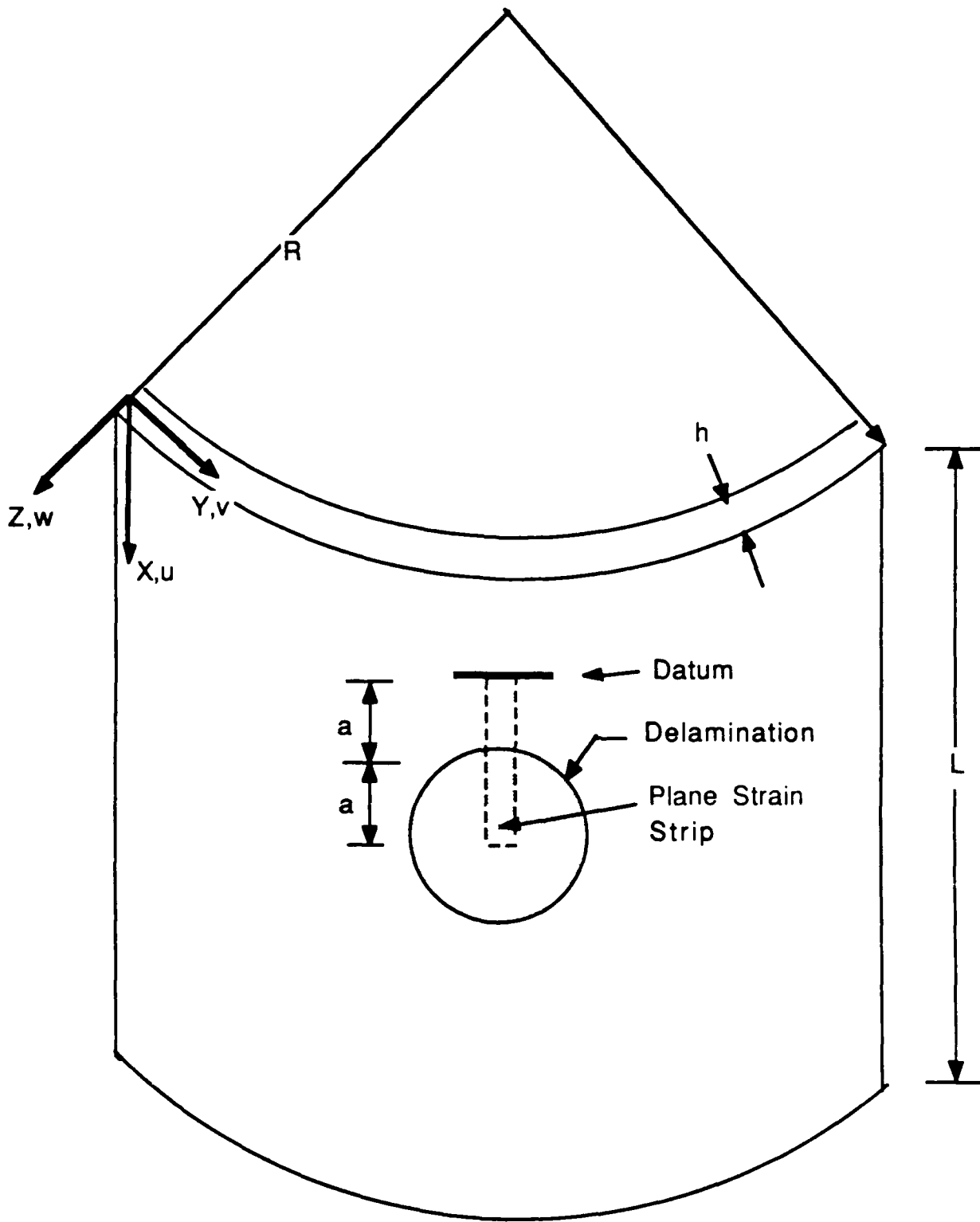


Figure 5.1 - Plane Strain Assumption

the y direction and free movement in the z direction. Hence, a plane strain assumption is valid for this region of the panel.

For the panel geometry investigated, a load applied to the top edge of the curved panel causes a displacement at the boundary of the delaminated plies. It was found that this displacement causes an apparent constant strain field through the curved panel in the direction of load, and introduces an effective strain to the delaminated plies via an axial deflection of the sublaminate boundary. The relation between strain in the curved panel and strain in the delaminated plies was used since strain is a convenient tool for associating the response of the curved panel with the behavior of the sublaminate plies. Since bending is negligible, the delamination is primarily affected only by the deflection in the axial direction that is transmitted by a constant strain in the curved panel. To investigate the effect of this deflection on the sublaminate, a finite element model of the sublaminate was loaded with an edge deflection. The N_x load and the related axial strain in the sublaminate were computed at local buckling. A plane strain finite element model was used to relate this value of N_x to the eight ply curved panel. This model represented the strip shown in figure 5.1, and has eight plies through the z-direction, and contains a two ply delaminated region. This model was loaded using the

strain which had caused buckling in the circular finite element model of the two ply sublaminates.

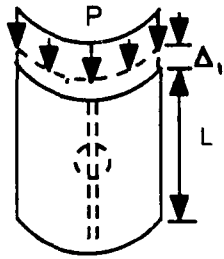
The resulting N_x value through the cross section of the plane strain model was calculated at a section of the model one delamination radius away from the delamination tip. This datum was chosen so that the calculated force resultant would be far enough from the discontinuity so that model responses due to the delamination tip could be avoided. This force resultant in the eight ply plane strain model could then be related to the global panel load, and would represent a force resultant in the eight ply laminate corresponding to the buckling strain in the (0/-45) sublaminates.

In summary, the prediction of the compressive load which will cause the delaminated region of a composite panel to snap was developed as follows, and is outlined in Table 5.1:

1. A model of the curved panel containing no delaminations was run using the STAGSC-1 finite element program for a normalized edge displacement. An N_x value at the top edge of the panel was calculated for this displacement, and the strain in the panel associated with this force was calculated at the datum shown in figure 5.1. The strain associated with the applied load in this model was then applied to a plane strain model in step four.

2. The delaminated area of the panel with (0/-45) orientation was modeled as a circular plate using STAGSC-1. This model was given a uniform edge displacement; the

What load P applied to curved panel will cause local buckling at the delamination?

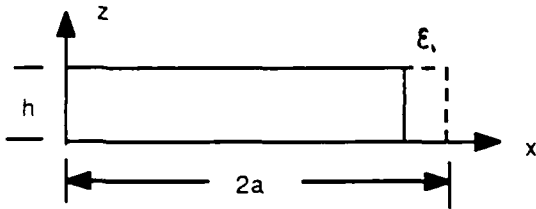


$$\epsilon_1 = \frac{\Delta_1}{L}$$

STAGSC-1 CURVED PANEL MODEL

1. Compute buckling load, P, for non-damaged panel.
2. Compute strain in panel at global buckling.
3. Use the plane strain model shown below to calculate a force resultant in a strip of the panel buckling.

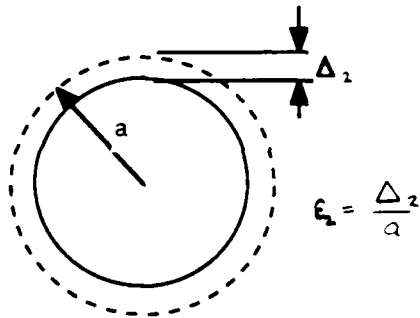
$$N'_x = N_{x1}$$



PLANE STRAIN - NO DELAMINATION

1. Use the strain computed in the curved panel model above to load the plain strain model.
2. Compute the force resultant in this 8 ply model associated with the strain obtained in the curved panel model above.

$$N_x = N_{x2}$$

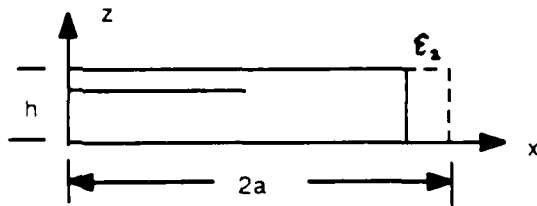


$$\epsilon_2 = \frac{\Delta_2}{a}$$

STAGSC-1 DISC MODEL (0/-45)

1. This is a model of the sublaminates created by the delamination.
2. Compute the force resultant associated with bifurcation for this model.
3. Compute the strain associated with bifurcation for this model.
4. This strain will be used to load an 8 ply plane strain model taken at the delamination.

$$N_x = N_{x3}$$



PLANE STRAIN WITH DELAMINATION

1. Load this model with the strain calculated at buckling for the disc model above.
2. Calculate the force resultant thru the 8 ply section associated with this strain

$$N_x = N_{x4}$$

Predicted Load at Local Buckling of Delaminated Plies

$$P_f = P \frac{N_{x2} N_{x3}}{N_{x1} N_{x4}}$$

Table 5.1 - Overview of Analytic Technique

bifurcation load was determined; and the strain in the disc and the N_x value at plate buckling were determined. The strain obtained at bifurcation for this model was then used to load the plane strain model in step three.

3. A finite element program [21] was used to run a plane strain analysis of an eight ply composite containing a delamination. This model was evaluated using the strain obtained at buckling for the circular plate of step two. This strain from step two is used to calculate an end displacement in the plane strain model which yields an equivalent strain at the delamination tip. For this value of strain, the N_x value thru the eight ply section of the model is calculated. This calculation is performed at a cross section that is one delamination radius away from the delamination tip so that stress concentrations due to the delamination are avoided, and so that a uniform N_x value can be calculated which corresponds to an eight ply section of the curved panel.

4. A plane strain model was also run for a section of panel that contained no delamination. This model was run using the strain in the curved panel of step one; and is used to determine an N_x value in a plane strain model which is equivalent to the load applied to the curved panel. The model was constructed such that the strain at the outer edge of the delaminated region calculated in step one was used as the input load for the plane strain model. The N_x value in an

eight ply section of the model located one delamination radius away from the delamination was calculated.

5. Now, the N_x values have been calculated in two plane strain models. One force resultant corresponds to a uniform load applied to the top edge of a curved panel; and the other force resultant corresponds to the buckling load for a (0/-45) circular plate. Using these force resultants, and the force resultants obtained in the two STAGSC-1 models, a load is computed which when applied to the top edge of the curved panel, will cause buckling of the circular delamination. This load is simply a percentage of the load applied to the curved 12 inch panel (see table 5.1).

The models used in this analytic method and the process of calculating a local sublaminar buckling load will be discussed in more detail in the balance of this chapter.

Curved Panel - STAGSC-1 Model

One of the standard geometries that STAGSC-1 is capable of generating is a curved cylindrical panel. For the finite element model used in this analysis, the surface of the shell was discretized into an 18 by 18 element mesh consisting of 2/3 inch square elements. Previous work done by Siefert [12] with this geometry had shown that accurate results could be obtained if the element size was between 1/2 and 1 inch. The

element selected for this analysis was the quadrilateral 410 element referred to as the QUAF 410 (fig 5.2) in the STAGSC-1 user manual [1]. This element was selected because it works well for linear analysis and for cylindrical shells, and because it has 12 fewer degrees of freedom than the more accurate QUAF 411 element. The QUAF 410 is a 20 degree of freedom four noded element with three translational displacements, two in-plane rotations, and one independent normal rotation at each node.

The shape functions for the u and v displacements within the QUAF 410 element are a cubic polynomial parallel to the edges and a linear polynomial perpendicular to the edges, and the bending shape functions are cubic polynomials.

Both linear material properties and linear buckling were used for this model. The model was loaded at its top edge with a constant end displacement in the positive x direction. The boundary conditions used for the model were the same constraints assumed in the experimental work. Using this STAGSC-1 model, the strains and stresses in the panel could be determined for a given value of load, P. Also computed was the force resultant at the top edge of the panel, N_{x1} , associated with this load.

The introduction of a load to the top edge of the curved composite panel causes a strain in the panel in the vicinity of the delamination tip. The critical strain at this point which will cause the sublaminates to buckle is discussed in the next section.

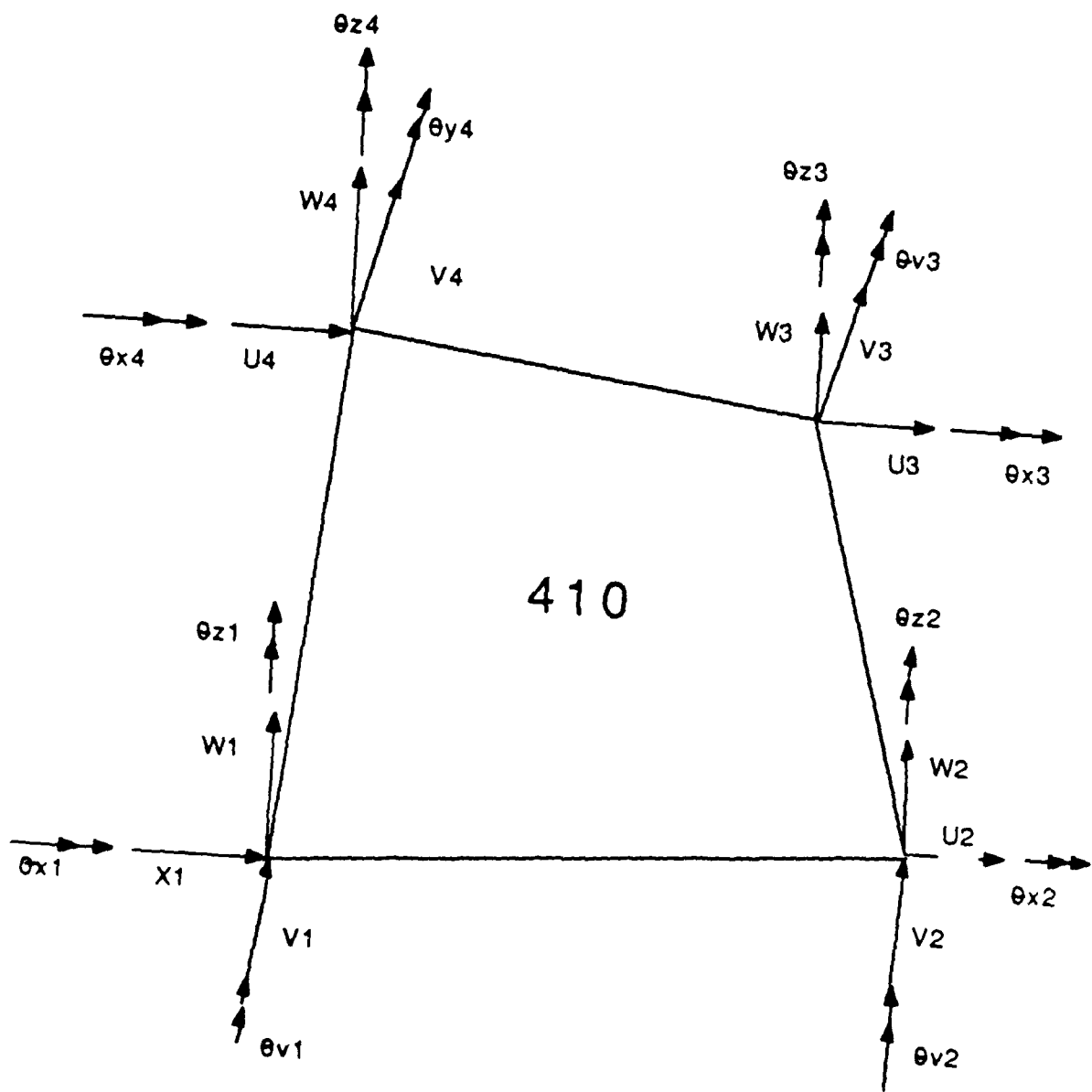


Figure 5.2 - STAGSC-1 QUAF 410 Element

Delaminated Plies - STAGSC-1 Model

The author was interested in modeling the buckling of a circular plate to characterize the plane strain strip concept previously discussed. The most obvious condition was one of complete geometric symmetry, and therefore, the subsequent convergence study and model was predicated on this strain feature.

The delaminations manufactured into the panels, as stated previously, were two and four inches in diameter. The STAGSC-1 model discussed in this section was used to determine the force resultant and the strain necessary to cause buckling of the (0/-45) circular delaminated region of the panels. The force resultant at the model boundary, N_{x3} , and the edge displacement of the boundary were determined using a STAGSC-1 annular ring shell geometry and various finite elements and mesh refinements.

A convergence study was first performed to determine an optimum finite element mesh for this geometry. Initially, a mesh having 12 elements and isotropic material properties was run using the QUA4 410 element. The mesh was identified as a 5x4 mesh since it had five nodes on any radius and four nodes around any arc. The mesh was modeled as a quarter of a circle since symmetric loading and boundary conditions could be applied. A closed form Bessel function solution exists for a uniform axisymmetric compressive load on a circular

plate. Therefore, a uniform edge displacement was applied radially inward at the outer boundary, and the N_x value at plate buckling was recorded. This model (fig 5.3) was run for both clamped and simple edge supports, and the STAGSC-1 buckling load was compared to the following Bessel function solutions for the buckling of circular discs [4]:

For clamped edges ($u=v=w,x=w,z=free w=w,y=constrained$):

$$N = \frac{14.65 D}{a^2} \quad (5.1)$$

For simple supports ($u=v=w,y=w,z=free w=w,x=constrained$):

$$N_x = \frac{4.20 D}{a^2} \quad (5.2)$$

where:

$$D = \frac{E h^3}{a^2 (1-\nu^2)} \quad (5.3)$$

$a \equiv$ the radius of the disc

It should be pointed out that the so called clamped edge condition best characterized the actual delaminated boundary with respect to the overall sublamine restraint. Therefore, the boundary condition incorporated in the completed analysis is the clamped support.

The STAGSC-1 model was run for increasing mesh refinements including 5x4, 10x8, and 20x16 for both simple and clamped edges. This study showed that convergence to the

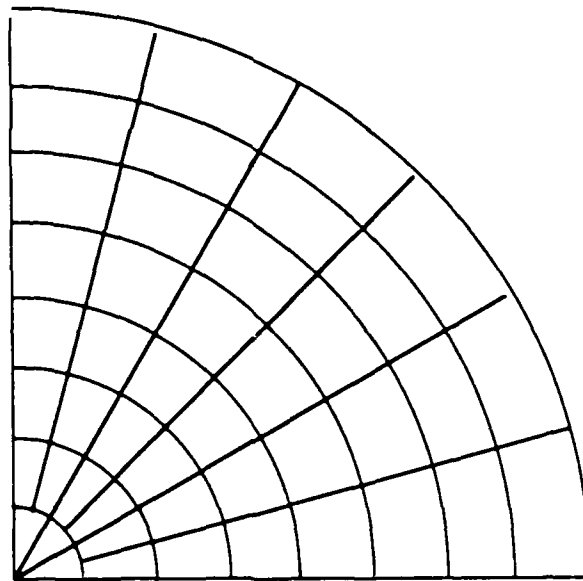
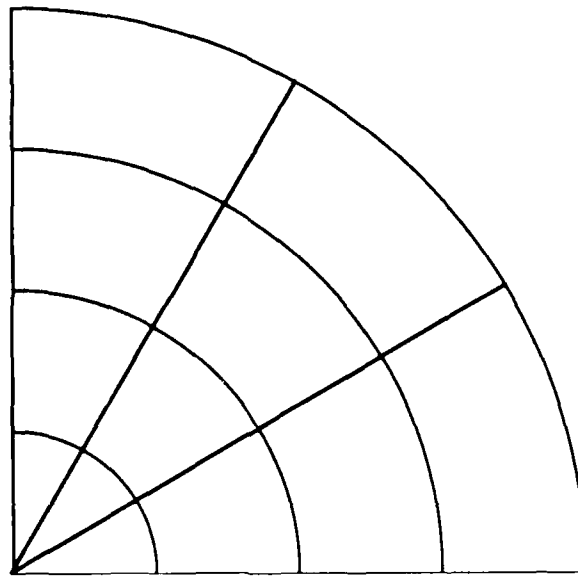
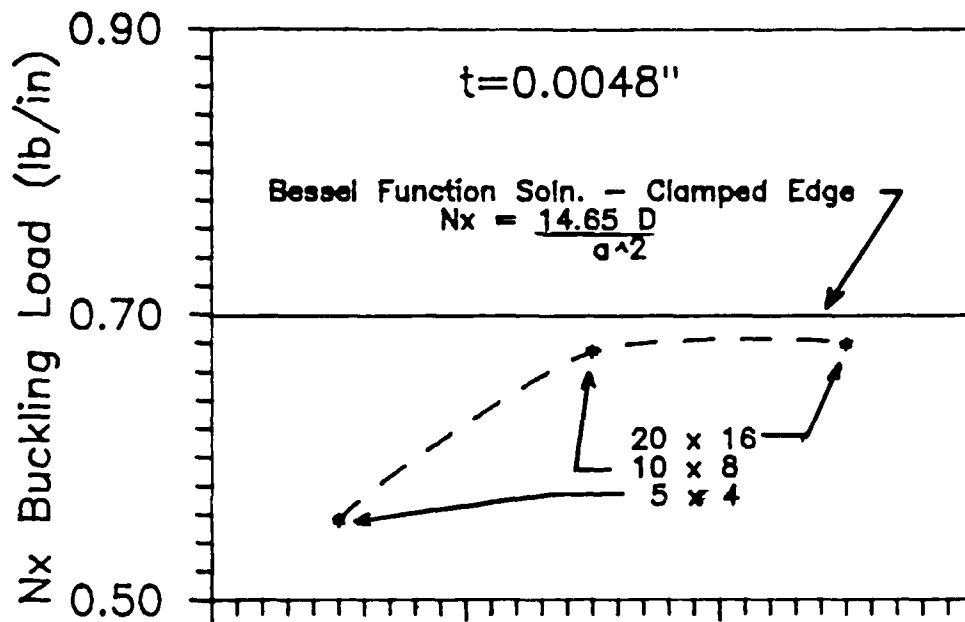


Figure 5.3 - Meshes used for Ckonvergence
Study 5 x 4 and 10 x 8

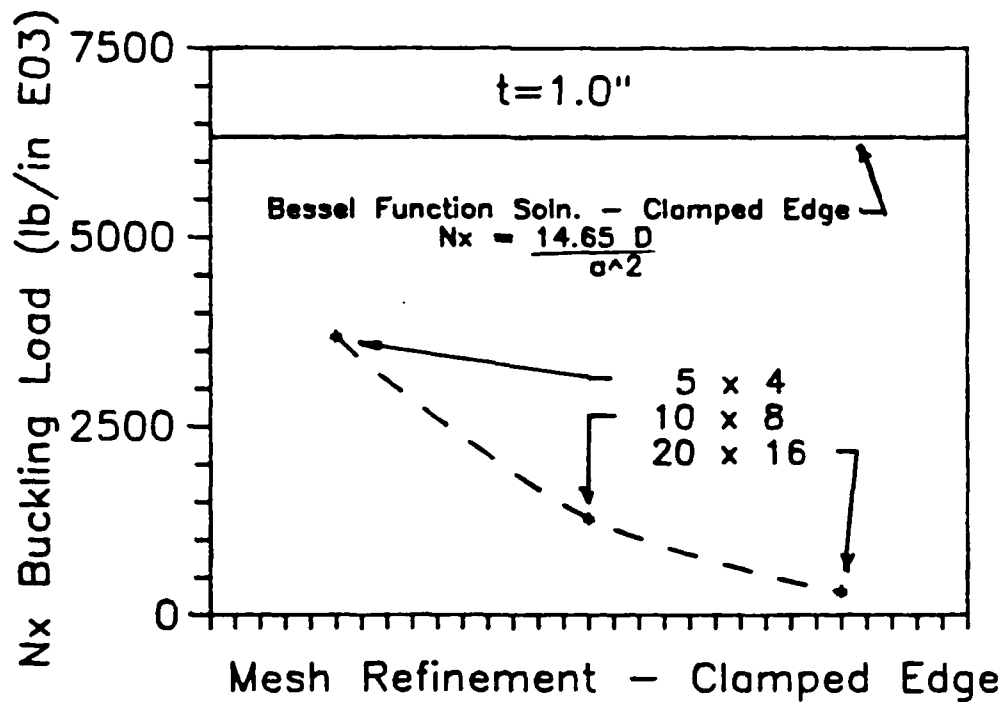
Bessel function solutions was obtained with the 10x8 mesh (fig 5.4 and table 5.2). During this convergence study, initial models were run with a thickness of one inch to speed the computations of the closed form solution. These models gave results that diverged from the closed form solutions as the mesh was refined (fig 5.5). This is probably due to the fact that STAGSC-1 was developed using thin shell theory with a small linear rotation assumption. Geometries that are clearly three dimensional (having a length to thickness ratio less than 10) should be avoided when using STAGSC-1.

A model used by Shivakumar and Whitcomb at NASA Langley Research Center [13] for their research with elliptical delaminations was also run (see fig 5.6). They had obtained convergence with this model for anisotropic lay-ups, so it was used in this study to check the accuracy of the 10 x 8 model. Shivakumar and Whitcomb's model uses the TRINC 320 triangular plate element (fig 5.7) which has 18 degrees of freedom: three translations and two rotations at each of the corner nodes plus edge rotations at midside nodes. The in-plane shape functions are linear for this element and bending is piecewise cubic [10]. This model had 738 degrees of freedom as opposed to the 377 degrees of freedom in the 10x8 model using the QUAFF 410. Therefore, it was a more expensive model to run. Whitcomb's model, using the 320 element, correlated well with the closed form Bessel solution, but not as closely as the models using the QUAFF 410 rectangular elements.



Mesh Refinement - Clamped Edge

Figure 5.4 - Convergence for Circular Disc - $h=0.0048''$



Mesh Refinement - Clamped Edge

Figure 5.5 - Divergence for Circular Disc - $h=1.000''$

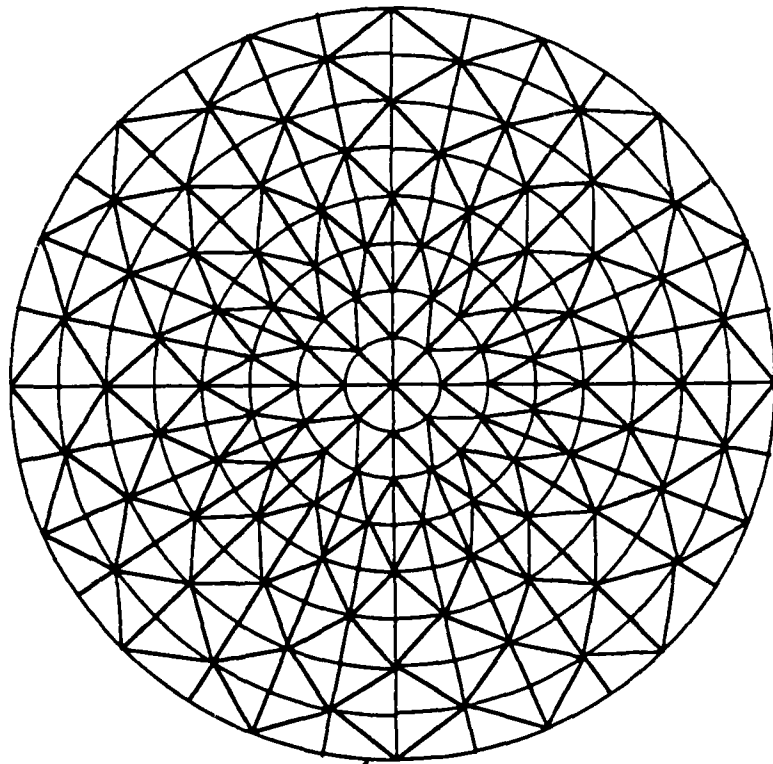
<u>Mesh Refinement</u>	<u>Element Type</u>	<u>90 Model DOF</u>	<u>360 Model DOF</u>
5 x 4	410	71	-
10 x 8	410	377	1502
20 x 16	410	1703	-
9 x 8	320	738	1841

Table 5.2 - Number of Degrees of Freedom for Various Circular Disc Models

<u>Mesh</u>	<u>Diam.*</u>	<u>h (in)</u>	<u>Element</u>	<u>BC</u>	<u>Nx (lb/in)</u>
5 x 4	4i	0.0048	410	SS	0.2028
5 x 4	4i	0.0048	410	CL	0.6990
5 x 4	4i	1.0000	410	CL	3,677,000
10 x 8	2i	0.0048	410	CL	2.915
10 x 8	2o	0.0048	410	CL	0.5227
10 x 8	4i	0.0048	410	CL	0.6791
10 x 8	4o	0.0048	410	CL	0.1307
10 x 8	4i	1.0000	410	CL	1,270,600
20 x 16	4i	0.0048	410	CL	0.6740
20 x 16	4i	1.0000	410	CL	311,600
10 x 29	2a	0.0048	410	CL	4.5731
10 x 29	4a	0.0048	410	CL	1.1572
10 x 29	4a	0.0052	410	CL	1.4713
9 x 33	4a	0.0048	320	CL	1.0670
9 x 33	2a	0.0048	320	CL	4.7170
9 x 33	2a	0.0052	320	CL	5.9452
9 x 33	2a	0.0048	320	CL	4.4947(y free)
9 x 33	2a	0.0048	320	CL	4.6300(\$G1)

Table 5.2a - Circular Disc STAGSC-1 Results

* a-(0/45) i-isotropic o-orthotropic



Boundary Conditions:
 $u=v=B, x=B, z$ Free
 $w=B, y$ Constrained

Figure 5.6 - 9 x 33 Mesh with 320 Element

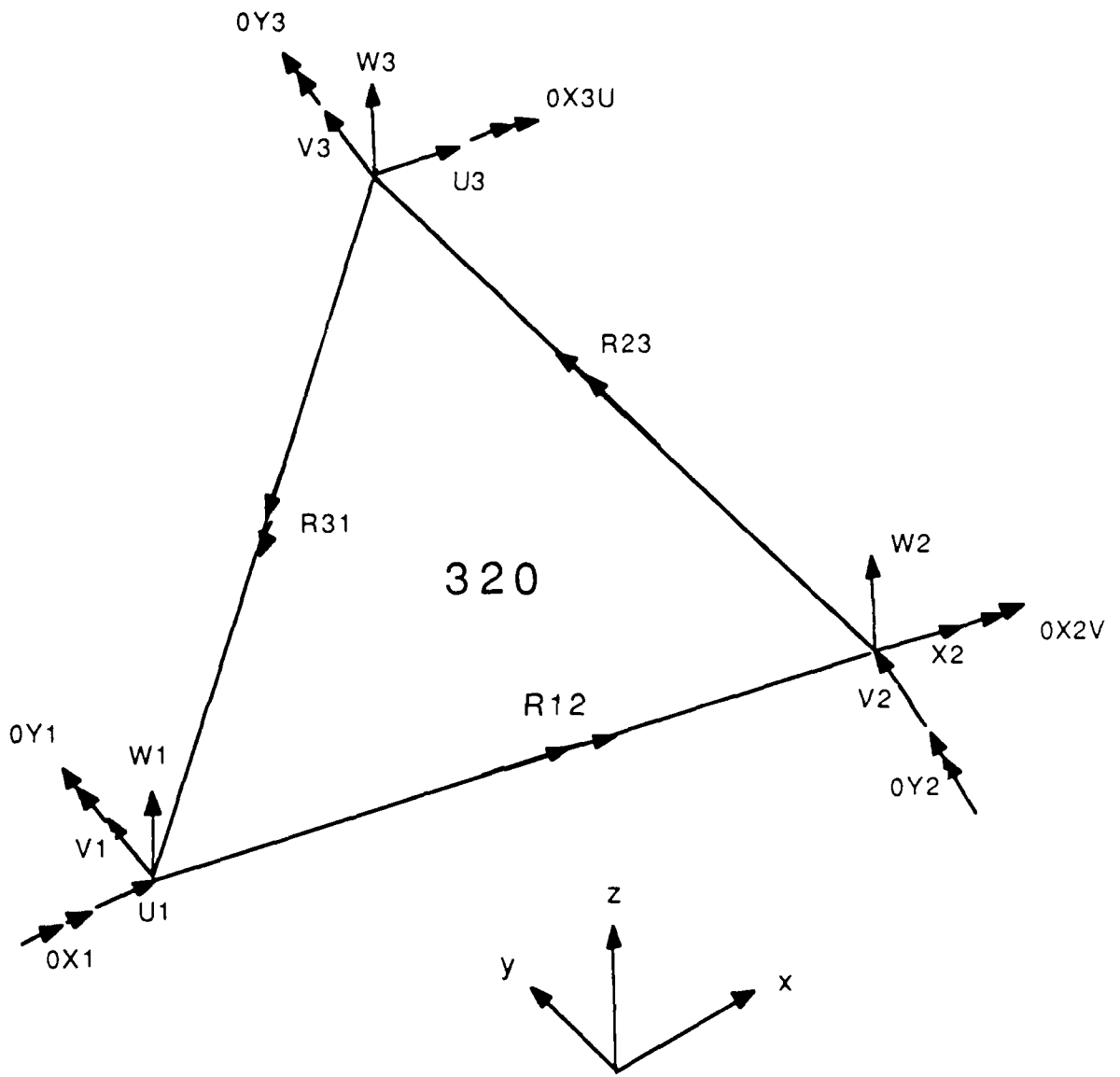


Figure 5.7 - STAGSC-1 TRINC 320 Element

Thus, the 10x8 QJAF 410 model shown in figure 5.7a was used to obtain N_x at buckling for the circular delaminated region, N_{x3} . Also determined using this model was the nominal ϵ_x strain in the sublaminde at local buckling. This strain was then used in the plane strain model discussed in the next section to determine an equivalent N_x value in an eight ply laminate, N_{x4} . This force resultant is the force resultant in an eight ply plane strain model associated with the strain at buckling for a two ply, (0/-45) circular sublaminde.

Also calculated for this STAGSC-1 model was the average normal stress at the sublaminde boundary at local buckling. From the STAGSC-1 output for a two inch delamination, the average N_x value for an axisymmetric edge displacement of 0.001 inches was 48.136 lb/in. This value was then multiplied by the eigenvalue, 0.095, to determine the average force resultant at the boundary at the onset of sublaminde instability. This force resultant was then divided by the cross section dimension of the (0/-45) plies, 2×0.0048 ", to determine the average normal stress, 476.3 psi, at the sublaminde boundary at local buckling of the model. This stress will be used in the next section as a comparison to check the validity of the plane strain model.

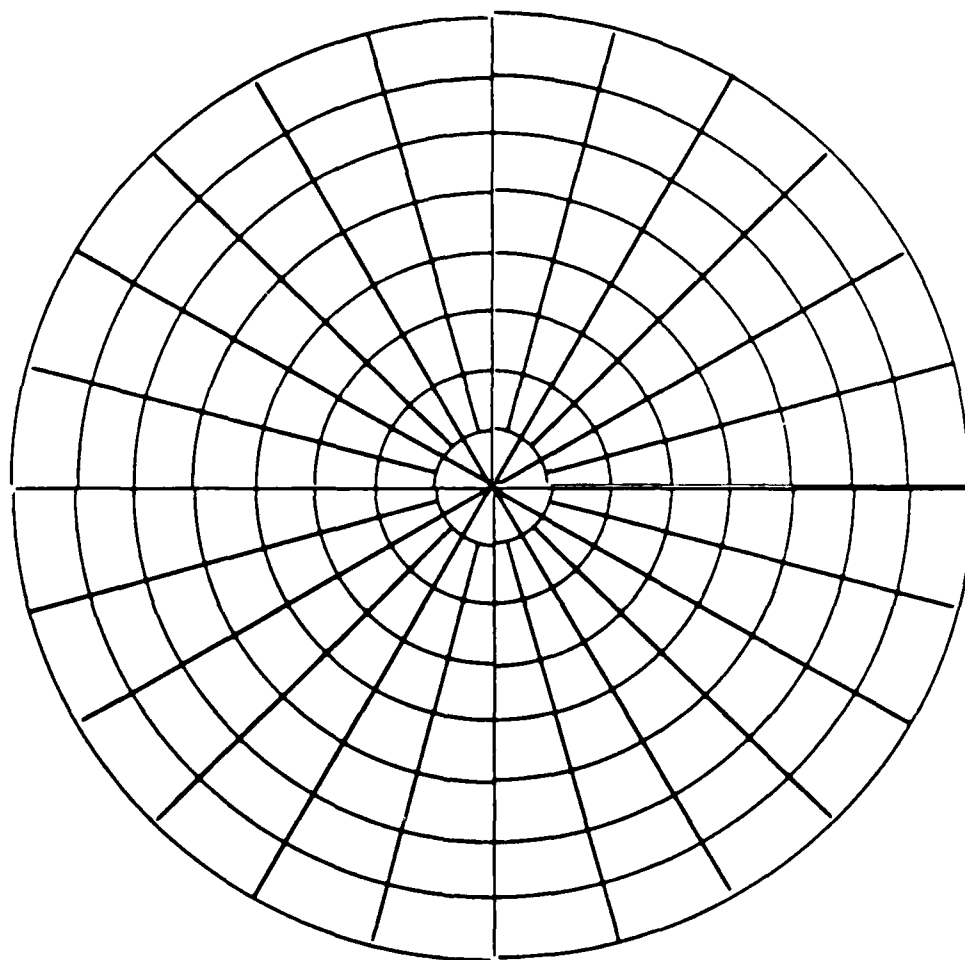


Figure 5.7a - 10 x 33 Mesh with 410 Element

Plane Strain Finite Element Model

The plane strain finite element code used for this analysis was developed by Dr. Sandhu [21] of the Air Force Flight Dynamics Lab. The model is used in this analysis to tie the strain at local sublaminar buckling to the strain in a plane strain section of the curved panel. The strain in this eight ply plane strain model could then be used to calculate a plane load which would cause the sublaminar to buckle.

The problem was modeled as an eight ply plane strain section containing a delamination between the second and third plies (see fig 5.8). This delamination was modeled as a crack having no thickness in the z-direction by defining two node points at each station along the delamination length. Also, the mesh is highly refined in the vicinity of the tip of the delamination since this is where the greatest stress concentrations were expected to occur (fig 5.9). Symmetry is used at the midlength of the delamination, with this boundary fixed against rotation and displacement in the x-direction while allowing freedom in the y-direction.

The model was loaded with an end displacement equivalent to the strain required to buckle the (0/-45) sublaminar. This displacement was applied one delamination radius away from the delamination tip so that a uniform cross sectional force resultant could be achieved.

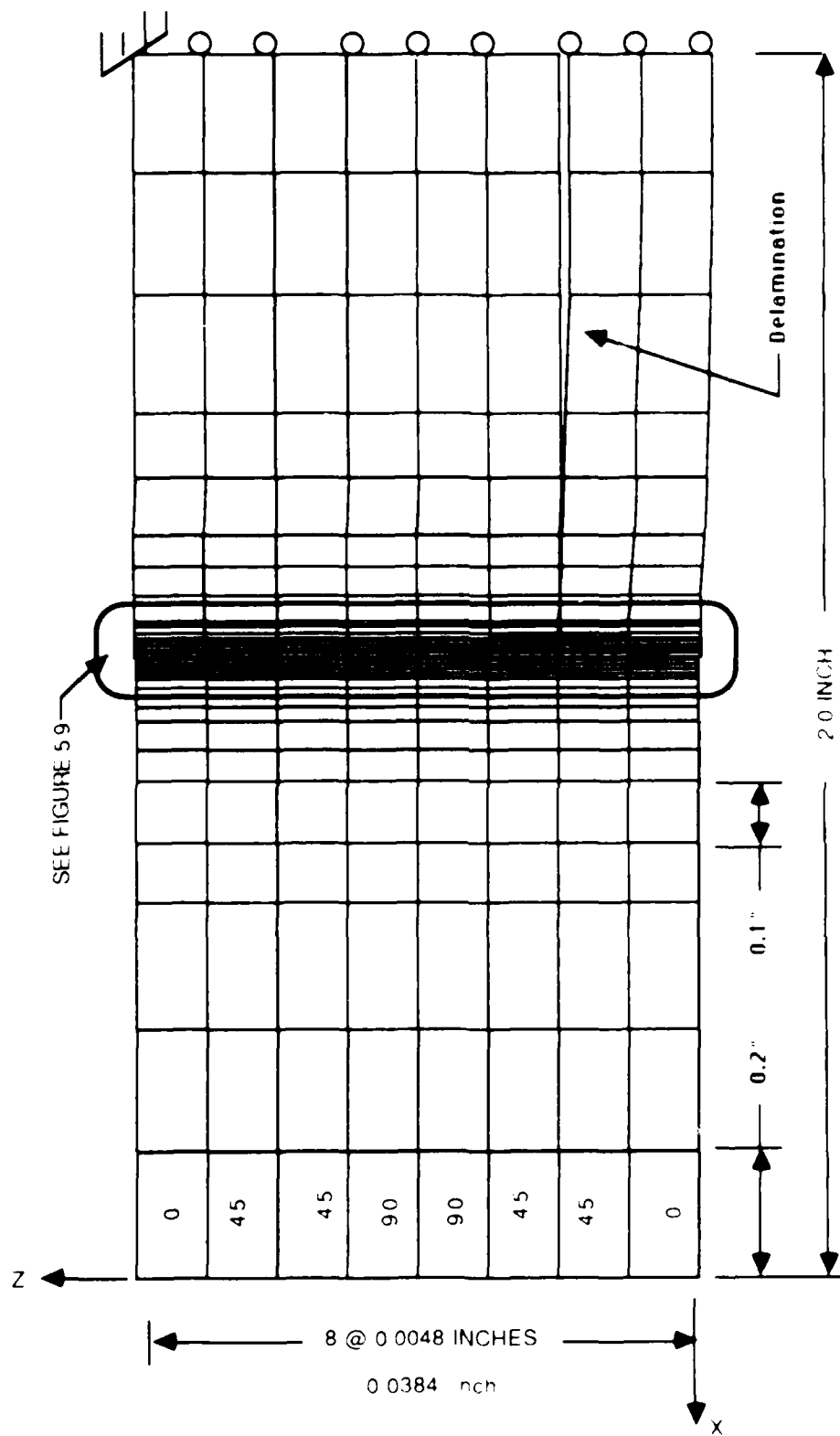


Figure 5.8 - Plane Strain Finite Element Mesh (distorted)

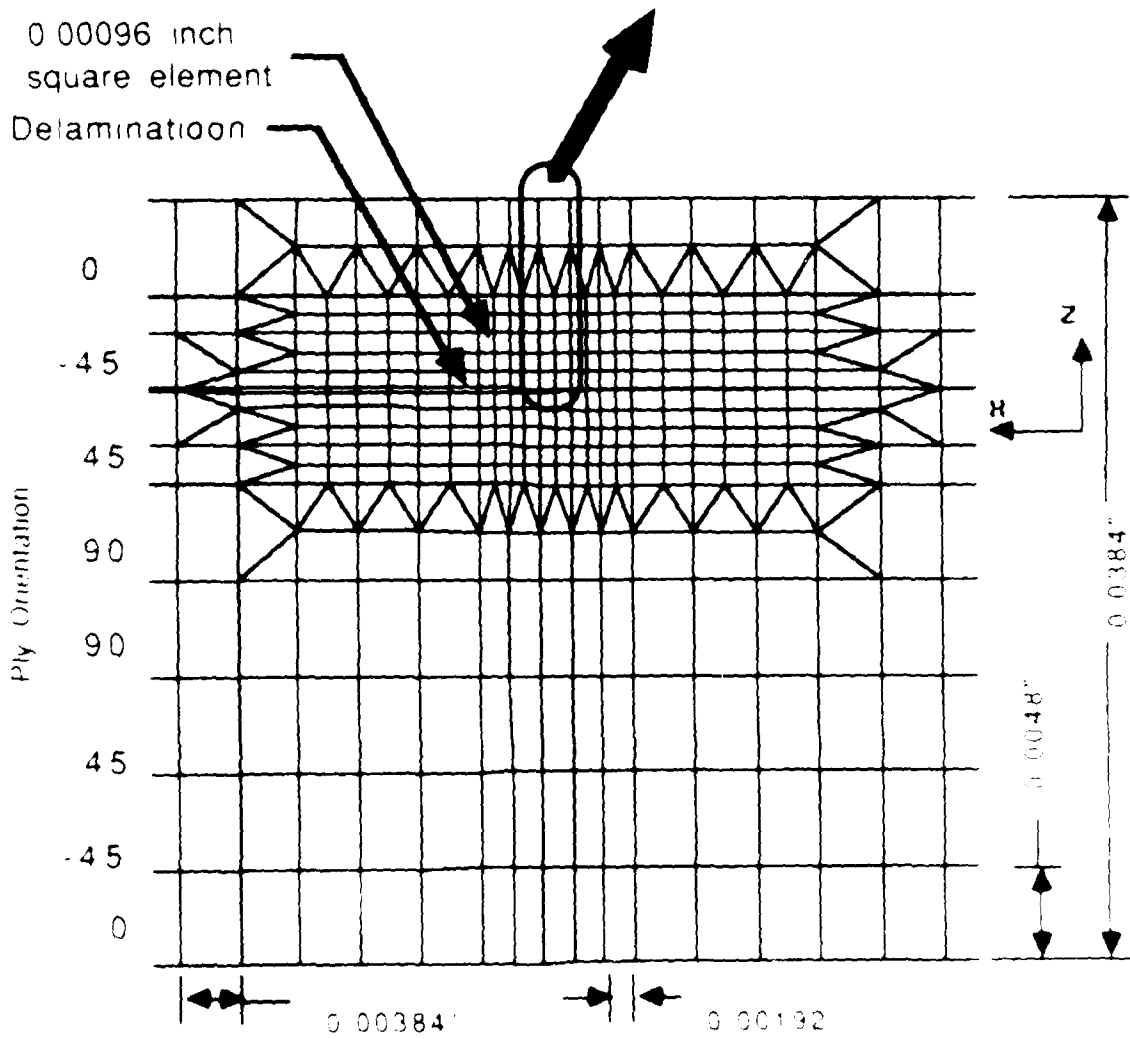
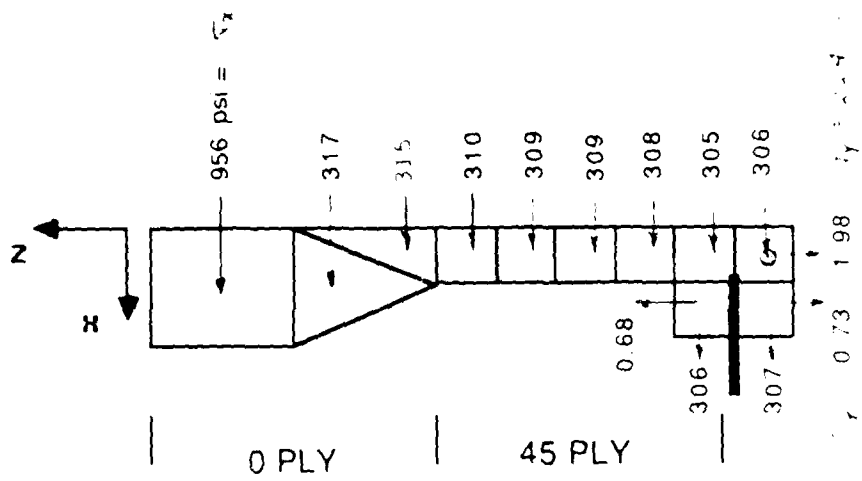


Figure 5.9 - Plane Strain Model at Delamination Tip

The stresses in the vicinity of the delamination tip were recorded and are shown in figure 5.9. The average axial stress in the 0/-45 section of the model was calculated from these stresses to be 472.1 psi. This value is for a plane strain calculation associated with the strain at buckling in the (0/-45) STAGSC-1 circular disc model. The STAGSC-1 circular disc model discussed previously yielded an average stress value of 476.3 psi for this same value of strain. The difference between these two stresses is only 0.88 percent. Therefore, it appears that by using a symmetrical loading pattern, a load distribution over the upper two plies is equivalent to a plane strain phenomenon. Also of note in this plane strain model is the magnitude of stresses in the z-direction. In the vicinity of the delamination tip these stresses varied from 0.68 psi to 1.98 psi. This level of stress is inconsequential, and it can be clearly seen that up to the point of sublaminate buckling, there is no danger of mode I crack growth due to these stresses (this was expected since the loading is assumed in the plane of the delamination). Further crack growth features would have to consider the delaminated region in the post-buckling regime, and is beyond the scope of this research.

This plane strain model was designed to determine a force resultant, N_{λ} , thru an eight ply plane strain section of the composite. This force resultant is the N_{λ} value in a past section of eight ply section associated with the strain

at sublaminar instability for a two ply (0/-45) delamination.

Now, the strain in the curved 12 inch panel resulting from a panel load has been related to a force resultant in a plane strain model; and now the strain in a circular disc at local buckling has been related to a force resultant in a plane strain model. It is now possible to calculate the load which when applied to the top edge of the 12 inch curved panel will cause local instability of a delaminated region of the panel. This calculation is explained in the next section.

Plane Strain Model - No Delamination

A plane strain analysis was performed for the laminate to correlate the force resultant and strain in a plane strain model with the force resultant and strain in a plane strain strip of the curved composite panel.

The average N_x value distributed through the model was calculated for the strain (obtained from the curved panel model) that was associated with a displacement at the top edge of the curved 12 inch panel.

First the Q values were calculated for the material:

$$Q_{11} = \frac{E_1}{1 - \nu_{12}\nu_{21}} \quad (5.4)$$

$$Q_{22} = \frac{E_2}{1 - \nu_{12}\nu_{21}} \quad (5.5)$$

$$Q_{66} = G_{12} \quad (5.6)$$

Then the \bar{Q}_{11} values were computed in the x-direction, where θ is the angle between the fiber direction and the panel's x-direction.

$$\bar{Q}_{11} = Q_{11}\cos^4\theta + 2(Q_{12} + 2Q_{66})\sin^2\theta\cos^2\theta + Q_{22}\sin^4\theta \quad (5.7)$$

The stress can be calculated:

$$[\sigma] = [\bar{Q}_{ij}] \{\epsilon\} \quad (5.8)$$

The strain, ϵ_x , is taken from the STAGSC-1 program. It was observed, as previously mentioned, that the panel yields a constant ϵ_x strain. One could quickly compute this strain by using the displacement at the panel's top edge, and dividing this value by the overall length of the panel, thus yielding a σ_x of:

$$\sigma_x = \bar{Q}_{11} \epsilon^o \quad (5.9)$$

The stress is obtained for each of the plies, and a stress resultant, N_{x2} , is calculated. This force resultant is then the value of N_x in the eight ply plane strain strip associated with a deflection induced through loading of the curved panel.

Analytic Prediction

Based on the finite element models discussed in the previous sections, and using linear superposition, the following equation was developed to predict local buckling of the sublaminates:

$$P_f = P * \alpha * \beta \quad (5.10)$$

Where α is the ratio of the force resultant at buckling in the STAGSC-1 circular disc with the force resultant in the curved panel associated with a load P applied to the panel. And β is the ratio of force resultants in the plane strain models.

$$\alpha = N_{x3} / N_{x1} \quad (5.11)$$

$$\beta = N_{x2} / N_{x4} \quad (5.12)$$

P_f \equiv Predicted load in pounds at which local sublaminates snapping will occur.

P \equiv Load in pounds at top edge of the curved panel

N_{x1} \equiv N_x value at buckling for Curved Panel

N_{x2} \equiv N_x value in plane strain model with No Delamination
This value is calculated for a strain equivalent to the strain in the curved panel due to a load, P .

N_{x3} \equiv N_x value at buckling for Circular Disc
Calculated using STAGSC-1 model of sublaminates.

N_{x4} \equiv N_x value for plane strain model containing a delamination. This force resultant is calculated using the strain at buckling for the circular disc model.

Substituting equations (5.11) and (5.12) into (5.10), the predicted load applied to the top of the curved 12 inch panel which would cause local buckling in the delaminated plies is:

$$P_f = P \frac{N_{x3} N_{x2}}{N_{x1} N_{x4}} \quad (5.13)$$

As the average thickness of the laminate plies increases, the value at which local sublaminate snapping will occur also increases. This is seen by noting that N_{x1} (the N_x value for the 12 inch curved panel) increases by panel thickness, h , raised to the 2.06 power (approximately by h^2). N_{x3} for the circular disc increases by approximately the cube of the panel thickness; and N_{x2} and N_{x4} both increase linearly with thickness. Therefore, the snapping of the sublaminate was expected to increase linearly with panel thickness. This linear variation of predicted snapping load was plotted as a linear prediction of snapping load versus panel thickness in figure 5.10. Using this relation, the load causing local instability of a sublaminate could be determined based on panel thickness. This relation appeared to be valid for the range of panel thicknesses used in this research.

The relations between analytic predictions and experimental snapping values are shown in figure 5.10 and in table 5.3. The data points shown in figure 5.10 are in pairs. Each pair represents two panels from the same mold

with the same panel thickness. These data pairs are shown connected by a line with a bar at midheight representing the average snapping load for that pair. The snapping loads for the two inch delaminations fell below the analytic predictions. This was expected since linear models were used in the analysis, which in general increases the load at which predicted failure will occur. For these panels, the experimental snapping loads differed from the analytic predictions by a mean of 31.3 percent with a standard deviation of 21.4 percent.

Only three data points were obtained for the snapping of the four inch delaminations. This is a very sparse data set; however, it was noted that these panels tended to snap at higher load values than were predicted. A possible explanation for this is that the four inch sublaminates were being restrained by the base laminate, and were therefore buckling at higher modes. These panels differed from the analytic predictions by a mean of 14.6 with a standard deviation of 5.2.

This analytic technique is seen to give predictions of local sublaminata buckling within approximately 30 percent of experimental values. These predictions are good engineering approximations obtained using a linear two dimensional model to predict a nonlinear, three dimensional local instability.

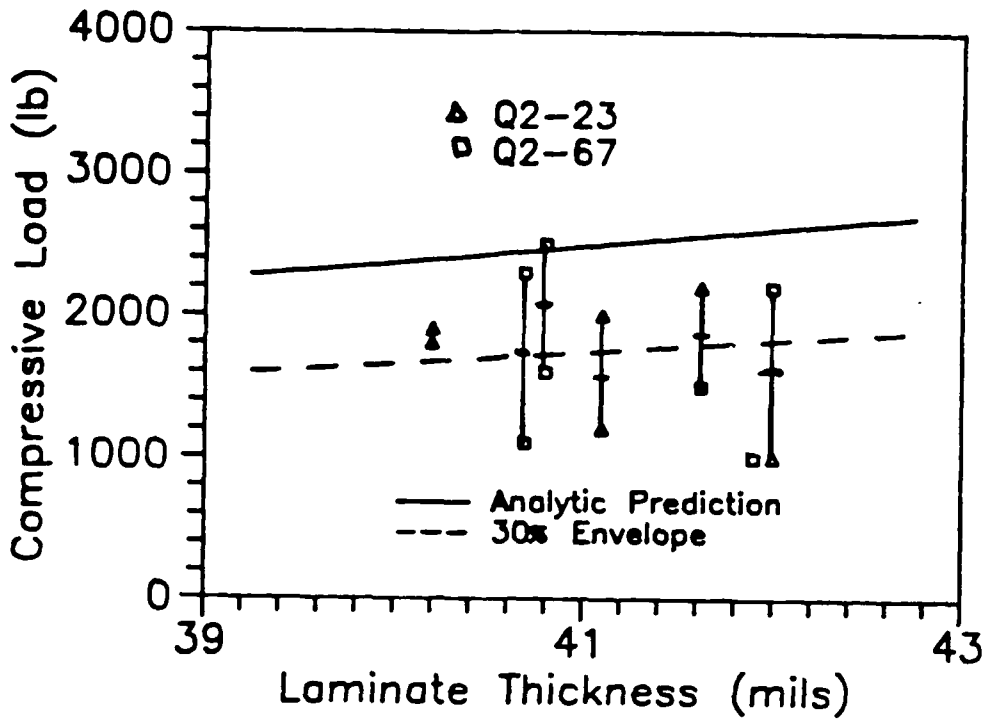


Figure 5.10 - Strain Reversal Load - 2" Delaminations

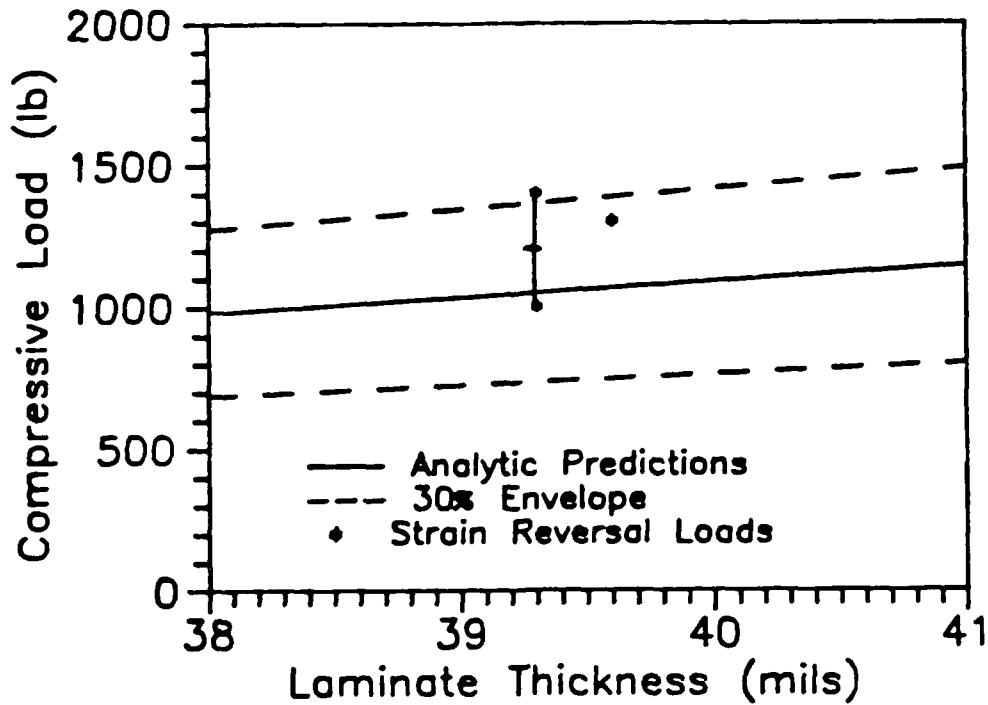


Figure 5.10 - Strain Reversal Load - 4" Delaminations

<u>PANEL</u>	<u>t (mils)</u>	<u>EXPER (lbs)</u>	<u>ANALYSIS</u>	<u>% DIFF</u>
Q2-23-1	40.69	1100	2451	55.1
Q2-23-2	40.69	2300	2451	6.2
Q2-23-3*	40.80	1600	2464	35.1
Q2-23-4*	40.80	2500	2464	-1.5
Q2-23-5*	41.90	1000	2599	61.5
Q2-23-6**	41.62	1500	2564	41.5
Q2-23-7**	42.00	2200	2611	15.7
Q2-67-1	40.20	1900	2392	20.6
Q2-67-2	40.20	1800	2392	24.8
Q2-67-3*	41.10	2000	2500	20.0
Q2-67-4*	41.10	1200	2500	52.0
Q2-67-5**	42.00	1000	2611	61.7
Q2-67-6**	41.62	2200	2564	14.2
Q4-23-1	39.30	1000	1168	14.4
Q4-23-2	39.30	1400	1168	19.9
Q4-67-1	39.60	????	1187	????
Q4-67-2	39.60	1300	1187	9.5

NOTES: * - 3000 lb seating load
 ** - 2 pieces of teflon, 3000 lb seating load

Table 5.3 - Experimental Delamination Snapping Loads

VI. CONCLUSIONS

Based on the experimental and analytic results, the following conclusions can be made for graphite/epoxy cylindrical composite panels which have been subjected to axially compressive loads:

1. In general, the linear bifurcation predictions obtained using the STAGSC-1 finite element code were in close agreement with experimental results. For undamaged panels, the experimental global buckling load was an average of 12.9 percent lower than predicted values with a standard deviation of 2.8 percent.

2. Surface damage to composite panels tends to decrease the panel stiffness resulting in a decrease in critical buckling loads. As the surface area that is damaged is enlarged, global buckling loads will in general decrease. However, this study found that for 2 inch diameter surface damage to the exterior ply, average buckling strength actually increased slightly. But, the standard deviation of buckling load also increased, indicating less consistency in panel strength.

3. Higher void contents also caused the global panel buckling strength to increase. This can be understood by considering that panel thickness increased linearly with percent voids, while the buckling load is seen to increase by the square of panel thickness for this geometry. Higher void contents are not desirable, however, as an increase in the void content of a panel increases the chance for moisture absorption and subsequent material degradation.

4. Delaminations in a composite panel, have the potential for more catastrophic failure than surface damage. Delaminations are usually not visually observable and can grow through the laminate with cyclic loadings. For the delamination sizes studied in this thesis, only slight decreases in global panel buckling were noted. However, in general, impact on a composite panel can potentially cause a number of delaminations through the panel thickness. This would decrease panel strength even further and would increase the severity of delamination growth. Buckled sublaminates also have relatively large deformations in the z direction, which could seriously affect the aerodynamics of the structure, and could conceivably result in aircraft instabilities.

5. The phenomenon of local sublaminates snapping of the delaminated plies can be predicted using superposition of a

series of linear finite element models. The use of these models results in a fairly accurate and inexpensive prediction of local instabilities caused by local buckling. It is thought that this analytic technique could be easily extended to shells with different geometries and loading conditions to get a ball park estimate of shell failure loads.

6. Seating loads should be applied to panels prior to experimental testing. These loads should be applied before all fixture supports are tightened to decrease the chance of non-symmetric loading and moments induced by differential fixture movements. Care should be taken to ensure that the panel is trimmed square and that the load is evenly introduced so that non-symmetric buckling can be avoided.

7. The STAGSC-1 bifurcation values for the curved cylindrical panels could be predicted by using a regression curve that related panel thickness to panel buckling loads. Relations were also found to exist for other geometries such as a flat plate and a circular disc. It is thought that similar relations could be easily established for other shell geometries, and that the amount of computer time required to predict buckling of a various thicknesses for a given shell geometry could be greatly reduced.

8. Teflon discs proved to be an excellent debonding material for creating delaminations, with 100 percent delamination observed in all samples. However, when the 0.5 mil teflon was placed adjacent to the exterior ply, a blister effect occurred. This blister was easily visible on the surface of the panel, and contained fractures in the matrix of the delamination running parallel to the fiber direction. Initial finite element models were run to determine the possible cause of this phenomenon. There was no indication in the model results that a temperature differential during curing caused the ply failure. It is postulated that volatiles formed during panel curing were trapped beneath the teflon disc resulting in a vapor pressure which caused an air bubble to form. A more thorough investigation of this problem needs to be attempted.

9. Normal stresses at a delamination were calculated through the (0/-45) cross section of a STAGSC-1 circular plate model. These normal stresses were then compared to an average stress through a (0/-45) cross section of a plane strain model subjected to the same value of strain. The stresses were within 0.88 percent of each other. This indicates that the assumption that the delaminated region of a curved panel can be modeled using a plane strain model is a valid approximation.

The stresses in the vicinity of a delamination crack tip were calculated in a plane strain model. The model was loaded with a strain sufficient to cause buckling of the 0/90-45 delaminated plies. At this load, the stresses in the z-direction at the crack tip were calculated. These stresses, normal to the plane of the delamination, ranged from 0.68 to 1.98 psi. This level of stress is much less than the stress required to initiate crack growth in this material.

APPENDIX A

Constitutive Matrices and Test Data

The Point Stress Laminate Analysis code, SQ5 [11], was used to determine the stiffness matrices for AS4/3501-6 graphite epoxy. For the quasi-isotropic symmetric (0/-45/45/90)_s layup, the coupling stiffness matrix B_{ij} is equal to zero. The matrices are computed for a laminate thickness of 0.0384 inches (corresponding to a ply thickness of 0.0048 inches) so that a comparison can be made to results reported in previous work with cylindrical composite panels [7,15]. Matrices are then computed for the median thickness (0.0416) of the panels tested in this study. Finally values are shown for a (0/-45) layup so that a plane strain evaluation could be made of the delaminated region of the panel.

For $h=0.0384$ inches, quasi-isotropic (ply thickness $t=0.0048$):

$$A_{ij} = \begin{bmatrix} 315.730 & 92.535 & 0.000 \\ 92.535 & 315.730 & 0.000 \\ 0.000 & 0.000 & 111.600 \end{bmatrix} \times 10^3 \text{ lb/in}$$

$$B_{ij} = 0$$

$$D_{ij} = \begin{bmatrix} 63.765 & 9.605 & -3.867 \\ 9.605 & 17.362 & -3.867 \\ -3.867 & -3.867 & 11.947 \end{bmatrix} \text{ lb-in}$$

For $h=0.0416$, $(0/-45/45/90)_s$ Ply thickness $t=0.0052$:

$$A_{ij} = \begin{bmatrix} 342.043 & 100.247 & 0.000 \\ 100.247 & 342.043 & 0.000 \\ 0.000 & 0.000 & 120.898 \end{bmatrix} \times 10^3 \text{ lb/in}$$

$$B_{ij} = 0$$

$$D_{ij} = \begin{bmatrix} 81.071 & 12.211 & -4.916 \\ 12.211 & 22.074 & -4.916 \\ -4.916 & -4.916 & 15.190 \end{bmatrix} \text{ lb-in}$$

For $(0/-45)$, Ply thickness $t=0.0052$ in:

$$A_{ij} = \begin{bmatrix} 130.966 & 25.062 & -22.728 \\ 25.062 & 40.056 & -22.728 \\ -22.728 & -22.728 & 30.225 \end{bmatrix} \times 10^3 \text{ lb/in}$$

$$B_{ij} = \begin{bmatrix} -172.161 & 53.978 & -59.092 \\ 53.978 & 64.206 & -59.092 \\ -59.092 & -59.092 & 53.973 \end{bmatrix} \text{ lb}$$

$$D_{ij} = \begin{bmatrix} 1.18044 & 0.22589 & -0.20485 \\ 0.22589 & 0.36103 & -0.20485 \\ -0.20485 & -0.20485 & 0.27242 \end{bmatrix} \text{ lb-in}$$

For (0/-45) ply thickness $t=0.0048$ in.:

$$A_{ij} = \begin{bmatrix} 120.890 & 23.134 & -20.979 \\ 23.134 & 36.974 & 20.979 \\ -20.979 & -20.979 & 27.900 \end{bmatrix} \times 10^3 \text{ lb/in}$$

$$B_{ij} = \begin{bmatrix} 146.690 & 45.993 & -50.350 \\ 45.993 & 54.708 & -50.350 \\ -50.350 & -50.350 & 45.993 \end{bmatrix} \text{ lb}$$

$$D_{ij} = \begin{bmatrix} 0.92845 & 0.17767 & -0.16112 \\ 0.17767 & 0.28396 & -0.16112 \\ -0.16112 & -0.16112 & 0.21427 \end{bmatrix} \text{ lb-in}$$

The lab measurements and experimental test data for this thesis are recorded in the tables on the following pages.

<u>PANEL</u>	<u>t (mils)</u>	<u>% VOIDS</u>	<u>EXPER (lbs)</u>	<u>STAGSC-1</u>	<u>% DIFF</u>
Q0-00-1	40.01	0.0972	4795	5263	8.9
Q0-00-2	40.01	0.0972	4445	5263	15.5
Q0-00-3	41.50	0.4341	4779	5662	15.6
Q0-00-4	41.50	0.4341	4995	5662	11.8
Q0-00-5	41.50	0.9621	4945	5662	12.7
Q2-12-1	42.07	4.3671	5085	5819	12.6
Q2-12-2	41.38	4.3583	5214	5630	7.4
Q2-12-3	41.38	4.3583	5321	5630	5.5
Q2-12-4	40.76	2.2760	4365	5462	20.1
Q2-12-5	40.15	2.1762	5100	5300	3.8
Q2-12-6	40.15	2.1762	5149	5300	2.8
Q2-12-7	41.61	1.2224	5356	5692	5.9
Q2-12-8	41.61	1.2224	5177	5692	9.0
Q2-23-1	40.69	0.1666	4692	5443	13.8
Q2-23-2	40.69	0.1666	4570	5443	16.0
Q2-23-3*	40.80	-0.0854	4697	5473	14.2
Q2-23-4*	40.80	-0.0854	4738	5473	13.4
Q2-23-5*	41.90	2.0222	4703	5772	18.5
Q2-23-6**	41.62	0.3211	5325	5695	6.5
Q2-23-7**	42.00	0.4244	5160	5800	11.0
Q2-67-1	40.20	0.3775	4233	5313	20.3
Q2-67-2	40.20	0.3775	4673	5313	12.0
Q2-67-3*	41.10	0.4962	5357	5554	3.5
Q2-67-4*	41.10	0.4962	4255	5554	23.4
Q2-67-5**	42.00	0.4244	5295	5800	8.7
Q2-67-6**	41.62	0.3211	5130	5695	9.9

Table A.1 - Panel Test Data (continued on next page)

<u>PANEL</u>	<u>t (mils)</u>	<u>% VOIDS</u>	<u>EXPER (lbs)</u>	<u>STAGSC-1</u>	<u>% DIFF</u>
Q2-78-1	42.61	3.5801	5567*	5969	6.7
Q2-78-2	42.61	3.5801	5524	5969	7.5
Q2-78-3	41.84	0.8887	4795	5755	16.7
Q2-78-4	41.84	0.8887	5659	5755	1.7
Q4-12-1	41.90	4.4354	5229	5772	9.4
Q4-12-2	41.90	4.4354	4885	5772	15.4
Q4-23-1	39.30	0.4781	5224	5078	-2.9
Q4-23-2	39.30	0.4781	4823	5078	5.0
Q4-67-1	39.60	0.7278	4437	5156	14.2
Q4-67-2	39.60	0.7278	4500	5156	11.4
Q4-78-1	41.77	0.1169	4787	5736	16.5
Q4-78-2	41.77	0.1169	4851	5736	15.4

NOTES: # - Nonsymmetric buckling mode
* - 3000 lb seating load
** - 2 pieces of teflon, 3000 lb seating load

For SN 1-12 SG1 and SG2 at bottom of panel

Table A.1 - Experimental Data continued

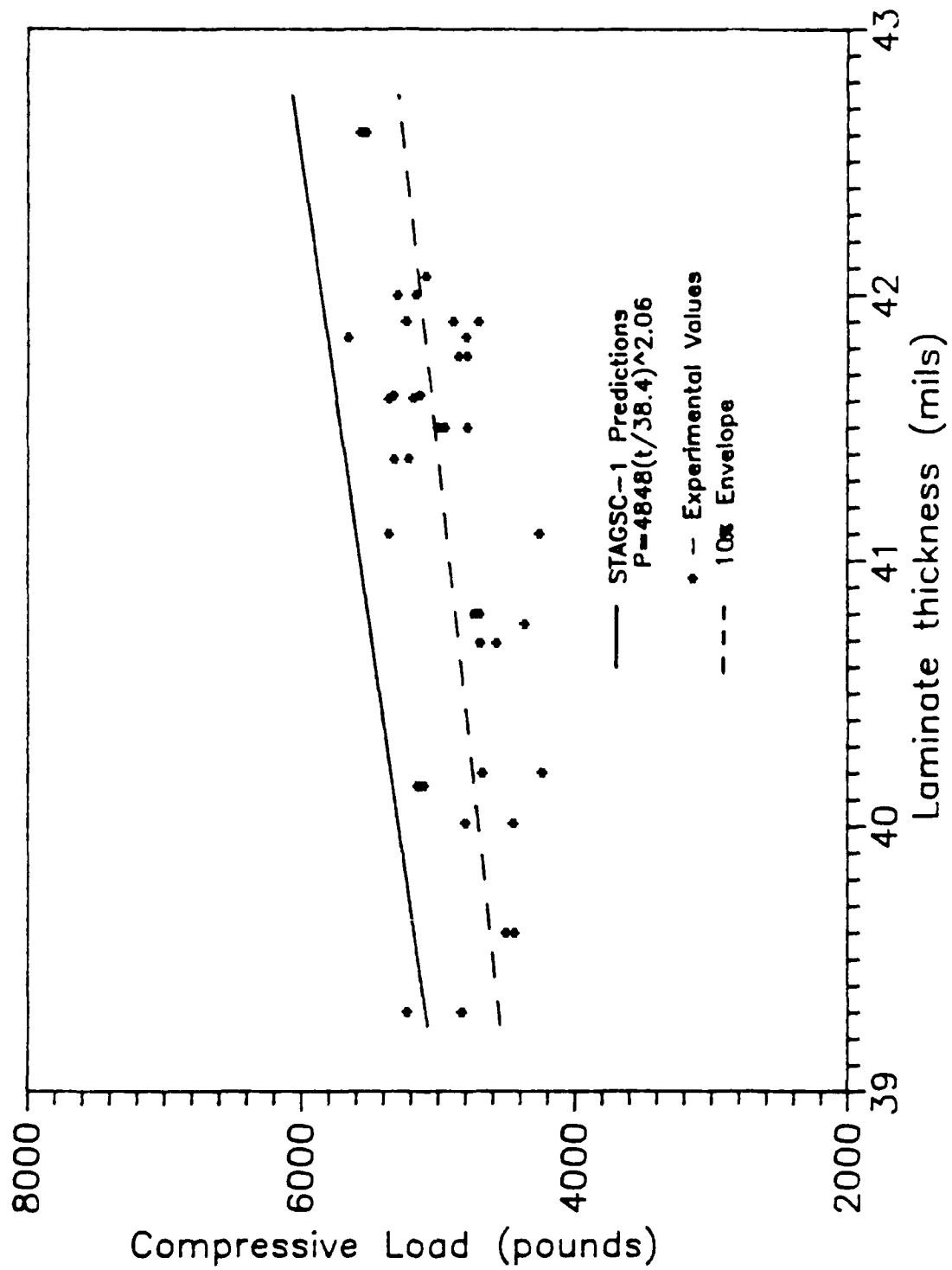


Figure A.1 - Load vs Thickness for all Panels Tested

Panel Number	Delam Size & Loc	Panel Size	Panel Thickness	Ply	Thickness	% Resin	% Voids
RW13987-1	NONE	15.5"x32"	0.0400769		5.01E-03	25.5997	0.0972
RW13987-2	NONE	20"x40"	0.0415		5.19E-03	26.2424	0.4341
RW16287-1	4" Center, plies 7-8	15.5"x32"	0.04169		5.21E-03	25.5123	0.1169
RW16287-2	4" Center, plies 1-2	15.5"x32"	0.0419		5.24E-03	26.7101	4.4354
RW16287-3	2" Center, plies 7-8	15.5"x32"	0.04261		5.33E-03	26.7125	3.5801
RW16287-4	2" Center, plies 1-2	15.5"x32"	0.0415		5.19E-03	26.356	2.1762
RW16787-5	4" Center, plies 7-8	20"x40"	0.0426		5.33E-03	27.6317	3.5806
RW16787-6	4" Center, plies 1-2	20"x40"	0.0409		5.11E-03	25.8153	-0.0091
RW16787-7	2" Center, plies 7-8	20"x40"	0.03969		4.96E-03	25.0684	-0.2282
RW16787-8	2" Center, plies 1-2	20"x40"	0.04207		5.26E-03	27.0426	4.3671
RW16987-9	2" On Left; plies 1-2	15.5"x32"	0.0406		5.08E-03	25.1299	0.125
RW16987-10	4" On Left; plies 1-2	15.5"x32"	0.0404		5.05E-03	25.8795	0.279
RW16987-11	2" On Left; plies 7-8	15.5"x32"	0.04438		5.55E-03	26.2323	3.9485
RW16987-12	4" On Left; plies 7-8	15.5"x32"	0.04192		5.24E-03	25.6153	0.9036
RW20387-9	2" At End; plies 7-8	15.5"x32"	0.04153		5.19E-03	26.0934	1.4018
RW20387-10	2" At End; plies 1-2	15.5"x32"	0.04138		5.17E-03	26.8	4.3583
RW20387-11	2" 1/4" Center; 7-8	20"x40"	0.04084		5.11E-03	25.4502	-0.1026
RW20387-12	2" 1/4" Center; 1-2	20"x40"	0.04076		5.10E-03	25.9062	2.276
RW20887-13	4" Center; plies 6-7	15.5"x32"	0.0396		4.95E-03	24.7026	0.7278
RW20887-14	4" Center; plies 2-3	15.5"x32"	0.0393		4.91E-03	25.4356	0.4781
RW20887-15	2" Center; plies 6-7	15.5"x32"	0.0402		5.03E-03	25.14	0.3775
RW20887-16	2" Center; plies 2-3	15.5"x32"	0.04069		5.09E-03	25.1062	0.1666
RW21087-17	2" Center; plies 7-8	15.5"x32"	0.04184		5.23E-03	25.6292	0.8887
RW21087-18	2" Center; plies 1-2	15.5"x32"	0.04161		5.20E-03	25.992	1.2224
RW32887-1	2" Center; plies 2-3	15.5"x32"	0.0408		5.10E-03		
RW32887-2	No Delaminations	15.5"x32"	0.0415		5.19E-03		
RW32887-3	2" Center; pl 2-3, 6-7	15.5"x32"	0.0419		5.24E-03		
RW32887-4	2" Center; plies 6-7	15.5"x32"	0.0411		5.14E-03		
RW01288-1	2" Center; plies 2-3	15.5"x32"					
RW01288-2	2" Center; plies 6-7	15.5"x32"					

Table A.2 - Panel Lab Data - Density, Thickness, Voids

Appendix B

Sample Computer Input Decks

A researcher can invest an extremely large amount of time learning a computer operating system, and then learning the various computer codes necessary to model his problem. This section of the thesis is presented as a guide for those not familiar with STAGSC-1 or the NOS operating system found on the AFWAL Cyber computer system. A sampling of STAGSC-1 input data decks for various shell geometries and SQ5 input decks are presented and briefly discussed along with some common commands that a NOS user will find useful.

Most of the jobs that were run on the Cyber for this research were STAGSC-1 finite element models. Since a typical linear STAGSC-1 run for this thesis used 50-150 cp seconds of computer time, these jobs must be submitted as batch jobs. The following batch job (fig B.1) can be given a filename such as bjob, and then submitted using the command {submit,bjob,to} where the {to} at the end of the command sends the dayfile output to the wait queue. A dayfile is useful in determining the amount of computer time used in a computer run, and in tracking the command sequence that was used by the batch job to run the program. After a job is submitted, the researcher should give the command {fi}. This command gives the status of all current executing jobs, and includes a four letter job name for the terminal.

```
/JOB
WILDER,P2.
/USER
CHARGE,*.
SETTL(*).
ATTACH,STAGS1/UN=D820090.
ATTACH,STAGS2/UN=D820090.
GET, filename.
STAGS1, filename.
RETURN,STAGS1.
STAGS2.
RETURN,STAGS2.
REWIND,*.
ROUTE,OUTPUT,DC=PR,UN=AL,UJN=BWILDER,ST=CSA.
/EOB
```

Figure B.1 - Typical STAGSC-1 Batch Job

The batch job shown above should be changed for another user. The new user's name should replace WILDER and BWILDER, and the filename of the STAGSC-1 input deck to be run should replace *filename*. The batch job shown is set up to send the output to the printer. Alternatively, the output could be sent to a file by changing the ROUTE command.

The STAGSC-1 input deck shown below is the input that was used to analyze the linear buckling load for the curved cylindrical panels used in this study. This model is a model for an eight ply laminate with 0.0048 inch thick plies. The (\$) seen in the input deck is a divider between fortran input and user comments. The \$C1 card is the load multiplier for the system and multiplies the load entered on the \$Q3 card to compute the total system load.

LINEAR ANALYSIS - 12 IN PANEL - BIFURCATION - DELTA=.001 - C1=1	
1,1,1,1,0,0,1	\$B 1 ANALYSIS TYPE
1	\$B2 # SHELL UNITS
1,0,1	\$B3
1.0	\$C1 LOAD INCR
1,0,650,0,0	\$D2 EIGENVALUE CNTRL
1,1.0	\$D3 CLUSTER DEFN
19,19	\$F1 NO. ROWS COLS
1	\$I1 MATL #1
18.844E06,0.0218128,.91E06,1.,1.,1.468E06,1.	\$I2 MATL PROP
1,1,8	\$K1 8 LAMINAE
1,0.00480,0.0	\$K2 PLY, T, ORIENT
1,0.00480,-45.0	\$K2
1,0.00480,45.0	\$K2
1,0.00480,90.0	\$K2
1,0.00480,90.0	\$K2
1,0.00480,45.0	\$K2
1,0.00480,-45.0	\$K2
1,0.00480,0.0	\$K2
5	\$M1 SHELL TYPE
0.0,12.0,0.0,57.3,12.0	\$M2A SHELL GEOMETRY
1	\$M5
410	\$N1 ELEMENT TYPE
0,0	\$P1
100,000	\$P2 BOUNDARY COND
110,100	\$P2
000,000	\$P2
110,100	\$P2
1	\$Q1
1,1,0	\$Q2
0.001,-1,1,1,0,0	\$Q3 LOAD
2,2,2,0,0,2	\$R1 OUTPUT FORMAT

Figure B.2 - STAGSC-1 Input Deck for a Curved 12 inch Panel

The input deck shown in figure B.3 below was one of the input decks used in this study to perform the convergence study for buckling of a circular plate under a uniform axial displacement. This particular input deck is for a 10x8, 90 degree model. The material property input card \$I2 shows the input required for an isotropic material. The shell geometry card \$M1 is the card which defines this shell as an annular ring. The \$M2A card gives the radius of the inner boundary, the radius of the outer boundary, and the angles in degrees swept out by the two side boundaries. The element type chosen for this model was the QUA4 410 element. Using this element and the given plate geometry, STAGSC-1 will automatically generate each element in the mesh at intervals defined by the user. The four \$P2 cards are the cards which define the constraints at the shell's boundaries in the following order: displacement in the x,y,z directions, rotations with respect to x, y, z. A one signifies freedom to move while a zero signifies a constrained node. The user has the option of specifying a separate load and constraint at each node as can be seen in figure B.5 or of maintaining the same constraints and loads at every node on a boundary as is done in figure B.4. For this case, the third card specifies a clamped edge condition for the outside arc of the model. The displacement load is defined by the \$Q3 card. This card not only gives the displacement value but the boundary to which it applied.

LINEAR ANALYSIS - 2IN DISK OPLY - BIFUR - DISK5 - ISOTROPIC	
1,1,1,1,0,0,1	\$B1 ANALYSIS TYPE
1	\$B2 NO. SHELL UNITS
1,0,1	\$B3
1.0	\$C1 LOAD INCR
1,0,650,0,0	\$D2 EIGENVALUE CNTRL
1,.001	\$D3 CLUSTER DEFN
10,8	\$F1 NO. ROWS COLS
1	\$I1 MATL #1
18.844E06,0.3	\$I2 MATL PROP
1,1,1	\$K1 8 LAMINAE
1,0.00480,0.0	\$K2 PLY THICK, ORIENT
4	\$M1 SHELL TYPE
00.0,1.0,0.0,90.0	\$M2A SHELL GEOMETRY
1	\$M5
410	\$N1 ELEMENT TYPE
0,0	\$P1
001,111	\$P2 BOUNDARY COND
101,011	\$P2
110,101	\$P2
101,011	\$P2
1	\$Q1
1,1,0	\$Q2
-.001,-1,1,10,0,0	\$Q3
1,1,1,0,0,1	\$R1 OUTPUT FORMAT

Figure B.3 - STAGSC-1 Input for Two Inch Circular Plate

The next input deck seen in figure B.4 below was used to generate a STAGSC-1 circular plate model similar to the model used by Shivakumar and Whitcomb [13] in their work with elliptical delaminations (see fig 5.7). This model was more difficult to generate, and didn't agree as well with the closed form solution as the 10x8 model. A couple of features of this model to note are the input cards \$N9A and \$N9B. These cards generate a series of similarly oriented elements around the model. The first card defines the number of cards necessary to define the model, and the other cards define the element, the number of elements in the series and the node numbers which define the first element.

LINEAR ANALYSIS - 2IN DISK OPLY - BIFUR - DISKA - 0/-45 PLYS	
1,1,1,1,0,0,1	\$B1 NO. SHELL UNITS
1	\$B2 NO. SHELL UNITS
1,0,1	\$B3
1.0	\$C1 LOAD INCR
1,0,650,0,0	\$D2 EIGENVALUE CNTRL
1,0.001	\$D3 CLUSTER DEFN
9,33	\$F1 NO. ROWS COLS
1	\$I1 MATL #1
18.844E06,0.0218128,.91E06,1.,1.,1.468E06,1.	\$I2 MATL PROP
1,1,2	\$K1 # LAMINAE
1,0.00480,0.0	\$K2 PLY THICK, ORIENT
1,0.00480,-45.0	\$K2
4	\$M1 SHELL TYPE
0.0,1.0,0.0,360.0	\$M2A SHELL GEOMETRY
1	\$M5
0,0,0	\$N1 ELEMENT TYPE
15	\$N9A
320,1,8,1,1,2,1,2,5	\$N9B
320,1,8,2,1,3,3,2,5	\$N9B
320,1,8,2,1,3,1,3,3,0,4	\$N9B
320,1,8,2,5,3,3,3,5,0,4	\$N9B
320,1,16,3,1,4,1,4,2,0,2	\$N9B ELEMENT ORIENTATION
320,1,16,3,1,4,2,3,3,0,2	
320,1,16,4,2,4,3,3,3,0,2	
320,3,16,4,1,5,1,4,2,2,2	
320,3,16,5,1,5,2,4,2,2,2	
320,3,16,4,2,5,2,5,3,2,2	
320,3,16,4,2,5,3,4,3,2,2	
320,2,16,5,1,6,1,6,2,2,2	
320,2,16,5,1,6,2,5,2,2,2	
320,2,16,5,2,6,2,5,3,2,2	
320,2,16,6,2,6,3,5,3,2,2	
0,0	\$P1
001,111	\$P2 BOUNDARY COND
101,011	\$P2
110,010	\$P2
101,011	\$P2
1	\$Q1
1,1,0	\$Q2
-.001,-1,1,9,0,0	\$Q3
2,2,2,0,0,2	\$R1 OUTPUT FORMAT

Figure B.4 - STAGSC-1 360 Degree Circular Plate Model Using
the TRINC 320 Element.

The following model is presented to illustrate the method of loading individual nodes on a structure while constraining others. Note that two load systems are defined by the use of two \$Q2 cards followed by a series of \$Q3 load records.

LINEAR ANALYSIS - 2IN DISK PLY - BIFUR - DISKA - 07-45 PLYES	
1,1,1,1,0,0,1	\$B1 NO. SHELL UNITS
1	\$B2 NO. SHELL UNITS
1,0,1	\$B3
1.0	\$C1 LOAD INCR
1,0,650,0,0	\$D2 EIGENVALUE CNTRL
1,0.001	\$D3 CLUSTER DEFN
9,33	\$F1 NO. ROWS COLS
1	\$I1 MATL #1
18.844E06,0.0218128,.91E06,1.,1.,1.468E06,1.	\$I2 MATL PROP
1,1,2	\$K1 # LAMINAE
1,0.00480,0.0	\$K2 PLY THICK, ORIENT
1,0.00480,-45.0	\$K2
4	\$M1 SHELL TYPE
0.0,1.0,0.0,360.0	\$M2A SHELL GEOMETRY
1	\$M5
0,0,0	\$N1 ELEMENT TYPE
15	\$N9A
320,1,8,1,1,2,1,2,5	\$N9B
320,1,8,2,1,3,3,2,5	\$N9B
320,1,8,2,1,3,1,3,3,0,4	\$N9B
320,1,8,2,5,3,3,3,5,0,4	\$N9B ELEMENT ORIENTATION
320,1,16,3,1,4,1,4,2,0,2	
320,1,16,3,1,4,2,3,3,0,2	
320,1,16,4,2,4,3,3,3,0,2	
320,3,16,4,1,5,1,4,2,2,2	
320,3,16,5,1,5,2,4,2,2,2	
320,3,16,4,2,5,2,5,3,2,2	
320,3,16,4,2,5,3,4,3,2,2	
320,2,16,5,1,6,1,6,2,2,2	
320,2,16,5,1,6,2,5,2,2,2	
320,2,16,5,2,6,2,5,3,2,2	
320,2,16,6,2,6,3,5,3,2,2	

Figure B.5 - STAGSC-1 Model of Circular Plate with Multiple Load Systems (Continued on Next Page)

Figure B.5 Continued

0,0	\$P1
001,111	\$P2 BOUNDARY COND
101,011	\$P2
110,101	\$P2
101,011	\$P2
2	\$Q1
1,33,0	\$Q2
-0.001,-1,1,9,8,0	\$Q3
-0.001,-1,1,9,9,0	\$Q3
-0.001,-1,1,9,10,0	\$Q3
0.000,-1,1,9,11,0	\$Q3
0.000,-1,1,9,12,0	\$Q3
0.000,-1,1,9,13,0	\$Q3
0.000,-1,1,9,14,0	\$Q3
0.000,-1,1,9,15,0	\$Q3
0.000,-1,1,9,16,0	\$Q3
0.000,-1,1,9,17,0	\$Q3
0.000,-1,1,9,18,0	\$Q3
0.000,-1,1,9,19,0	\$Q3
0.000,-1,1,9,20,0	\$Q3
0.000,-1,1,9,21,0	\$Q3
0.000,-1,1,9,22,0	\$Q3
0.000,-1,1,9,23,0	\$Q3
0.000,-1,1,9,24,0	\$Q3
0.000,-1,1,9,25,0	\$Q3
0.000,-1,1,9,26,0	\$Q3
0.000,-1,1,9,27,0	\$Q3
0.000,-1,1,9,28,0	\$Q3
0.000,-1,1,9,29,0	\$Q3
0.000,-1,1,9,30,0	\$Q3
0.000,-1,1,9,31,0	\$Q3
0.000,-1,1,9,32,0	\$Q3
0.000,-1,1,9,33,0	\$Q3
2,1,0	\$Q2
0,-1,2,9,0,0	\$Q3
2,2,2,0,0,2	\$R1 OUTPUT FORMAT

Figure B.5a (Continued) - STAGSC-1 Circular Plate with
Multiple Load Systems

The Point Stress Laminate program SQ5 was used to determine the constitutive relations used in this research. A sample input deck is given in the figure below. SQ5 can be used to compute most of the values necessary to perform classical laminate calculations. Models can be run which compute force resultants and moment resultants for a temperature differential, which compute resultants for a given strain, and which compute average material properties for a given laminate.

```

PROPERTIES OF A LAMINATE (0,-+45,90)S
      0      0      0      0      0      2      1      0
18844000. 1468000. 0.28      910000. 0.      0.
      1      1      0.      0.0048
      2      1 -45.      0.0048

```

Figure B.6 - Sample SQ5 Input Deck

A selection of common NOS commands used on the AFWAL Cyber computer system is presented here for subsequent students who must learn to use STAGSC-1 on the current system. It is first suggested that the new user load the AFWAL profile into his account by following the directions

outlined in the "An Introduction to AFIT Computer Systems" pamphlet. The Procfile contains a library of abbreviated commands which are similar to UNIX commands. A help file is also available which gives a summary of most of the abbreviated commands and which can be sent to the printer so that the user has a handy reference.

`get,filename` - retrieves a file from the library into the working environment. The file must be retrieved into the working environment before it can be operated on or executed by the user.

`save,filename=newfilename` - used after an editing session to save the new version of a file to the user's library

`replace,filename` - used after an editing session to replace an old file with a new version in the library

`rts,filename` - routes a file to the printer

`submit,batchjob,to` - submits a batchjob and sends the dayfile to the waitque.

`fi` - gives the status of all current executing jobs and tells which jobs are in the wait queue.

`qg,jobname` - retrieves a job's dayfile from the waitque. The `jobname` is a four character code assigned by the computer which defines the job and is seen using `fi`.

`purge,filename` - deletes a file from the directory

`ls` - a Procfiler command which shows all of the files in the user's directory

`more,filename` - prints a file to the screen one page at a time. Hitting the space bar or the carriage return bring up the next page of the file.

BIBLIOGRAPHY

1. Almroth, B.O., Brogan, F.A., and Stanley, G.M., Structural Analysis of General Shells, Volume II User Instruction for STAGSC-1, Lockheed Palo Alto Research Laboratory, California, January, 1981.
2. Brush, D.O., and Almroth, B.O., Buckling of Bars, Plates and Shells, McGraw-Hill, New York, 1975.
3. Croop, H.C., AFWAL-TM-87-188-FIBC, Fabrication of Curved Graphite/Epoxy Compression Test Panels, Flight Dynamics Laboratory, Ohio, August, 1987.
4. Dym, C.L., Shames, I.H., Solid Mechanics - A Variational Approach, McGraw-Hill, New York, 1973.
5. English, Lawrence K., "Fabricating the Future with Composite Materials - Part II - Reinforcement", Engineering Materials, September, 1987.
6. Hebert, J.S., Analytical/Experimental Linear Bifurcation of Curved Cylindrical Panels, MS Thesis, AFIT/GAE/AA/83D-14, Air Force Institute of Technology, WPAFB, Ohio, December, 1983.
7. Horban, B.A. and Palazotto, A.N., "Experimental Buckling of Cylindrical Composite Panels with Eccentrically Located Circular Delaminations", Journal of Spacecraft and Rockets, AIAA, Vol 24, August 1987
8. Jones, Robert M., Mechanics of Composite Materials, McGraw-Hill, New York, 1975.

9. O'Brien, T.K., "Characterization of Delamination Onset and Growth in a Composite Laminate", Damage in Composite Materials, ASTM STP775, American Society for Testing and Materials, 1982, pp. 140-167.
10. Rankin, C.C., Stehlin, P., Brogan, F.A., NASA Contractor Report 4000, Enhancements to the STAGS Computer Code, NASA Scientific and Technical Information Branch, Virginia, 1986.
11. Reed, D.L., Point Stress Laminate Analysis, FZM-5494, General Dynamics, Fort Worth Division, April, 1970.
12. Seifert, G.R. and Palazotto, A.N., "The Effect of a Centrally Located Midplane Delamination on the Instability of Composite Panels", Experimental Mechanics, pg 330, December 1986.
13. Shivakumar, K.N., Whitcomb, J.D., "Buckling of a Sublaminar in a Quasi-Isotropic Composite Laminate", Journal of Composite Materials, Vol. 19, Jan. 1985.
14. Sobel, L.H. and Thomas, K., Evaluation of the STAGSC-1 Shell Analysis Computer Program, WARD-10881 Westinghouse Advanced Reactors Division, Madison PA, Aug 1981
15. Tisler, Thomas W. Jr., Collapse Analysis of Cylindrical Composite Panels With Large Cutouts Under an Axial Load, MS Thesis, AFIT/GAE/AA/86-D-18, School of Engineering, Air Force Institute of Technology, WPAFB, Ohio, December, 1986.

16. Tsai, Stephen W., Composite Design, Think Composites, Dayton, Ohio, 1987.
17. Whitcomb, J.D., "Finite Element Analysis of Instability Related Delamination Growth", Journal of Composite Materials, Vol. 15, Sept. 1981, p. 403.
18. Whitcomb, J.D., "Strain-Energy Release Rate Analysis of Cyclic Delamination Growth in Compressively Loaded Laminates", Effects of Defects in Composite Materials, ASTM STP 836, American Society for Testing and Materials 1984, pp. 175-193.
19. Woytowitz, Peter J., AFWAL-TR-84-3088 Sample Problems for STAGSC-1, AFWAL/FIBRA, WPAFB, Ohio, 1984.
20. Wilkens, D.J., "Compression Buckling Tests of Laminated Graphite/Epoxy Curved Panels", AIAA Paper No. 74-32, Presented at the AIAA 12th Aerospace Sciences Meeting, Washington, DC, January 30, 1974.
21. Sandhu, R.S., "Alternate Strength Analysis of Symetric Laminates", Technical Report AFFDL-TR-73-137, AD 779927, Air Force Flight Dynamics Laboratory, Wright-Patterson AFB, Ohio, February 1974.

VITA

Captain Brendan L. Wilder was born on 12 June 1959 in DeQueen, Arkansas. He graduated from high school in Humboldt, Tennessee in 1977 and attended the University of Tennessee at Knoxville from which he received the degree of Bachelor of Science in Civil Engineering in June 1982. Upon graduation, he received his Air Force Commission through OTS, and was assigned to George AFB where he served as a design engineer in the 831st CSG Civil Engineering Squadron for three years. In June 1986 he was assigned to the Air Force Institute of Technology, School of Engineering.

Permanent Address: Rt.1 Box 159
Fayette, MO 65428

REPORT DOCUMENTATION PAGE

Form Approved
OMB No 0704-0188

1a REPORT SECURITY CLASSIFICATION UNCLASSIFIED			1b RESTRICTIVE MARKINGS			
2a SECURITY CLASSIFICATION AUTHORITY			3 DISTRIBUTION / AVAILABILITY OF REPORT Approved for public release; distribution unlimited.			
2b DECLASSIFICATION DOWNGRADING SCHEDULE						
4 PERFORMING ORGANIZATION REPORT NUMBER(S) AFIT/GA/AA/88M-3			5 MONITORING ORGANIZATION REPORT NUMBER(S)			
6a NAME OF PERFORMING ORGANIZATION School of Engineering		6b OFFICE SYMBOL (if applicable) AFIT/EN		7a NAME OF MONITORING ORGANIZATION		
6c ADDRESS (City, State, and ZIP Code) Air Force Institute of Technology Wright-Patterson AFB, Ohio 45433			7b ADDRESS (City, State, and ZIP Code)			
8a NAME OF FUNDING SPONSORING ORGANIZATION		8b OFFICE SYMBOL (if applicable)		9 PROCUREMENT INSTRUMENT IDENTIFICATION NUMBER		
8c ADDRESS (City, State, and ZIP Code)			10 SOURCE OF FUNDING NUMBERS			
			PROGRAM ELEMENT NO	PROJECT NO	TASK NO	WORK UNIT ACCESSION NO
11 TITLE (Include Security Classification) See Box 19						
12 PERSONAL AUTHOR(S) Brendan L. Wilder, M.S., Capt, USAF						
13a TYPE OF REPORT MS Thesis		13b TIME COVERED FROM _____ TO _____		14. DATE OF REPORT (Year, Month, Day) 1988 March		
15 PAGE COUNT 151						
16 SUPPLEMENTARY NOTATION						
17. COSATI CODES			18 SUBJECT TERMS (Continue on reverse if necessary and identify by block number) Composites, Cylindrical Panels, Delaminations, Experimental Shell Analysis, STAGSC-1, Graphite Epoxy, Finite Elements			
FIELD	GROUP	SUB-GROUP				
11	04					
19 ABSTRACT (Continue on reverse if necessary and identify by block number) 11) Title: A STUDY OF DAMAGE TOLERANCE IN CURVED COMPOSITE PANELS Thesis Advisor: Dr. Anthony N. Palazotto						
20 DISTRIBUTION / AVAILABILITY OF ABSTRACT <input checked="" type="checkbox"/> UNCLASSIFIED/UNLIMITED <input type="checkbox"/> SAME AS RPT <input type="checkbox"/> DTIC USERS			21 ABSTRACT SECURITY CLASSIFICATION UNCLASSIFIED			
22a NAME OF RESPONSIBLE INDIVIDUAL Dr. Anthony N. Palazotto			22b TELEPHONE (Include Area Code) (513) 255-3517		22c OFFICE SYMBOL AFIT/EN	

Approved for public release; distribution unlimited.

UNCLASSIFIED

This thesis investigated the behavior of a cylindrical composite panel made of AS4/3501-6 graphite/epoxy with ply orientations $[0/-45/45/90]_s$. Abrasion and burn surface damage was physically modeled in the panels by removing a portion of the exterior plies. The panels were then tested by compressively loading them and a comparison was made to buckling predictions obtained using a STAGSC-1 shell program. These tests indicated that panels which have suffered minor surface damage do not deviate significantly from buckling predictions obtained using a STAGSC-1 linear bifurcation model.

Panels were also tested which had varying thicknesses and variations in void content due to faulty manufacturing techniques. These panels were also compressively loaded, and it was found that high void content increased panel thickness, which resulted in higher compressive strengths.

Composite laminates subjected to a low speed impact, such as a dropped tool or a manufacturing load, often develop an internal delamination. This delamination may result in the reduction of the panel's strength when subjected to compressive load.

Since curved panels are 3-dimensional, and buckling is a non-linear phenomenon, the compressive load which will cause curved panels to become unstable is extremely hard to predict analytically. This thesis presents a technique whereby the local buckling loads at the delamination may be predicted using a 2-dimensional model with a plane strain correction. This model yielded predictions of local instability within 30 percent of experimental values.

UNCLASSIFIED

END
DATE
FILMED
DTIC
4/88